CHALMERS
UNIVERSITY OF TECHNOLOGY

Land subsidence caused by pore pressure reduction due to a local groundwater extraction

A study on modelling approaches to predict and describe land subsidence caused by a local groundwater extraction

Master's thesis in Infrastructure and Environmental Engineering

MÅNS PAULSSON
MARCUS TRAPP

DEPARTMENT OF ARCHITECTURE AND CIVIL ENGINEERING

CHALMERS UNIVERSITY OF TECHNOLOGY
Gothenburg, Sweden 2024
www.chalmers.se

Master's thesis 2024

Land subsidence caused by pore pressure reduction due to a local groundwater extraction

A study on modelling approaches to predict and describe land subsidence caused by a local groundwater extraction

MÅNS PAULSSON

MARCUS TRAPP

CHALMERS
UNIVERSITY OF TECHNOLOGY

Department of Architecture and Civil Engineering
Division of Geology and Geotechnics
Geotechnics Research Group
Chalmers University of Technology
Gothenburg, Sweden 2024

Land subsidence caused by pore pressure reduction due to a local groundwater extraction
A study on modelling approaches to predict and describe land subsidence caused by a local groundwater extraction
Måns Paulsson
Marcus Trapp

Supervisors:
Ayman Abed, Department of Architecture and Civil Engineering
Peter Jansson, Sweco Sverige AB
Examiner:
Ayman Abed, Department of Architecture and Civil Engineering

Master's Thesis 2024
Department of Architecture and Civil Engineering
Division of Geology and Geotechnics
Geotechnics Research Group
Chalmers University of Technology
SE-412 96 Gothenburg
Telephone +46 31 772 1000

Typeset in LaTeX
Printed by Chalmers Reproservice
Gothenburg, Sweden 2024

Land subsidence caused by pore pressure reduction due to a local groundwater extraction
A study on modeling approaches to predict and describe land subsidence caused by a local groundwater extraction
MÅNS PAULSSON
MARCUS TRAPP
Department of Architecture and Civil Engineering
Chalmers University of Technology

Abstract

Land subsidence caused by the extraction of groundwater is a well known problem that could cause large and costly damages to the built infrastructure. This master's thesis explores the land subsidence resulting from reduced pore pressure due to local groundwater extraction in Gothenburg, Sweden. The study employs 1D and 2D consolidation models to simulate the effects of groundwater withdrawal on subsidence, providing a comprehensive analysis of vertical displacements and soil behavior. By integrating geotechnical site characterization with hydrogeological data, the research validates the predictions of the model against field measurements. The findings highlight that the 1D analytical solution correlates well with both the 1D Plaxis model and the field measurements. In addition, the results suggest that the extraction rate is the governing factor for the magnitude of land subsidence at close distances to the pumping well; meanwhile, the clay thickness is the governing factor at further distances from the well. The findings also indicate that the reduction in pore pressure will extend further in the soil profile for thicker clays, resulting in a larger land subsidence over longer periods of time. Furthermore, the findings highlight the need for validation with field measurements and the difficulties of modeling groundwater extraction and predicting subsequent land subsidence using an axisymmetric Plaxis 2D model.

Keywords: pore pressure, land subsidence, groundwater extraction, Plaxis 2D, analytical modeling, settlements, drawdown, aquifer, soft soil.

Acknowledgements

This Master's Thesis was written at the Division of Geology and Geotechnics at Chalmers University of Technology in collaboration with Sweco Sverige AB during the spring semester 2024.

We would like to express our gratitude for the support and insightful thoughts provided during the last months of our studies. Our thanks go to Ingrid Johansson at the Chalmers Library for your inspiring persona and support with the literature search. We also thank Ulf Johansson, consultant at Trafikverket, and Otto Graffner, project manager at Trafikverket, for their assistance in providing data for the Hamnbanan railway project. Our greatest gratitude is directed towards our examiner and supervisor at Chalmers Ayman Abed and our supervisor at Sweco Peter Jansson. Ayman has been contributing to the thesis throughout the semester with his expertise in geotechnical engineering, the modeling process, and excellent support throughout the journey. Peter has with his years of experience working with geotechnics and high level of expertise been of great importance during the process and constantly reminded us to keep a foot in the real world. Thanks to both of you for all the hours of interesting and educational conversations. Lastly, we would like to thank the entire geotechnics group at Sweco for their support and great fika.

Måns Paulsson, Gothenburg, June 2024
Marcus Trapp, Gothenburg, June 2024

Nomenclature

Roman letters

a	Factor in the "general soil model" describing the soil type and anisotropy	[-]
b	Material constant in the "general soil model"	[-]
c'_{ref}	Reference cohesion intercept	[kPa]
c_k	Compression index	[-]
c_u	Undrained shear strength	[kPa]
E'_{ref}	Effective Young's modulus	[kPa]
E_s	Compression modulus in the analytical solution	[kPa]
e_{init}	Initial void ratio	[-]
g	Gravitational acceleration constant, $g = 9.81$	$[m/s^2]$
h_0	Initial groundwater head of all soil layers	[m]
h	Head of groundwater	[m]
H	Thickness of soil layer	[m]
Hfa_{netto}	Ram sounding penetration resistance	$[sl/0.2m]$
K_0	Lateral earth pressure coefficient at rest	[-]
K_0^{nc}	Lateral earth pressure coefficient at rest for normally consolidated soils	[-]
$K_{0,OC}$	Lateral earth pressure coefficient at rest for overconsolidated soils	[-]
k	Hydraulic conductivity	[m/s]
M_0	Compression modulus for $\sigma'_v \leq \sigma'_c$	[kPa]
M_L	Compression modulus for $\sigma'_v \leq \sigma'_c \leq \sigma'_L$	[kPa]
n	Porosity	[-]
Q	Water flow	$[m^3/day]$
q_c	Cone resistance	[kPa]

S	Settlement	[m]
T_v	Time factor	[-]
u	Pore pressure	[kPa]
W_L	Liquid limit	[%]
W_N	Water content	[%]
z	Depth from ground surface	[m]

Greek letters

α_s	Creep parameter	[-]
γ	Unit weight	$[kN/m^3]$
γ_{sat}	Saturated unit weight	$[kN/m^3]$
γ_{unsat}	Unsaturated unit weight	$[kN/m^3]$
γ_w	Unit weight of water	$[kN/m^3]$
κ^*	Modified swelling index	[-]
λ^*	Modified compression index	[-]
μ	Correction factor for undrained shear strength	[-]
μ^*	Modified creep index	[-]
ν	Poisson's ratio	[-]
ν'	Effective Poisson's ratio	[-]
ν_{ur}	Poisson's ratio for unloading-reloading	[-]
ρ	Density	$[kg/m^3]$
σ'_c	Preconsolidation stress	[kPa]
σ'_L	Limit effective stress where the compression modulus begins to increase	[kPa]
σ'_v	Vertical effective stress	[kPa]
σ'_z	Vertical effective stress	[kPa]
$\tau_{v,k}$	Undrained shear strength from vane test and fall cone test	[kPa]
$\tau_{vb,corr}$	Corrected undrained shear strength from vane test	[kPa]
ϕ	Friction angle	[°]
ψ	Dilation angle	[°]

Contents

List of Figures

List of Tables

1
Introduction

In this chapter, relevant background information on land subsidence is presented along with the aim, limitations, and research questions of the thesis.

1.1 Background

Land subsidence is a phenomenon in which the land surface sinks gradually or suddenly (Esteban et al., 2024). There can be many causes for subsidence, both natural and anthropogenic (Galloway and Burbey, 2011). A common cause of subsidence is the extraction of fluids in the soil such as natural gas, crude oil, or most commonly groundwater. Groundwater is extracted from the ground for several different reasons. The most well-known reason is to use it as raw water for drinking water supply and irrigation, but groundwater is also frequently extracted during the construction phase of underground projects. Land subsidence could, for example, lead to surface cracking, pipe breaks, differential settlements, and subsequently leaning buildings or even damage to the building structure and other costly damage to infrastructure (Cigna and Tapete, 2021).There are many examples in which groundwater drawdown induced subsidence has had severe consequences (Merisalu et al., 2023).

It has long been known that land subsidence is related to the removal of fluids in the soil. One of the first observations was made in the 1920s by two American geologists, Pratt and Wallace (1926). In Sweden, groundwater was first suspected in the 1960s to have a great impact on subsidence (Lindskoug and Nilsson, 1974). In 1925 Karl Terzaghi introduced the principle of effective stress (He et al., 2020). This principle explains that a reduction in the pore pressure in a soil leads to an increase in the effective stress. This increase can cause the aquifer (and the adjacent soil skeleton) to compact, resulting in land subsidence.

Three important and related topics on anthropogenic land subsidence are geomechanical and hydraulic properties, numerical solutions, and monitoring techniques (He et al., 2020). Geomechanical and hydraulic properties can differ considerably between sites, due to the stress history at the site, which can greatly impact important parameters such as the compressibility and creep of soft clays (Wikby et al., 2023). Since pore pressure in soft soils has a direct correlation with effective stresses and subsequently the magnitude of land subsidence, it is crucial to understand the mechanisms of change in pore pressure when extracting groundwater (He et al., 2020). Numerical modeling supported by laboratory tests and field analyses is a

powerful tool to understand changes in pore pressure. The modeling of these kinds of problem is best achieved by using advanced constitutive models (Wikby et al., 2023). To verify and ensure reliable results from the use of an advanced constitutive model, it is important to perform a sensitivity analysis (Tahershamsi and Dijkstra, 2021; 2022). Previous studies have shown that some parameters are more sensitive to change than others in similar numerical models.

Although numerical modeling is a powerful tool, the results must be verified with real-life data. In recent years, many monitoring tools have been developed to measure the magnitude of land subsidence worldwide (Gambolati et al., 2006). InSAR (Interferometric Synthetic Aperture Radar) and DGPS (Differential Global Positioning System) are examples of monitoring tools that can measure land subsidence from space, which can act as a replacement for the old spirit leveling tools.

1.2 Aim

The aim of this master thesis is to describe the reduction in pore pressure and the ensuing subsidence in a layer of clay when groundwater is extracted from an underlying confined aquifer. Furthermore, this master thesis aims to examine how the relationship between the depth of the clay layer and the duration of groundwater extraction affects both the proportion and the time perspective of the dissipation of pore pressures and the subsequent subsidence. This will be performed by conducting a literature study, modeling the problem in the Plaxis 2D computational software in both 1D and 2D, as well as using an 1D analytical solution. The consolidation process after a pump test within the Hamnbanan railway project in Gothenburg, Sweden, will be modeled using the computational software Plaxis 2D and a 1D analytical solution. The performance of the different approaches will be assessed and discussed by comparing the results with the measured field data.

1.3 Limitations

1. This study is limited to existing data; that is, no additional measurements of soil or hydraulic properties will be carried out.
2. The heterogeneity of geological and hydrogeological characteristics within the soil has been abstracted. The parameters were selected following a rigorous analysis of test data to represent reality.
3. The effect on the reduction of the pore pressures of aquifer recharge has been simplified. Infiltration from the ground surface and recharge within the aquifer have not been evaluated in this thesis.
4. The 2D Plaxis models have been constructed with axisymmetric assumptions based upon a selected cross section, representing a rudimentary approximation of the majority of real-world scenarios.

1.4 Research questions

1. How does the pore pressure reduction and the subsequent land subsidence develop over time?
2. Is there a viable analytical solution to predict land subsidence due to a uniform extraction of groundwater?
3. How do the thickness of the clay and distance from the pumping well affect the consolidation process that follows a groundwater extraction?
4. How can a local groundwater extraction be modeled in Plaxis 2D?

2
Theoretical background

In this chapter, a theoretical background is provided on the relationship between groundwater extraction and land subsidence. In addition, there is an introduction to an analytical solution for the consolidation process of a 1D soil column subject to drawdown.

2.1 Relationship between groundwater extraction and land subsidence

When extracting groundwater from a confined aquifer, there will be a decrease in water level and the upward pressure produced by the fluid will decrease and cause the soil skeleton to experience higher pressure (Sun et al., 1999). The soil skeleton of the aquifer and the confining layer is non-rigid and when it experiences a load greater than the preconsolidation stress, the soil can undergo extensive irreversible compaction (Galloway et al., 1999). Both the aquifer and the confining soft soil will experience deformations when extracting groundwater, but to various degrees.

When extracting groundwater, the pore pressures in the aquifer will decrease and the effective stresses will increase provided that the downward pressure of the underlying soil and the loads on the surface remain constant (Shen et al., 2004). The reduced water level or pore pressures in the aquifer will lead to drainage from the confining layer to the aquifer to even out the pressure differences. Together, this will eventually lead to the dissipation of pore pressures and increase the effective stresses in the confining layer as well. Drainage of pore fluids out of the confining layer is irreversible, which means that the volume of pore space available to fluids will permanently decrease with drainage and lead to compaction of the soft soil, that is, land subsidence (Galloway et al., 1999).

Due to infiltration from surface water, for example, rainfall or snowmelt, the pore pressures in the soil close to the surface will not change as much as further down in the soil profile (Shen et al., 2004). Consequently, there will be a difference in total head both between the aquifer and the overlaying soil, as well as within the soil layer itself, which will cause a flow of water from the ground surface towards the aquifer (Sun et al., 1999; Shen et al., 2004). There are differences between consolidation due to surcharge loading and due to groundwater extraction. The ultimate stage of consolidation caused by the surcharge loading is the full dissipation of excess pore pressures and a zero water flow rate, while the ultimate stage of consolidation

caused by groundwater extraction is steady-state water flow (Shen et al., 2004). If the clay layer is relatively large, it can take up to 30 years for excess pore pressure to dissipate (Broms et al., 1976) .

Studies have been made on the pore pressure distribution in western Swedish clays, while subject to drawdown in a lower aquifer. A study conducted by Berntson (1983) examined two sites with a clay thickness of 10 and 20 meters respectively. The sites were subject to a drawdown of 15 kPa in the lower boundary during a period of three months. Berntson found that the pore pressure distribution in the 10 meters thick clay was impacted throughout the whole profile. However, in the 20-meter thick clay, some parts of the pore pressure distribution remained unaffected after three months subject to the drawdown. Another study by Blomén (2017) show that in a typical western Swedish soil profile, it can be assumed that the uppermost 5 meters of clay are not affected by a drawdown in the lower aquifer. This means that the pore pressure distribution in the upper part of the clay will remain hydrostatic. Blomén's findings were based on field measurements at two sites, where the pore pressures were monitored for 1.5-3 years.

2.2 1D analytical solution

Xie et al. (2012) proposed an analytical solution of a one-dimensional consolidation analysis due to a reduction in groundwater level for an aquitard in a leakage system. The authors present analytical solutions for the compression, the average degree of consolidation, and the pore pressure distribution for the aquitard at any given time. The equations used in this thesis are presented in Equations 2.1 - 2.6. Their results showed that the increase in effective stress is the central mechanism for the compression of the aquitard, which is caused by and directly proportional to the change in pore pressure. Ten assumptions were made for the proposed analytical solution (Xie et al., 2012). The assumptions are as follows:

1. The soil is completely saturated.
2. The soil is homogeneous.
3. The soil particles and pore water are incompressible.
4. The deformation from consolidation in the soil is small.
5. The seepage in the soil obeys Darcy's law.
6. The deformation and seepage in the soil is one-dimensional.
7. The vertical conductivity and compression coefficient of the soil are constant during consolidation.
8. h_0 is the initial head of all soil layers.
9. The water head loss Δh due to extensive pumping of water in the aquifer occurs instantly and remains constant.
10. The groundwater level layer remains unchanged due to natural recharge.

$$u = \gamma_w(h_0 + z - \frac{\Delta h z}{H}) + \sum_{m=1}^{\infty} \frac{2\gamma_w \Delta h}{m\pi}(-1)^{m-1} sin(\frac{m\pi z}{H}) e^{-m^2\pi^2 T_v} \tag{2.1}$$

$$\Delta u = -\frac{\gamma_w \Delta h z}{H} + \frac{2\gamma_w \Delta h}{\pi} \sum_{m=1}^{\infty} \frac{(-1)^{m-1}}{m} sin(\frac{m\pi z}{H}) e^{-m^2\pi^2 T_v} \tag{2.2}$$

$$\Delta\sigma'_z = -\Delta u \tag{2.3}$$

$$S = \frac{\gamma_w \Delta h H}{2E_s}(1 - \sum_{m=1}^{\infty} \frac{2}{M^2} e^{-4M^2\pi^2 T_v}) \tag{2.4}$$

$$T_v = \frac{kE_s t}{\gamma_w H^2} \tag{2.5}$$

$$M = \frac{2m-1}{2}\pi, m = 1, 2, 3... \tag{2.6}$$

3
Methods

In the following chapter, the methodology of the thesis is described in detail. Initially, a literature study was conducted to acquire valuable information on the subject and previous studies conducted to familiarize the Hamnbanan rail project, decide on a cross section subject to numerical modeling, and collect the data and tests needed for further analysis. After the literature study, the three different Plaxis models were created and the modeling approaches decided. Furthermore, the writing of the code for the analytical solution suggested by Xie et al.(2012) was initiated. The data and tests collected in the case study were then evaluated to obtain the soil and aquifer properties, which was used as input and to refine the Plaxis models, as well as to adapt and compute the analytical solution. The results of the three different Plaxis models and the analytical solution were analyzed and conclusions were drawn. An overview of the methodology is shown in Figure 3.1.

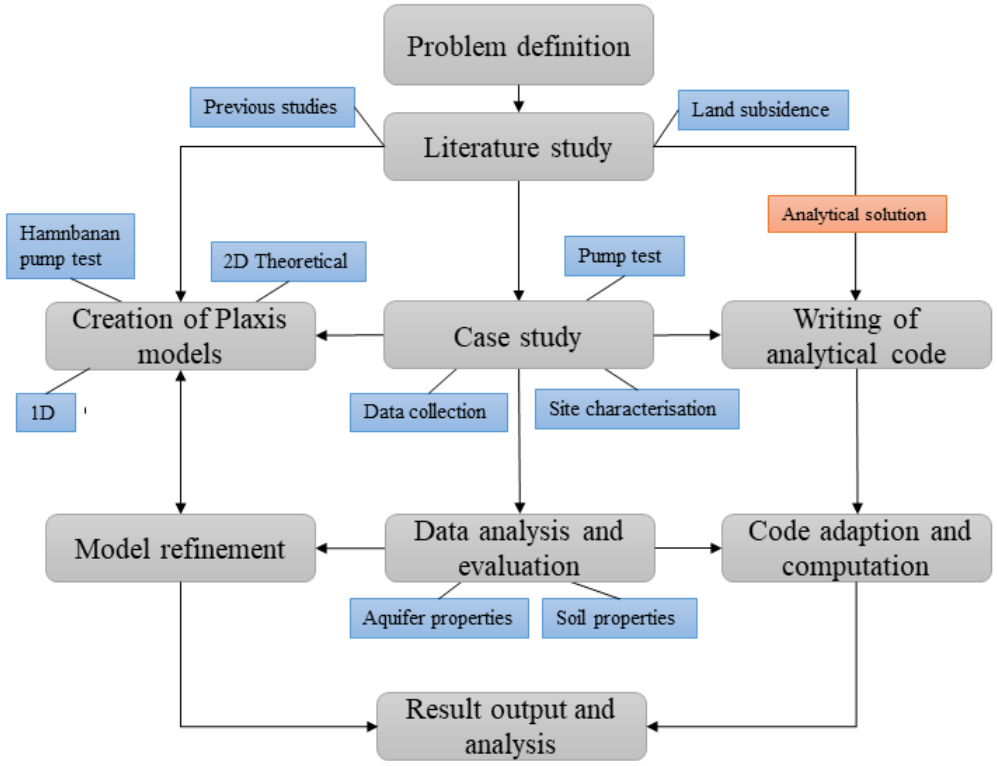

Figure 3.1: Summary of the thesis methodology.

3.1 Case study

The area subject to the case study is part of the Hamnbanan rail project in Gothenburg. Hamnbanan is an existing railway line that connects the port of Gothenburg to the national railway (Swedish Transport Administration, 2022). The construction phase of the project began in 2020 and is expected to be completed in 2024. The purpose of the project is to enhance the railway capacity to transport goods by replacing certain sections of the current single track with a double track. The section of the project that will be subject to the case study is located just north of the Eriksberg area on the island Hisingen in Gothenburg, Sweden. The approximate area is highlighted in Figure 3.2.

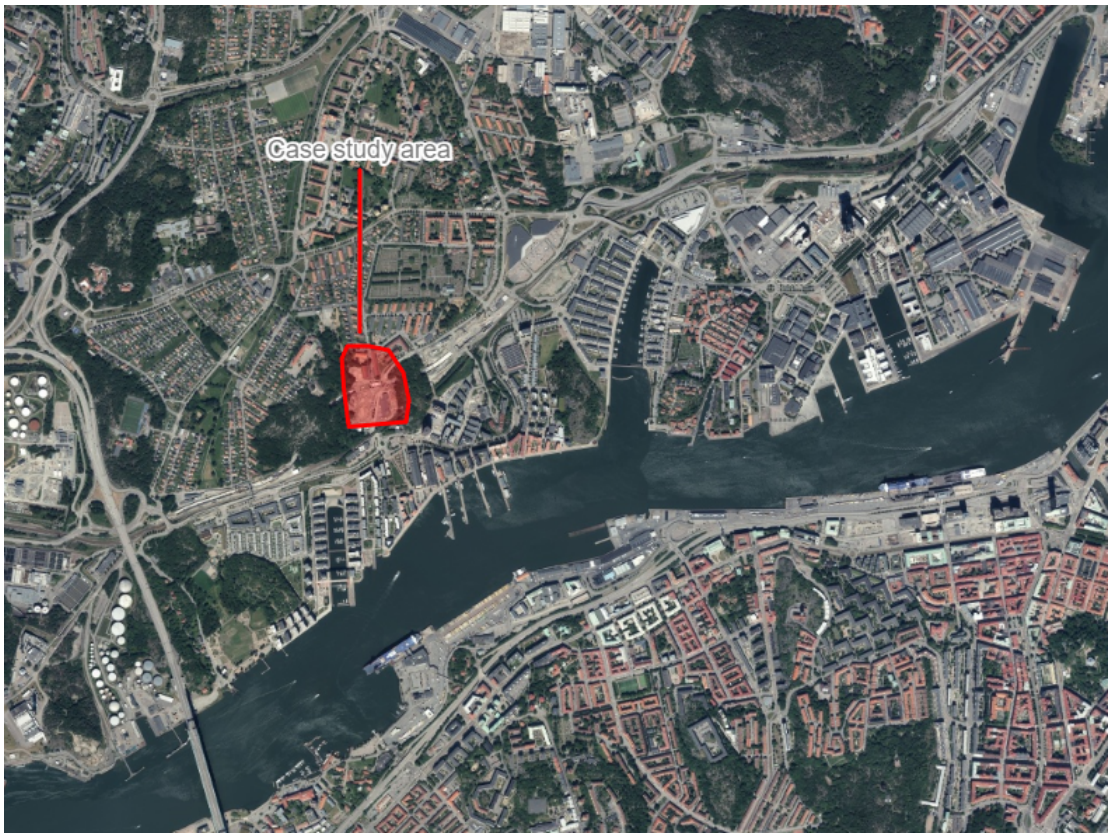

Figure 3.2: Approximate location of the area subject to the case study. Background map retrieved and modified from Lantmateriet.se. ©Lantmäteriet.

Several geotechnical and hydrogeological investigations have been conducted previously within the Hamnbanan project. Data from boreholes, wells and soil tests within the scope of the investigations have been used to assess the geotechnical and hydrogeological situation within the case study area. The investigations used are listed below.

- Hamnbanan Göteborg, dubbelspår Eriksberg Pölsebo, Vattenverksamhet, PM, Sättningsrisker på grund av grundvattensänkning (Swedish Transport Administration, 2018a).
- Markteknisk undersökningsrapport (MUR), Hydrogeologi (Swedish Transport Administration, 2015a).
- Markteknisk undersökningsrapport (MUR), Hydrogeologi (Swedish Transport Administration, 2018b)
- Projekterings PM, Geoteknik (Swedish Transport Administration, 2015c).
- Projekterings PM - Hydrogeologi (Swedish Transport Administration, 2015b).
- Teknisk handling Geoteknik (Swedish Transport Administration, 2015d).

The case study area is located to a large extent in a valley between the two mountains Krokängsberget and Bratteråsberget. The level of the ground surface varies between +7 and +10 (RH2000) within the area, where the highest areas are found along the edges of the mountains. The soil strata in the area generally consist of 1-3 m of fill or dry crust, followed by a layer of clay, with varying thicknesses from 1-12 m. The clay contains silt, and there is occasionally also the presence of sand and shells. Below the clay, there is a frictional soil with thicknesses ranging from 10 to 30 m, which overlays the bedrock. The highest soil depths are found in the center of the area, and the lowest depths are found along the edges of the mountains. The frictional soil is part of an aquifer that is in hydraulic contact with the river Göta Älv, which the groundwater flow in the aquifer is directed (Lång, 2009). An overview of the soil types and soil depths in the area is shown in Figures 3.3 and 3.4.

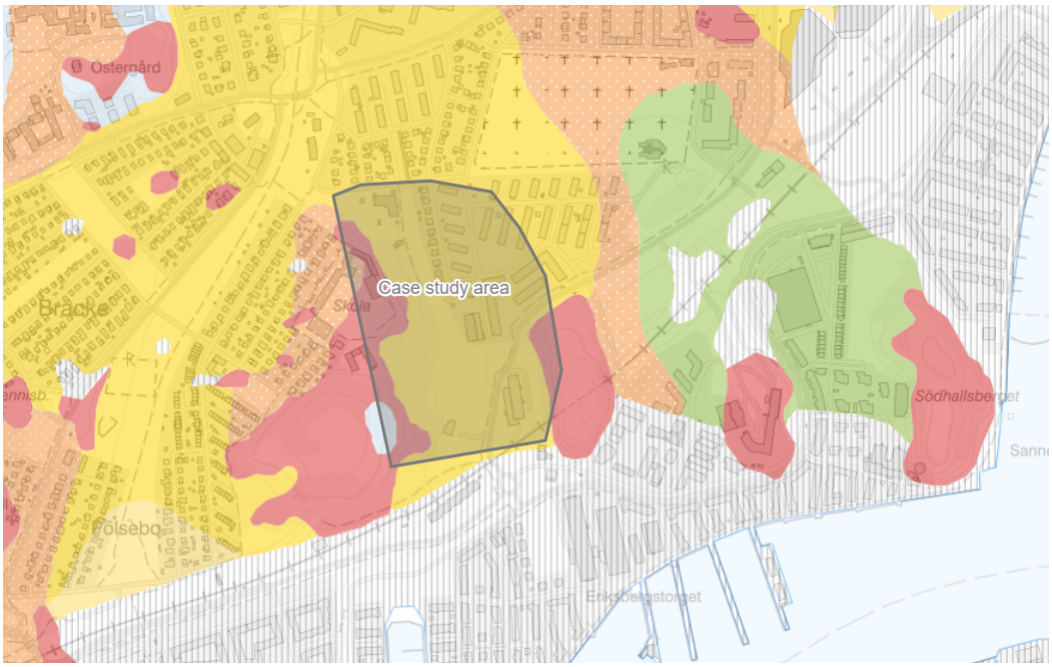

Figure 3.3: Map showing the soil types in the case study area. Yellow indicates clay and red bedrock. Background map retrieved and modified from Lantmateriet.se. ©Lantmäteriet.

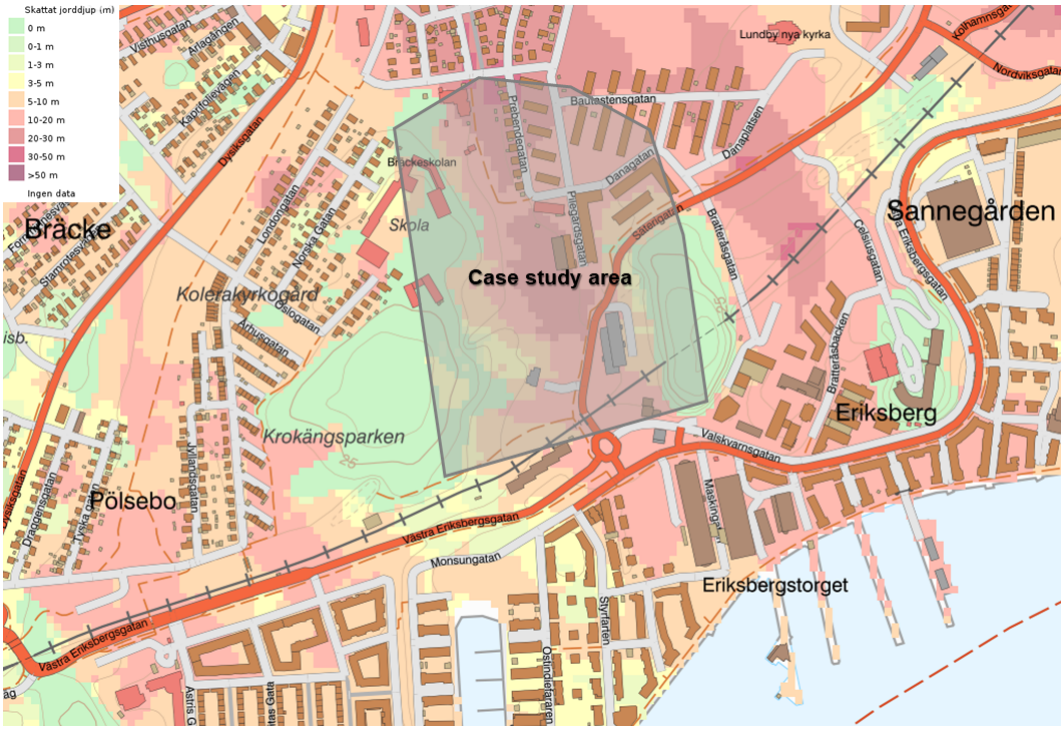

Figure 3.4: Map showing the soil depths in the case study area. Background map retrieved and modified from Lantmateriet.se. ©Lantmäteriet.

Ramböll conducted a pump test on behalf of the Swedish Transport Administration during February-March 2018, within the case study area. The pump test started on

February 26 and ended on March 26. The pump was installed in borehole VD4767 at a depth of approximately 13 meters. During the course of the test, the groundwater level was monitored in the pumping well and in 17 observation wells. Furthermore, BAT sensors monitored the pore pressure at varying depth in the overlaying clay layer in 4 wells. The pump flow was initially measured at 216 m^3/day, but after 1.5 hours it was changed to 190 m^3/day to obtain a more stable flow of water. The measurements during the test showed rather constant flow, with variations between 184-191 m^3/day. The location of the pumping well and relevant observation wells are shown in Figure 3.5.

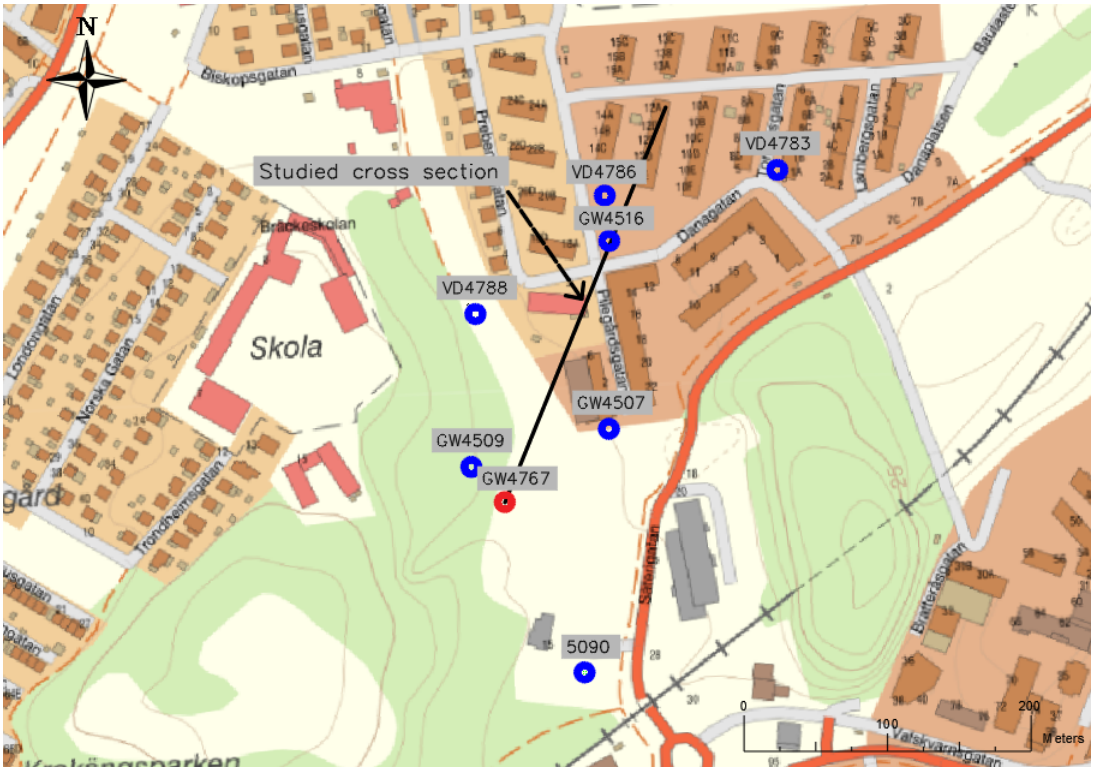

Figure 3.5: The location of the pumping well and relevant observation wells. Background map retrieved and modified from Lantmateriet.se. ©Lantmäteriet.

3.1.1 Geotechnical site characterisation

The soil test data obtained from the previous investigations presented in Section 3.1 have been compiled and evaluated. Engineering assumptions have been made to obtain profiles for certain parameters. The evaluation is based on the sounding methods pyramid penetration test (Tr), cone penetration tests (CPT), and ram soundings (Hfa), as well as vane tests. The piston samples have been tested for basic parameters, water content W_N, liquid limit W_L, density ρ, porosity n, and undrained shear strength c_u. In addition, constant rate of strain (CRS) tests have been performed to evaluate settlement moduli M_0 and M_L, hydraulic conductivity k, compression index c_k, as well as pre-consolidation pressure σ'_c. Vane tests have also been performed to further assess undrained shear strength. In addition, the friction angle ϕ has been evaluated on the basis of the Hfa and the CPT soundings.

The soundings and test data were obtained through Swecos' borehole database and from the Swedish Transport Administration.

The soil test data has been evaluated from 14 boreholes, their locations are shown in Figure 3.6. The piston samples, which have been subject to further testing, have been taken in 7 boreholes. VD4783, VD4786, VD4788, 4518, 4585, 5006 and 5090. The test data from VD4783 and 5090 are considered to be of less relevance in the evaluation of soil parameters, since they are considerably further away from the cross section, but have still been included in the graphs as references. In the graphs, their data points are distinguished from the rest by not having a fill color.

Figure 3.6: Location of the boreholes used for evaluation of the soil parameters. Background map retrieved and modified from Lantmateriet.se. ©Lantmäteriet.

To create a general soil profile in the area of the case study, soil parameters were evaluated against depth to take into account the variation in ground surface level. The clay has been evaluated to consist of two layers, the first at a depth of 2-6 meters, and a more dense and compact layer at a depth of 6-12 meters. As mentioned above, the thickness of the dry crust varies from 1-3 meters. This entails some deviating values for some boreholes between 2-3 meters, which has been disregarded for the evaluation of the clays' properties, but included in the evaluation of the dry crust.

The data compiled and evaluated for density and undrained shear strength are presented in Figures 3.7 and 3.8. The undrained shear strength has been corrected against the liquid limit according to equations 3.1 and 3.2, which is obtained from the Swedish Geotechnical Institutes information report *Soil properties* (2008). The

evaluated data for the liquid limit are presented in Appendix A, together with the evaluated water content.

$$c_u = \mu * \tau_{v,k} \tag{3.1}$$

$$\mu = (\frac{0.43}{W_L})^{0.45} \tag{3.2}$$

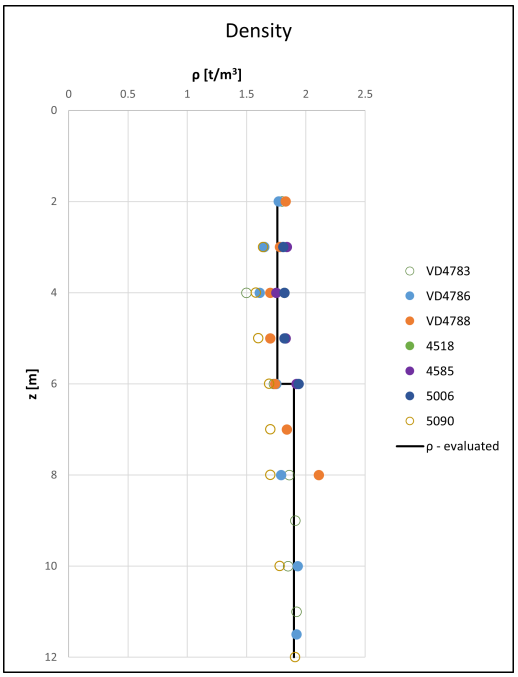

Figure 3.7: Test data and the evaluated profile for the density ρ.

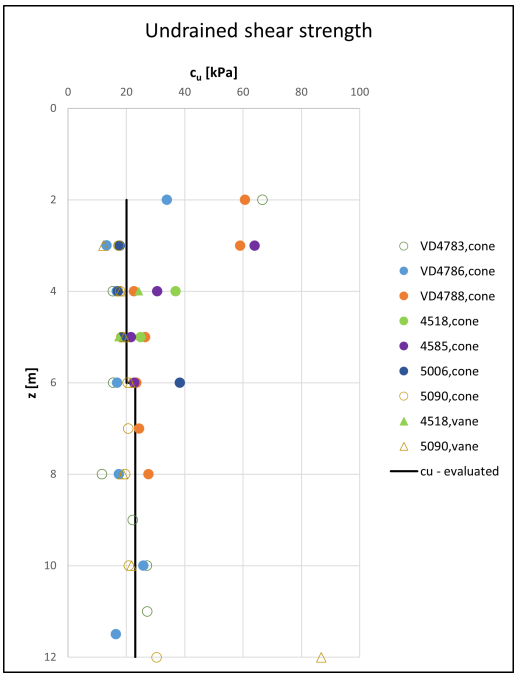

Figure 3.8: Test data and the evaluated profile for the undrained shear strength c_u.

The pore pressure in the clay has been measured over time with BAT-sensors placed at multiple depths in the four boreholes VD4783, VD4786, VD4788, and 5090. The measurements were evaluated and an pore pressure profile that represents the area was chosen. To assign the pore pressure profile, the measured pore pressures were plotted and evaluated over time for each borehole. The pressure profile was then validated by plotting it together with the pore pressure measurements on nearby dates during February 2018 and August 2019, see Figures 3.9 and 3.10. The pore pressure measurements over time for the four boreholes are presented in Appendix C.

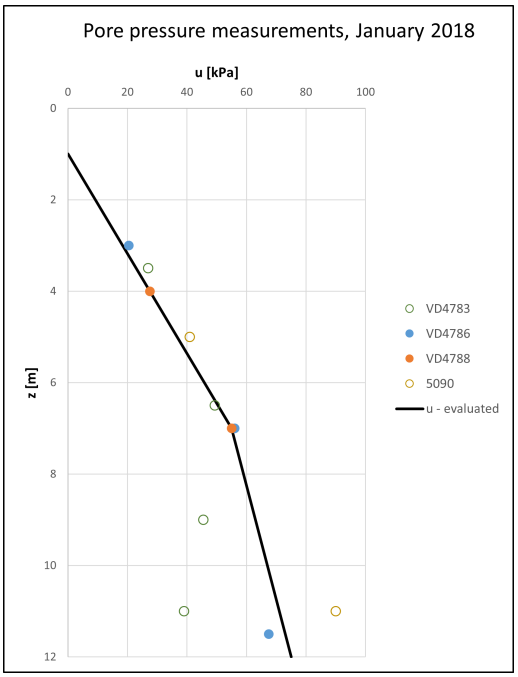

Figure 3.9: Pore pressure measurements in January 2018 compared to the evaluated pore pressure profile.

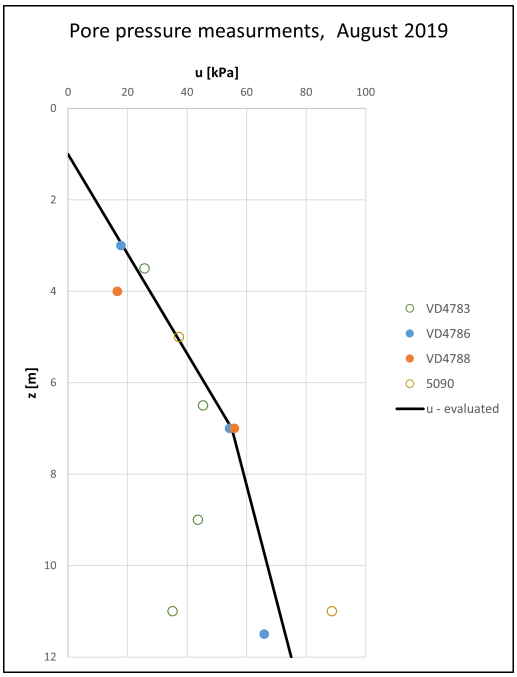

Figure 3.10: Pore pressure measurements in August 2019 compared to the evaluated pore pressure profile.

The preconsolidation pressure of the clay was evaluated using data from CRS tests at multiple depths in seven boreholes. In boreholes where vane tests had been conducted, the two empirical relations "Hansbos formula" (Equation 3.3) and "the general soil model" (Equation 3.4) presented by Larsson et. al (2007), was included in the evaluation of the preconsolidation pressure. The data along with the evaluated profiles are shown in Figure 3.11. The effective stress in the soil was evaluated using the assigned density and the pore pressure profile. Furthermore, 80% of the preconsolidation pressure was also included in the graph, which is the pressure at which consolidation and creep settlements occur, according to Swedish practice. With the profile evaluated for the preconsolidation pressure and the effective stress, the overconsolidation ratio OCR and the pre-overburden pressure were evaluated; see Figures 3.12 and 3.13.

$$\tau_{v,k} = \sigma'_c * 0.45 W_L \tag{3.3}$$

$$\sigma'_c = \sigma'_v \left(\frac{\tau_{vb,corr}}{a * \sigma'_v}\right)^{1/b} \tag{3.4}$$

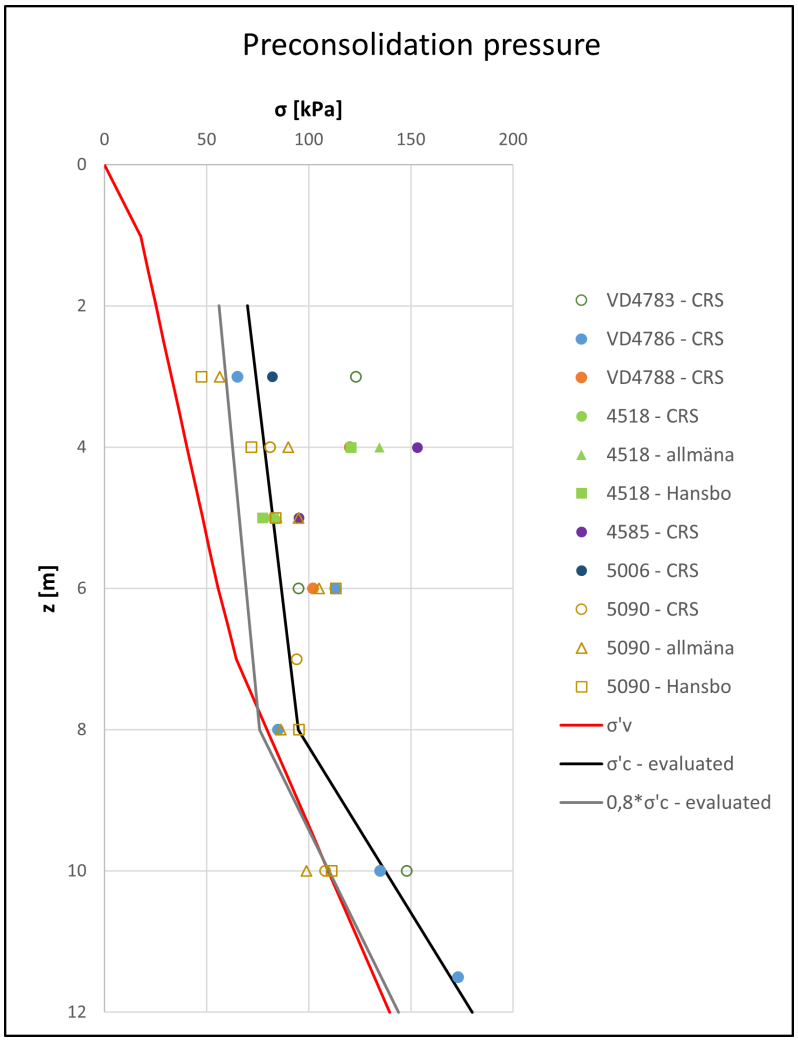

Figure 3.11: Effective stress and the evaluated preconsolidation stress plotted over depth.

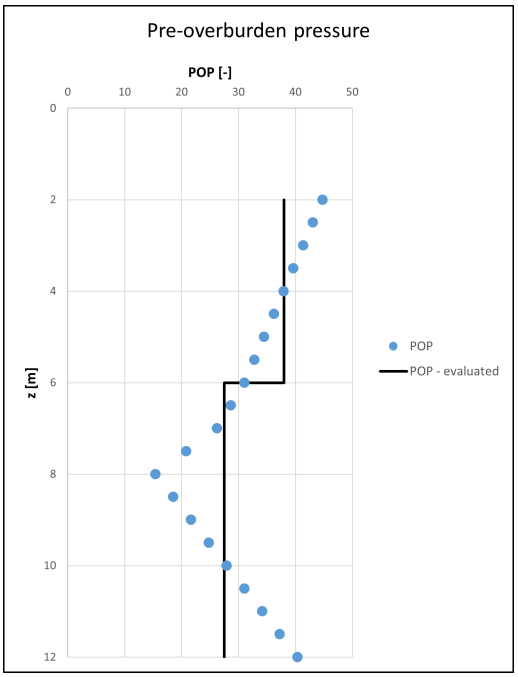

Figure 3.12: POP plotted over depth, along with the evaluated profile.

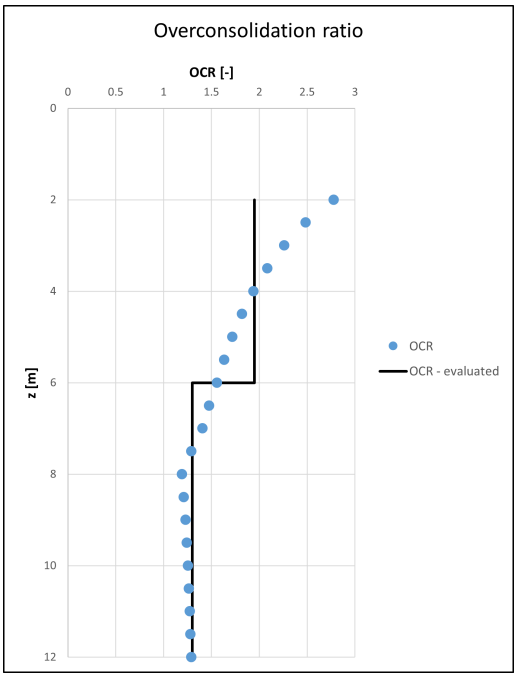

Figure 3.13: OCR plotted over depth, along with the evaluated profile.

The settlement moduli M_0 and M_L were evaluated using data from CRS tests at multiple depths for 7 boreholes. The evaluated data are shown in Figures 3.14 and 3.15. There is a large data scatter for the settlement moduli, which is probably due to the occasional presence of silt, shells, and plant parts in the clay.

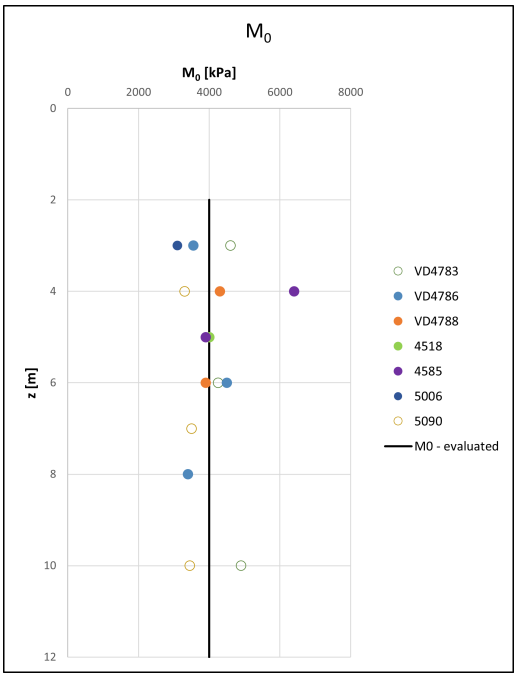

Figure 3.14: Test data and the evaluated profile for the settlement modulus M_0.

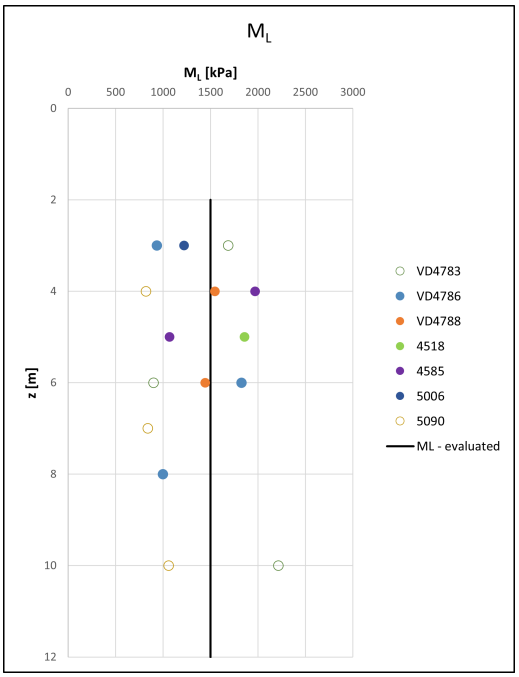

Figure 3.15: Test data and the evaluated profile for the settlement modulus M_L.

The lateral earth pressure coefficient K_0 was evaluated according to the Swedish Transport Administration (2011). Equation 3.5 is used for normal consolidated clays, while 3.6 is used for overconsolidated clays. As presented in Figure 3.13, the overconsolidation ratio is at least 1.3 in the profile and therefore is considered overconsolidated; therefore, Equation 3.6 is used. The evaluated values for K_0 for the soil profile can be seen in Figure 3.16.

$$K_0 = 0.31 + 0.71(W_L - 0.2) \tag{3.5}$$

$$K_0 = K_0 * OCR^{0.55} \tag{3.6}$$

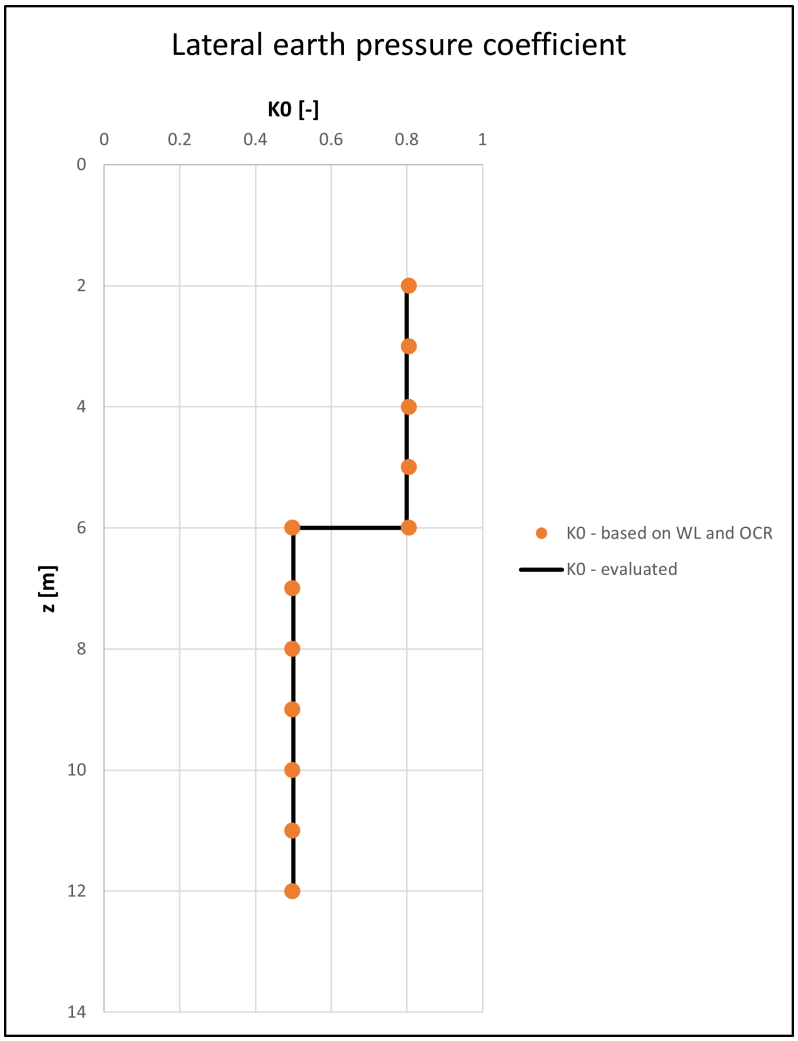

Figure 3.16: The evaluated lateral earth pressure coefficient K_0.

The friction angle was evaluated on the basis of the ram soundings and cone penetration tests conducted conducted within the case study area. Equation 3.7 was used to evaluate the CPTs and Equation 3.8 to evaluate the Hfa soundings, according to the Swedish Transport Administration (2023). The evaluated data are presented in Figure 3.17.

$$\phi' = 29 + 2.8 * q_c^{0.45} \tag{3.7}$$

$$\phi' = 29 + 2.3 * (Hfa)_{netto}^{0.46} \tag{3.8}$$

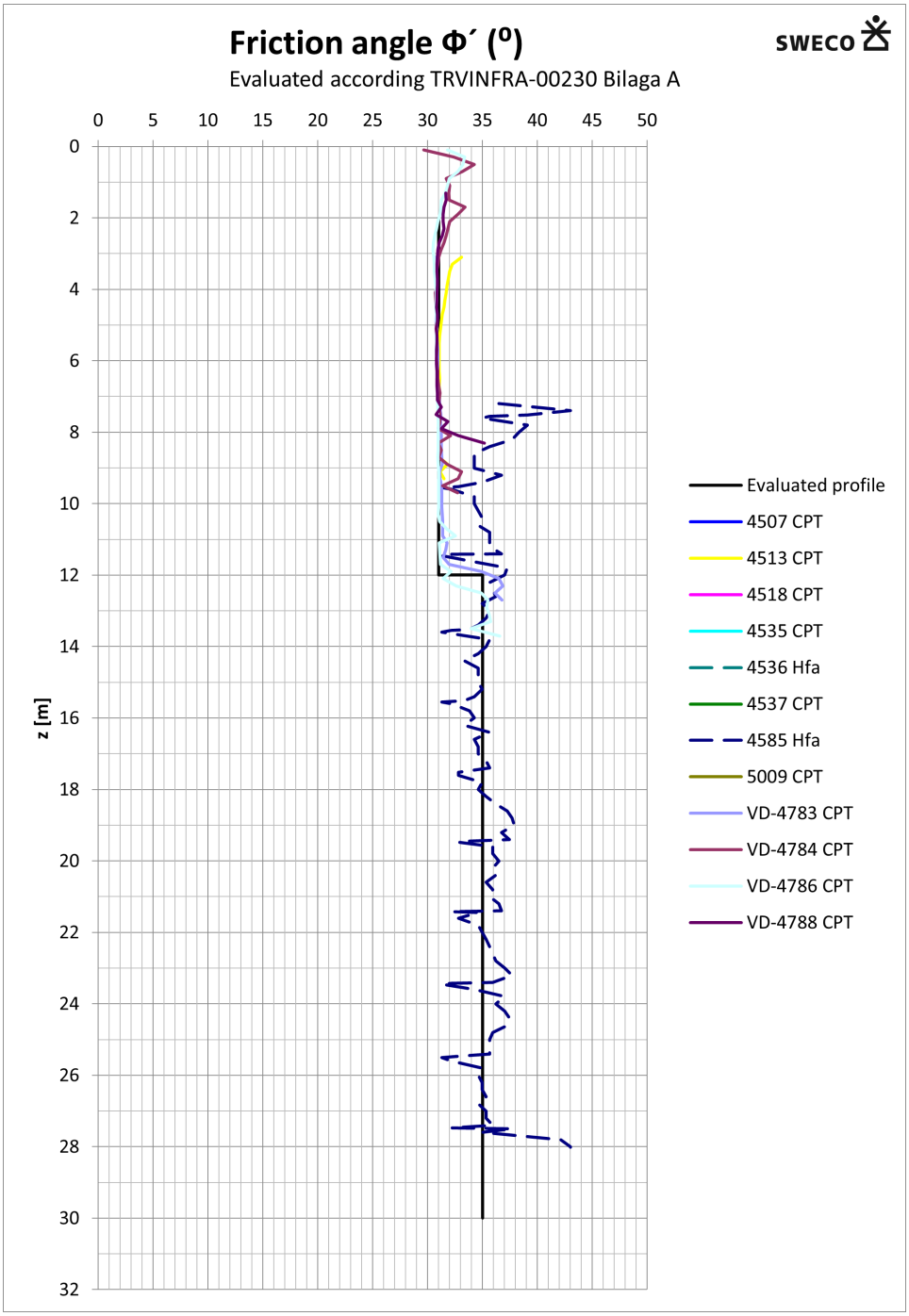

Figure 3.17: Evaluated test data and the evaluated profile for the friction angle ϕ.

3.1.2 Hydrogeological site characterisation

In the case study area there is a frictional layer that is part of a large aquifer that is in hydraulic contact with the river Göta Älv, which the groundwater flow within the aquifer is mainly directed towards (Lång, 2009). The aquifer has been evaluated to consist of sand, silty sand in the first few meters that transitions to sand and gravelly sand at depth. The thickness of the aquifer varies between 12 and 35 meters

in the case study area and follows the same general pattern as for the depth of the soil, see Figure 3.4.

The groundwater head in the aquifer has been measured in the long term on behalf of the Swedish Transport Administration, which spans over the course of the pumping test. The measurements were done both manually and with divers in several wells in proximity to the investigated cross section. Figure 3.18 shows the groundwater head in the boreholes of interest during the pumping test and approximately 6 weeks before and after.

The hydraulic conductivity of the aquifer was evaluated when the pumping test was conducted in the GW4767 well. The response in several observation wells was measured and the hydraulic conductivity was calculated. The hydraulic conductivity calculated in the pumping well and the observation wells is presented in Table 3.1 together with the average value used for the upcoming calculations.

Table 3.1: Hydraulic conductivity in the frictional soil.

Borehole	**Hydraulic conductivity [m/s]**
GW4509	$1.4 * 10^{-4}$
GW4516	$6 * 10^{-5}$
GW4517B	$3.4 * 10^{-5}$
GW4767	$2.3 * 10^{-4}$
GW4767 (recharge)	$1.2 * 10^{-4}$
Average	$1.17 * 10^{-4}$

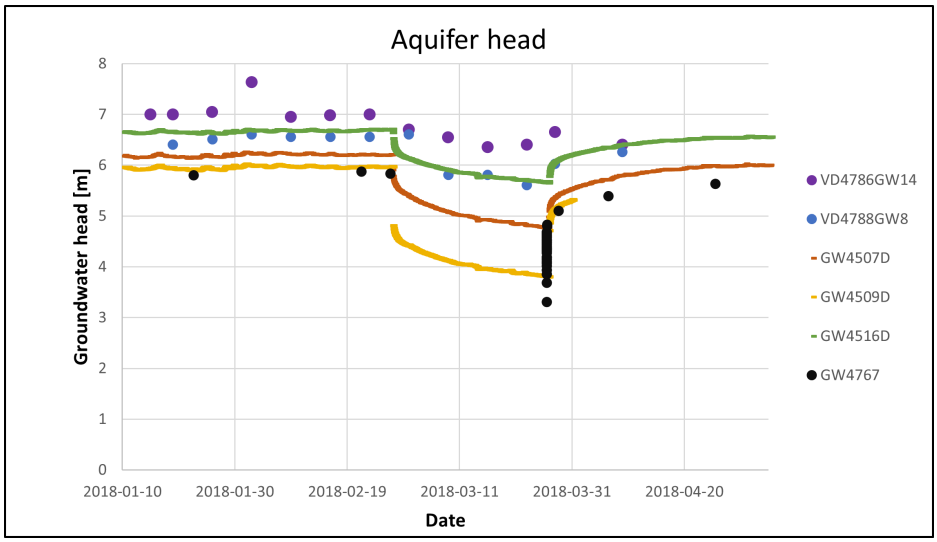

Figure 3.18: Groundwater head in the aquifer during the period January - May 2018.

3.2 1D consolidation analyses

The consolidation of a 1D soil column due to a drawdown in an underlying aquifer was analyzed with a Plaxis 2D model (from now on referred to as Plaxis) and the analytical model presented in Section 2.2. This was done to compare the two different approaches for analyzing the consolidation process by investigating deformations and the reduction of the pore pressure over time.

3.2.1 Input parameters for the 1D Plaxis model

When modeling the 1D model in Plaxis, the constitutive soil model "Mohr-Coulomb" was used as input for all soil layers. For the clay layer, the unit weights γ_{unsat} and γ_{sat} were calculated with Equation 3.9, while the void ratio e_{init} was calculated using Equation 3.10, both according to SGI (2008). Furthermore, the cohesion intercept c'_{ref} was calculated using Equation 3.11, according to SGI (2007). The stiffness parameter $E'ref$ was evaluated based on the oedometer moduli M_0. To convert this value to the E'_{ref} value used as input in Plaxis, Equation 3.12 was used. The input values needed to calculate Equations 3.9 - 3.11 along with the rest of the clay parameters were evaluated and are presented in Subsection 3.1.1.

For the dry crust and frictional soil, there is a lack of tests conducted to evaluate all the properties of the soil. Based on the available test data, γ_{unsat}, γ_{sat}, c'_{ref}, and ϕ were evaluated for the dry crust. Meanwhile, only ϕ, k_x, and k_y of the frictional soil were evaluated. For the remainder of the parameters, empirical and typical values were chosen. All input data for the soil are presented in Table 3.2.

$$\gamma = g * \rho \tag{3.9}$$

$$e_{init} = \frac{n}{1-n} \tag{3.10}$$

$$c'_{ref} = 0.1 c_u \tag{3.11}$$

$$E'_{ref} = \frac{E'_{oed}(1+\nu')(1-2\nu')}{(1-\nu')} \tag{3.12}$$

Table 3.2: Input data used for the 1D model in Plaxis.

Input data	Unit	Dry crust	Clay	Frictional soil
Soil model	-	Mohr-Coulomb	Mohr-Coulomb	Mohr-Coulomb
Drainage type	-	Undrained A	Undrained A	Drained
γ_{unsat}	kN/m^3	18	17.3	10
γ_{sat}	kN/m^3	18	17.3	18
e_{init}	–	0.5	1.3	0.5
E'_{ref}	kN/m^2	5 000	3 600	30 000
ν'	–	0.2	0.2	0.2
c'_{ref}	kN/m^2	6	2	1
ϕ	°	33	31	35
ψ	°	0	0	0
k_x	m/day	$0.864 * 10^{-3}$	$0.0864 * 10^{-3}$	10
k_y	m/day	$0.864 * 10^{-3}$	$0.0864 * 10^{-3}$	10
K_0	–	0.4554	0.8	0.4264

3.2.2 1D Plaxis model

In Plaxis a plain strain model with 15 noded elements was studied. The soil section was constructed as a one-meter-wide soil column with a depth of 30 meters. The soil stratification considered is 3 meters of dry crust, followed by a 9-meter thick clay layer on top of an 18-meter thick layer of frictional soil. The mesh quality was set to very fine with additional local refinements until the results converged. The geometry of the 1D Plaxis model is presented in Figure 3.19.

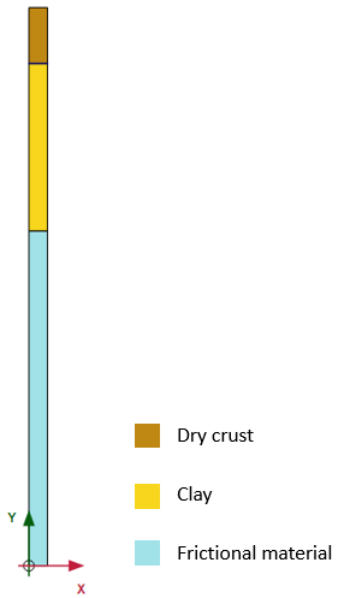

Figure 3.19: Geometry of the 1D Plaxis model.

The hydraulic boundary conditions were set as open in the y direction and as closed in the x direction to achieve a vertical flow of water. The global groundwater level was set at the bottom of the dry crust. The head of the aquifer (frictional material) was set at ground surface, and the pore pressure distribution in the clay was interpolated between the two using the "interpolate" function in Plaxis.

The methodology used to simulate a groundwater extraction was to first establish the initial conditions using the K_0 procedure and then introduce a pumping phase in which the head of the aquifer was lowered by 2 meters, followed by several consolidation phases of varying duration. The details of the phases are shown in Table 3.3. For the end of consolidation phase (EOC), the loading type "minimum excess pore pressure" was used and set at 1 kPa.

Table 3.3: Calculation phases for the 1D model in Plaxis.

Phase number	Phase	Calculation type	Time [Days]
1	Initial phase	K0 procedure	-
2	Pumping	Plastic	0
3	Consolidation 1	Consolidation	2
4	Consolidation 2	Consolidation	5
5	Consolidation 3	Consolidation	23
6	Consolidation 4	Consolidation	150
7	Consolidation 5	Consolidation	185
8	Consolidation 6	Consolidation	1460
9	Consolidation 7	Consolidation	EOC

3.2.3 1D analytical solution

The analytical solution for the consolidation of a 1D soil column suggested by Xie et al. (2012) was presented in Section 2.2. The solution suggested by the authors has been adjusted to manage initial non-hydrostatic pore pressure distributions, where the pressure level of the underlying aquifer is different from the groundwater level. The non-hydrostatic conditions are taken into account by adding the extra term u_{adj} (Equation 3.13) to Equation 2.1, resulting in Equation 3.14. Figure 3.20 presents a figure that describes the geometric input data for the 1D analytical solution. Note that the term z in the analytical solution refers to the depth from the top of the clay, as shown in Figure 3.20.

$$u_{adj} = \frac{\gamma_w h_a - \gamma_w (H + h0)}{H} z \tag{3.13}$$

$$u = \gamma_w (h_0 + z - \frac{\Delta h z}{H}) + \sum_{m=1}^{\infty} [\frac{2\gamma_w \Delta h}{m\pi} (-1)^{m-1} sin(\frac{m\pi z}{H}) e^{-m^2\pi^2 T_v}] + u_{adj} \tag{3.14}$$

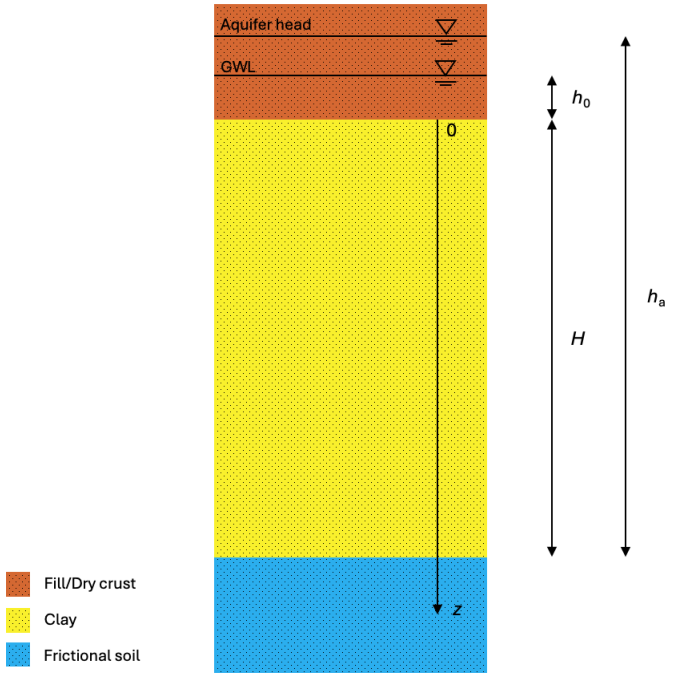

Figure 3.20: Description of the geometric input data for the 1D analytical solution.

3.3 2D consolidation analyses

In this section, the consolidation process of a two-dimensional cross section was analyzed with two different Plaxis models. A theoretical local groundwater extraction model was studied to describe how clay thickness and distance from the pumping well impact pore pressure reduction and soil subsidence over time. In addition, a model emulating the pump test within the Hamnbanan project was created to study modeling approaches for a land subsidence problem.

3.3.1 Input parameters for the 2D Plaxis models

In the 2D Plaxis models, the constitutive models "Soft Soil" (SS) and "Soft Soil Creep" (SSC) were used. In these models, the basic stiffness parameters κ^* and λ^* are used, and for the SSC model, the modified creep index μ^* is also included. These parameters were evaluated with Equation 3.15 - 3.17 in accordance with Olsson (2010).

σ'_v is defined by Olsson (2010) as "the average stress in the range before the pre-consolidation stress". This stress has been estimated with Equation 3.18. Additionally, Olsson (2010) defines σ'_{vc} as "The average between the pre-consolidation stress and the defined stress σ'". Since the defined stress, or the peak stress, varies in this category of drawdown problems, σ'_L is chosen as the defined stress. The evaluated profile for κ^* and λ^* can be seen in Figures 3.21 and 3.22.

The creep parameter α_s was retrieved from Table 1 in *Prediction of settlements of embankments on soft, fine-grained soils* by Larsson et al. (1997). The value of K_0^{nc} is calculated according to Jaky (1944) using Equation 3.19. Furthermore, according to Karstunen and Amavasai (2017) the value for Poissons ratio for unloading and reloading ν_{ur}, can be assumed to be in the range of $0.1 \leq \nu_{ur} \leq 0.2$, hence the value of 0.2 was chosen in this study. The assembly of all the input parameters needed for the constitutive models SS and SSC is presented in Table 3.4.

The bedrock was also modeled in the 2D Plaxis models. However, the effect of bedrock on drawdown and land subsidence is beyond the scope of this thesis. Hence, the input parameters were chosen so that no deformation would occur in the bedrock. In addition, the drainage type of the bedrock was set as nonporous. That is, the bedrock is set as an impermeable hydraulic boundary. The input parameters for the bedrock were retrieved from (Ma et al., 2006).

$$\kappa^* = \frac{2\sigma'_v}{M_0} \tag{3.15}$$

$$\lambda^* = \frac{1.1\sigma'_{vc}}{M_L} \tag{3.16}$$

$$\mu^* = \frac{\alpha_s}{2.3} \tag{3.17}$$

$$\sigma'_v = \frac{\sigma'_c}{2} \tag{3.18}$$

$$K_0^{nc} = 1 - \sin(\phi') \tag{3.19}$$

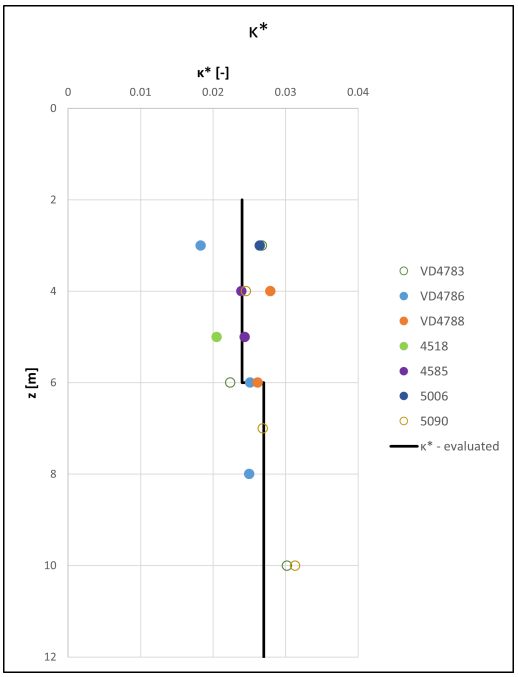

Figure 3.21: The evaluated soil test data and profile for the modified swelling index κ^*.

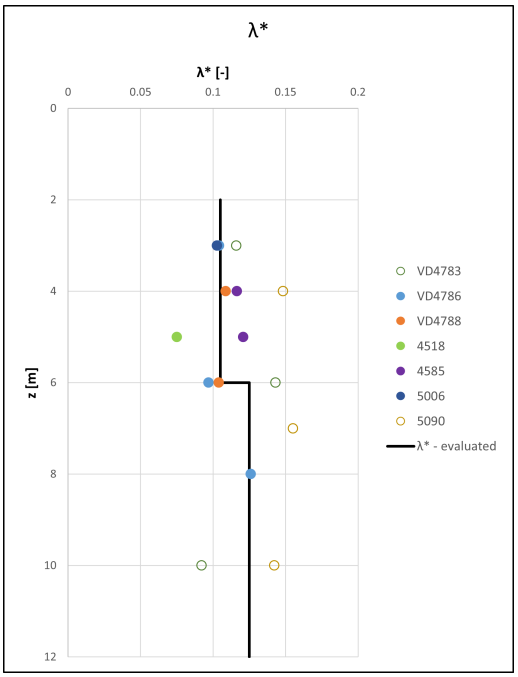

Figure 3.22: The evaluated soil test data and profile for the modified compression index λ^*.

Table 3.4: Evaluated input parameters for clay 1 and clay 2 needed for the Soft Soil and Soft Soil Creep models in Plaxis.

Parameter	Unit	Clay 1	Clay 2
γ_{unsat}	kN/m^3	17.3	18.6
γ_{sat}	kN/m^3	17.3	18.6
e_{init}	–	1.3	1.05
κ^*	–	0.024	0.027
λ^*	–	0.105	0.125
μ^*	–	0.0043	0.0022
υ_{ur}	–	0.2	0.2
c'_{ref}	kN/m^2	2	2.3
ϕ	°	31	31
ψ	°	0	0
K_0^{nc}	–	0.485	0.485
k_x	m/day	$8.64 * 10^{-5}$	$4.32 * 10^{-5}$
k_y	m/day	$8.64 * 10^{-5}$	$4.32 * 10^{-5}$
c_k	–	4.8	4.5
$K_{0,x}$	–	0.8	0.5
$K_{0,z}$	–	0.8	0.5
POP	–	38	27.5
OCR	–	1	1

3.3.2 Theoretical local groundwater extraction model

A local drawdown for a theoretical case was modeled in Plaxis, where an axisymmetric model with 15 noded elements was considered. This model was created for four different clay thicknesses, 10, 15, 20 and 30 meters, where the thicknesses of the dry crust and frictional soil remained constant at the assumed thicknesses of 2, respectively, 20 meters. In the results later on, Section 4.3, 100 meters along the x-axis will be examined, but the model was built as 200 meters long in the x-axis to eliminate any possible boundary effects that may emerge in Plaxis. The model with a 10 meter thick clay layer is presented in Figure 3.23 as an example for the soil strata and geometry of the models. The input parameters used in the model for the clay layers are presented in Table 3.4, whereas for the dry crust and frictional layer, the input parameters can be found in Table 3.2. Additionally, the model mesh was set to very fine and was locally refined until the results converged.

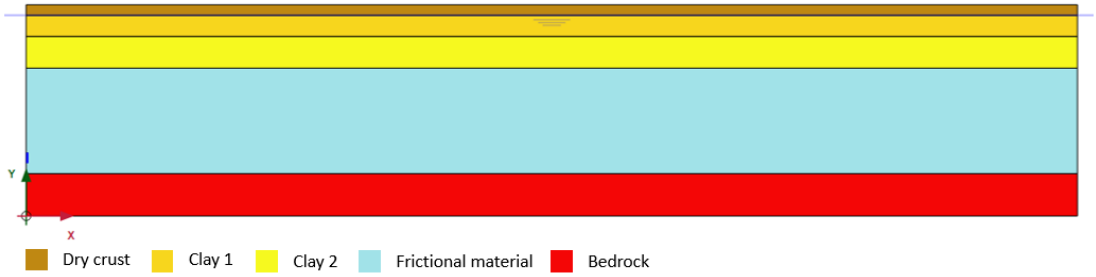

Figure 3.23: Geometry of the theoretical local groundwater extraction Plaxis model, with a clay thickness of 10 meters.

The hydraulic boundary conditions were set closed in x_{min} and open in the other directions to achieve a flow of groundwater that resembles reality. The global groundwater level and the groundwater level of the aquifer were set as the bottom of the dry crust, 2 meters below the ground surface.

The calculation of the theoretical model began with an initial phase in which the "K0 procedure" was used as the calculation type. Following this, six phases with different time intervals were modeled. A local groundwater extraction was modeled using the Plaxis well function. The well extraction rate was set as 190 m^3/day, which was the extraction rate used in the Hamnbanan test pumping (see Section 3.1). The well was placed as close to the x_{min} boundary as possible. Ideally, the well would have been placed at the boundary of the model. However, since the x_{min} hydraulic boundary in an axisymmetrical model must be closed, it overrides the pumping of the well if it is placed on this boundary. In this model, the well was at a depth of 13 meters, 0.2 meters from the x_{min} boundary.

In addition, the six phases were also calculated without any pumping to isolate the creep behavior of the model. An overview of the phases can be seen in Table 3.5.

Table 3.5: Calculation phases for the theoretical model in Plaxis.

Phase	Calculation type	Time [Days]
Initial phase	K0 procedure	
Scenario 1		
Pumping 7 days	Fully coupled flow-deformation	7
Pumping 1 month	Fully coupled flow-deformation	21
Pumping 3 months	Fully coupled flow-deformation	60
Pumping 6 months	Fully coupled flow-deformation	90
Pumping 1 year	Fully coupled flow-deformation	187
Pumping 5 years	Fully coupled flow-deformation	1460
Scenario 2		
Creep 7 days	Fully coupled flow-deformation	7
Creep 1 month	Fully coupled flow-deformation	21
Creep 3 months	Fully coupled flow-deformation	60
Creep 6 months	Fully coupled flow-deformation	90
Creep 1 year	Fully coupled flow-deformation	187
Creep 5 years	Fully coupled flow-deformation	1460

3.3.3 Hamnbanan pump test model

The pump test conducted within the Hamnbanan project was modeled in Plaxis, where a 15-noded element, axisymmetric model was considered. The geometry of the model was created on the basis of the boreholes along the cross section presented in section 3.1. The model is presented in Figure 3.24, where the soil strata and geometry are shown. The mesh quality was set as very fine and refined locally until the results converged. In this model, the constitutive model soft soil was used for the clay layers. The creep effects had to be ignored to obtain an operational model. However, due to the modeling time of 28 days, no substantial creep displacements that would affect the results are expected to occur. The input data for the dry crust and frictional soil was the same as in the 1D model and can be seen in Table 3.2, while for the clay, the input data are presented in Table 3.4.

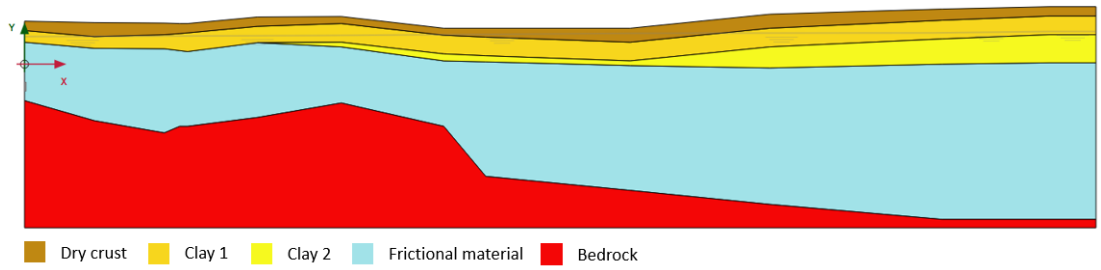

Figure 3.24: Geometry of the Hamnbanan pump test Plaxis model.

The hydraulic boundary conditions were set as closed in both x_{max} and x_{min} and open in the y-boundaries. The decision to close the x_{max} boundary was forced by software limitations, as Plaxis was unable to run the model while the x_{max} boundary was open. These issues will be discussed further in Section 5.5. The global

groundwater level was set at 1 meter below the ground surface, according to the evaluation in Subsection 3.1.1. The groundwater level of the aquifer was based on the data presented in Figure 3.18. The measurements taken just before the start of the pumping tests were chosen as input data to better resemble the conditions during the pump test. These values and the corresponding coordinates in the model are presented in Table 3.6 below.

Table 3.6: Input data for groundwater head in the aquifer.

Head [m]	**X coordinate [m]**
5.9	0
6	25
6.2	75
6.6	130
6.7	195
7	220+

The calculation of the Hamnbanan pump test model started with an initial phase in which "gravity loading" was used as the calculation type. Following this, a 28-day pumping phase was introduced. The local extraction of groundwater was modeled in two different ways.

The first procedure was to include a well in the model, as in the theoretical model. In this model, the placement of the well placement was based on the real location, which is located at a depth of 13 meters with a filter length of 2 meters described in (Swedish Transport Administration, 2018b). This corresponds to coordinates (0.2,-3.8) to (0.2,-5.8) in the Plaxis model. Furthermore, the well extraction rate was set to 190 m^3/day in the model.

The other method was by introducing a drain to the model, this drain was placed along the aquifer at the x_{min} boundary. The drain head was set to correspond to the drawdown measured during the pump test (Swedish Transport Administration, 2018b), which was 6.9 meters or coordinates (0,-1) in the model. The details surrounding the calculation phases for these methods are presented in Table 3.7.

The calculation process for both the well and the drain procedure was repeated for different model lengths, as this will have a great impact on the total volume of water in the aquifer, since the x_{max} boundary is closed. The three lengths simulated for each of the two extraction methods were 230, 500 and 1000 meters.

Table 3.7: Calculation phases for the well and drain procedure in Plaxis

Phase number	**Phase**	**Calculation type**	**Time [Days]**
1	Initial phase	K0 procedure	
Well			
2	Pumping 1 month	Fully coupled flow-deformation	28
Drain			
2	Pumping 1 month	Fully coupled flow-deformation	28

4
Results

In this chapter, the results of the 1D consolidation analyses, the theoretical local groundwater extraction model, and the Hamnbanan pump test model are presented.

4.1 Results of the 1D consolidation analyses

The results of the 1D consolidation analysis of a soil column subject to a uniform drawdown in the underlying aquifer for both the analytical solution and Plaxis are presented in this section. The models are compared in terms of vertical displacement, pore pressure distribution, and change in pore pressure in the clay.

In Figure 4.1, the distribution of the pore pressure in the clay is presented over time. As can be seen, the distributions of the pore pressures over time are very similar for both the analytical solution and the Plaxis model. At the final time step, after 5 years of pumping, it can be seen that both models predict that the end of consolidation is reached, or, at a minimum, are nearing completion. This observation is attributed to the fact that the profiles exhibit near-linear characteristics and have attained a steady-state condition.

The change in pore pressure in different time steps compared to the initial pore pressure distribution is presented in Figure 4.2. The figure shows a maximum difference between the models of approximately 1 kPa.

The vertical displacements at the top of the clay for the different models are presented in Figure 4.3. Since the analytical solution does not calculate the vertical displacement of the frictional soil, the Plaxis results are shown with and without the vertical displacement of the frictional soil. As can be seen, the different models predict similar vertical displacements, with a maximum difference of 0.15 cm after 5 years. The vertical displacements of the frictional soil occur immediately and are equal to approximately 1 cm.

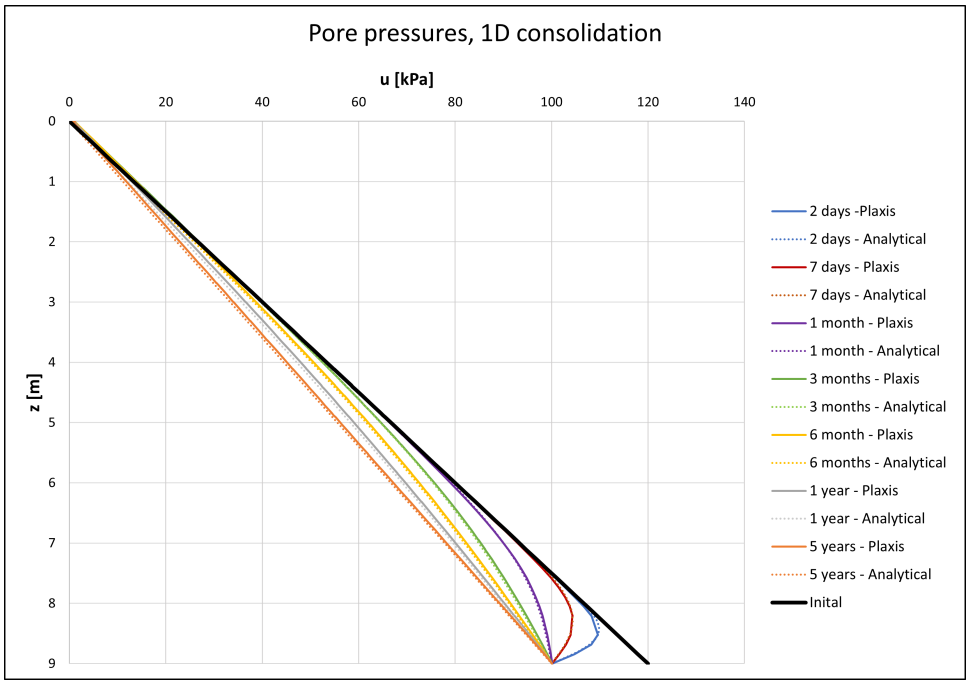

Figure 4.1: Distribution of pore pressure due to a uniform drawdown of 2 meters for the 1D Plaxis model and analytical solution. Plotted over clay depth for different pumping durations.

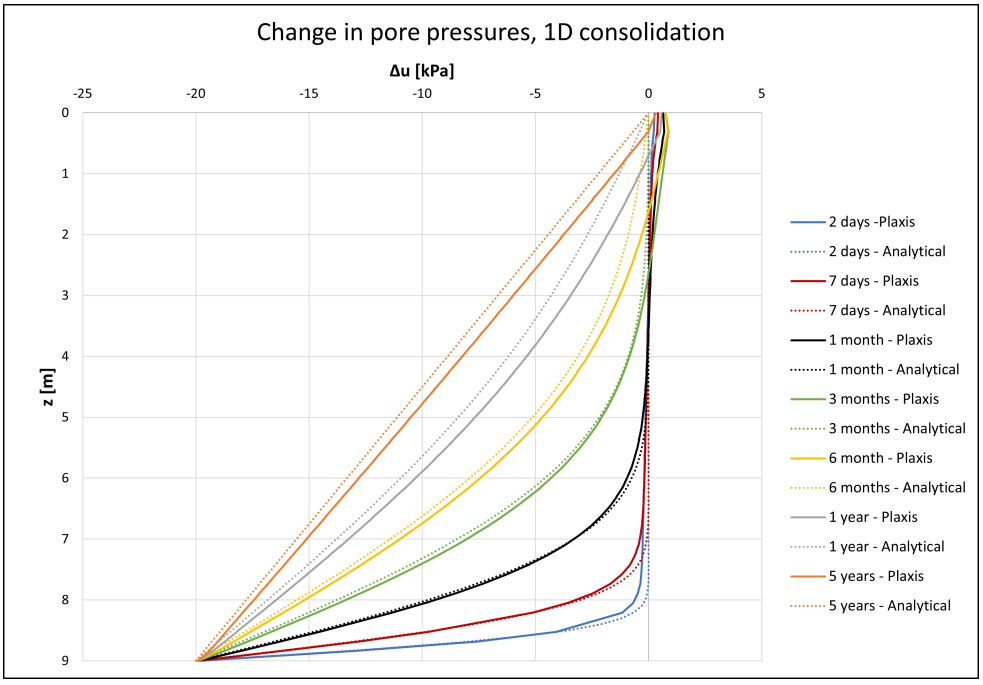

Figure 4.2: Change in pore pressure due to a uniform drawdown of 2 meters for the 1D Plaxis model and analytical solution. Plotted over clay depth for different pumping durations.

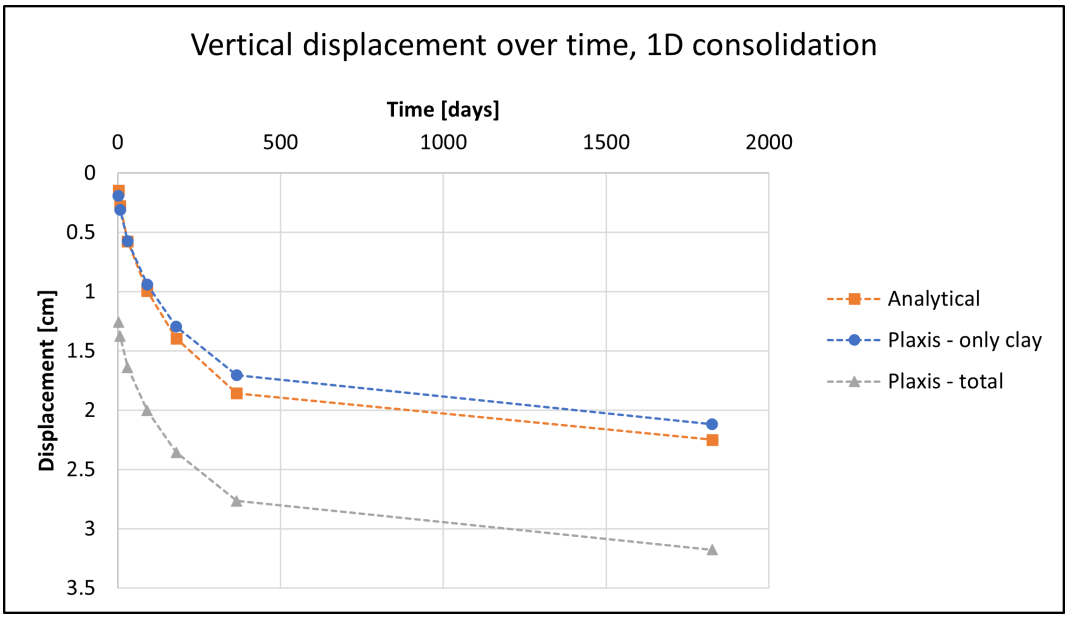

Figure 4.3: Vertical displacement for a uniform drawdown of 2 m. Plotted at several time steps for the Plaxis- and analytical solution. The analytical solution only takes the displacements of the clay into consideration. The vertical displacements for the Plaxis model is shown with and without the vertical displacement of the frictional soil.

4.2 Validation of the 1D analytical solution

The pore pressure distribution predicted by the analytical solution was compared with the measured data in boreholes VD4786 and VD4788, at two, respectively, three depths, at the start and at the end of the pumping test. The measured data are presented in Figures C.5 and C.6 in Appendix C. The distribution of pore pressures at the beginning and end of the pumping test for VD4786 is shown in Figure 4.4, and for VD4788 in Figure 4.5. As seen in the figures, the initial pore pressure distribution of the 1D analytical solution is not in complete agreement with the measured data, especially for VD4786. This is because the analytical solution is restricted to linear initial pore pressure distributions. A stepwise linear pore pressure distribution would be needed for a better fit with the measured data. However, the analytical solution seems to predict similar drawdowns as the measured data shows. This is because the differences between the pore pressures before and after the pumping test are similar for both the measured data and the analytical solution. The depth z of the analytical solution was adjusted from the depth from the top of the clay to the depth from the surface of the ground to comply with the measured data; see Section 2.2.

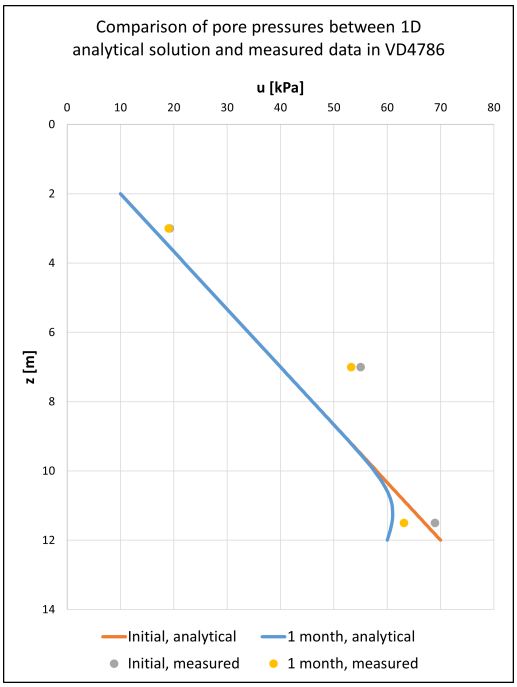

Figure 4.4: Comparison of pore pressures of the 1D analytical solution and measured data in borehole VD4786.

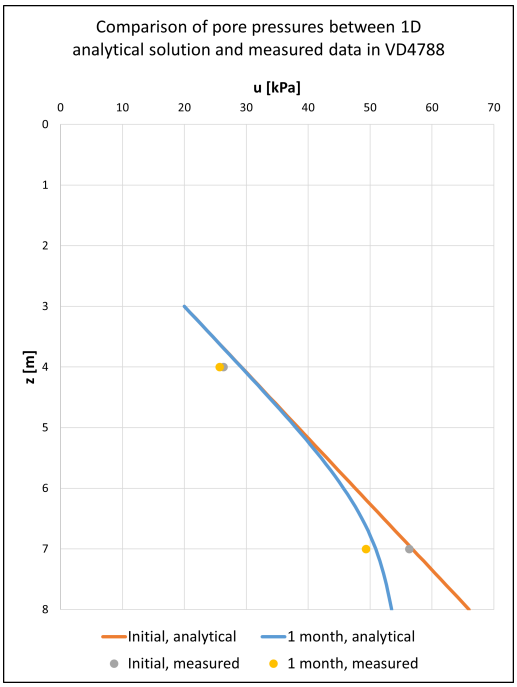

Figure 4.5: Comparison of pore pressures of the 1D analytical solution and measured data in borehole VD4788.

4.3 Results of the theoretical local groundwater extraction model

The results of the theoretical model subject to a local drawdown are presented in this section. The results are compared in terms of vertical displacements for varying thicknesses of the clay, including and excluding the effects of background creep. The thickness of the clay has been varied between 10-30 meters. Four points have been chosen for further analysis at the distances of 0, 10, 50 and 100 meters from the pumping well.

Vertical displacements have been corrected for heave in the upper part of the soil profile. The heave is caused by pore pressures exceeding the initial level, which is considered a numerical error in Plaxis. The creep in Plaxis has been identified as the factor causing the increase in pore pressure and subsequent heave. The phenomenon occurs with the constitutive model SSC, regardless of whether the pump is activated or not. However, when the constitutive model SS is used, the pore pressures remain at or below the initial level. The heave reduces with distance from the pumping well, and this has been corrected for by a stepwise linear function based on the examined heave at 4 distances.

The vertical displacements in the clay for the pumping rate 190 m^3/day, including creep, are shown in Figures 4.6 - 4.9, and the vertical displacements excluding creep are shown in Figures 4.10 - 4.13. As can be seen in the figures, the vertical displace-

ments after 1 year of pumping, with creep effects included, range from approximately 2.5 cm at the pumping well to 0.4-1.5 cm at a distance of 100 meters from the well. Vertical displacements after 1 year of pumping excluding background creep range from 1.5-2.3 cm at the pumping well to approximately 0.5 cm at a distance of 100 meters from the well. Several observations can be made regarding the dispersion of vertical displacements across varying clay thicknesses. This dispersion exhibits an increase over time, regardless of the influence of background creep and proximity to the pumping well. The impact of distance on this dispersion is reversed, depending on whether creep effects are considered. Specifically, the inclusion of creep effects leads to an increase in dispersion with increasing distance, whereas its exclusion results in a decrease in dispersion.

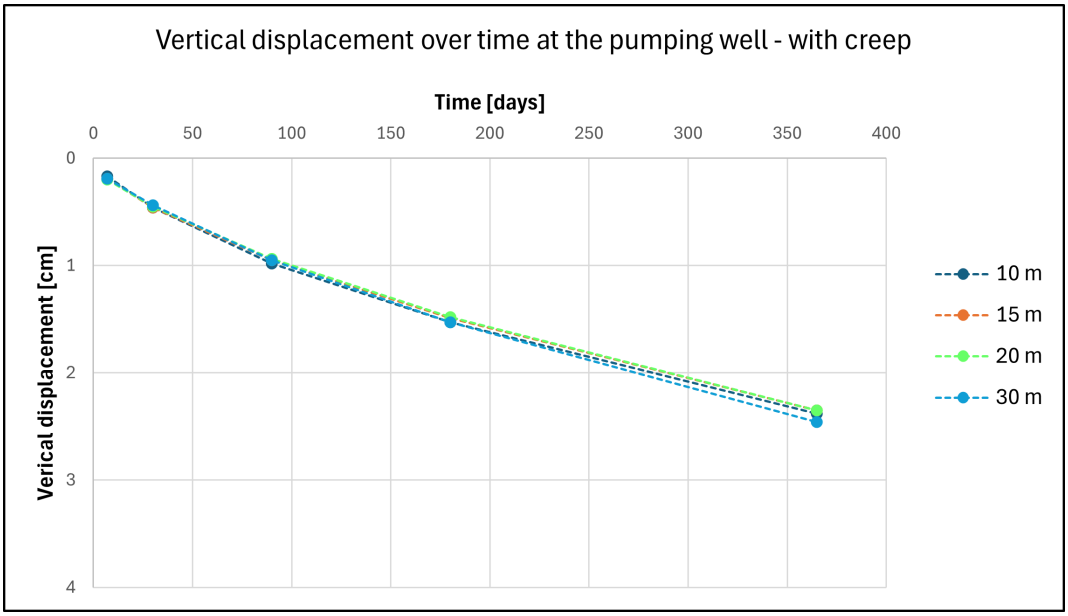

Figure 4.6: Vertical displacement of the clay, including creep, at the pumping well. Plotted over time for clay thicknesses 10, 15, 20 and 30 meters.

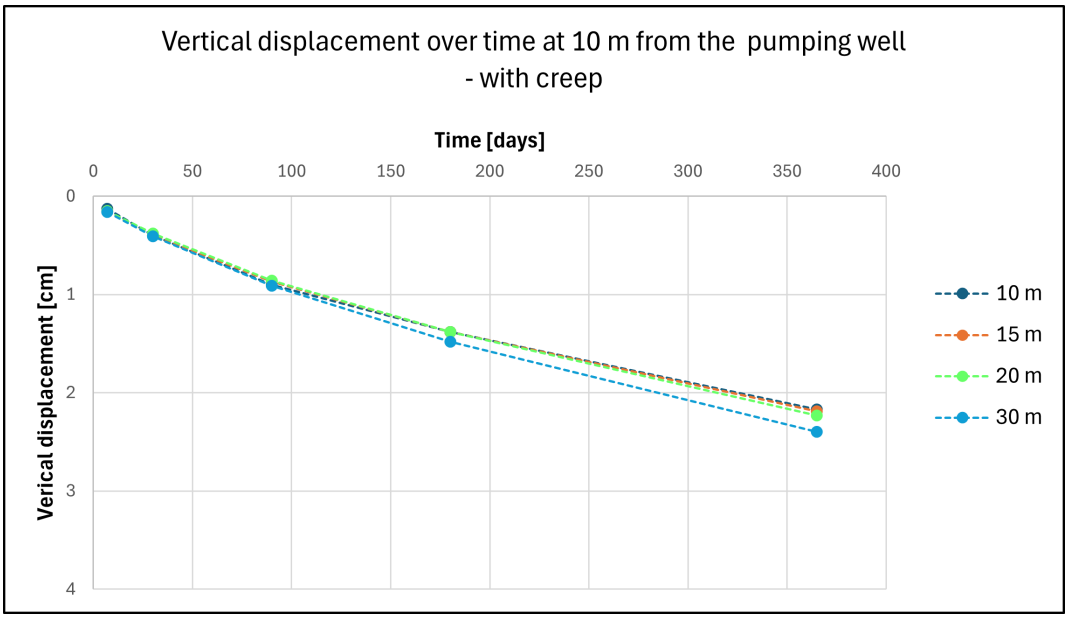

Figure 4.7: Vertical displacement of the clay, including creep, at the distance of 10 meters from the pumping well. Plotted over time for clay thicknesses 10, 15, 20 and 30 meters.

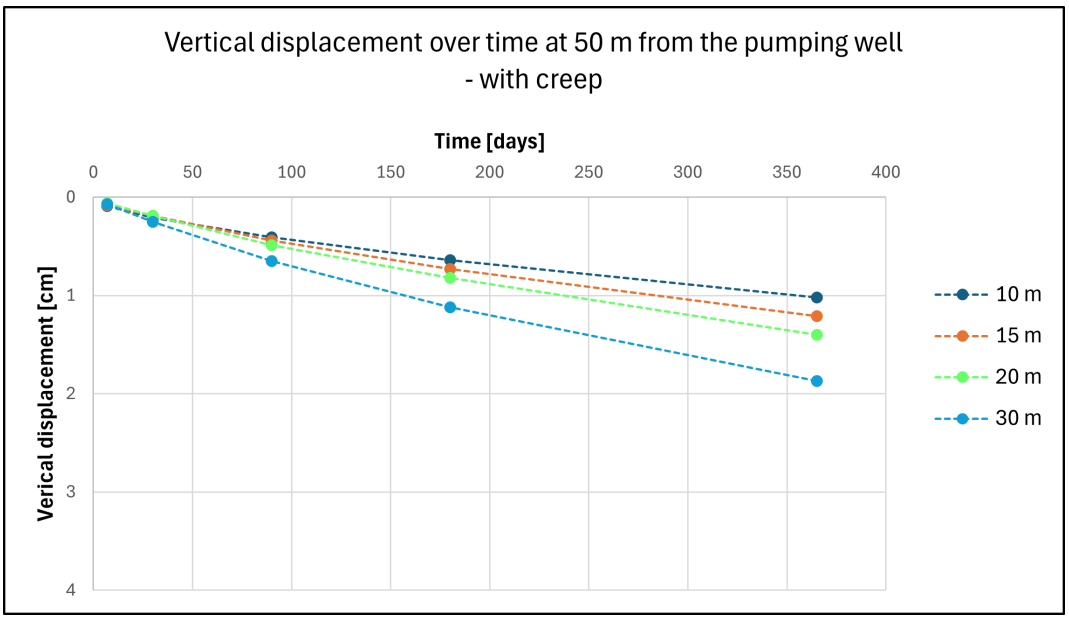

Figure 4.8: Vertical displacement of the clay, including creep, at the distance of 50 meters from the pumping well. Plotted over time for clay thicknesses 10, 15, 20 and 30 meters.

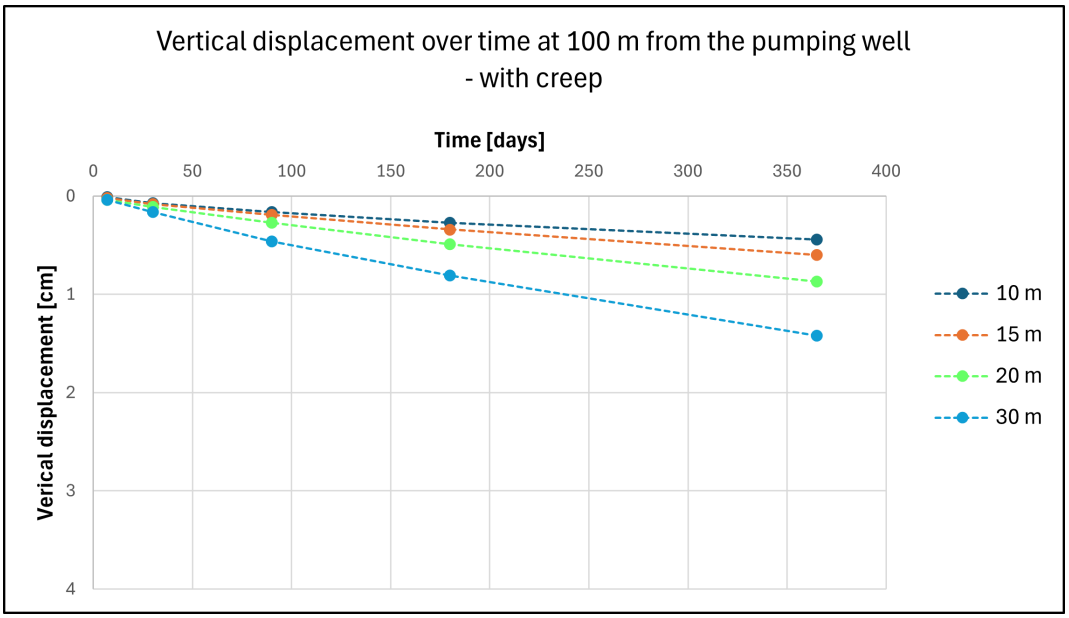

Figure 4.9: Vertical displacement of the clay, including creep, at the distance of 100 meters from the pumping well. Plotted over time for clay thicknesses 10, 15, 20 and 30 meters.

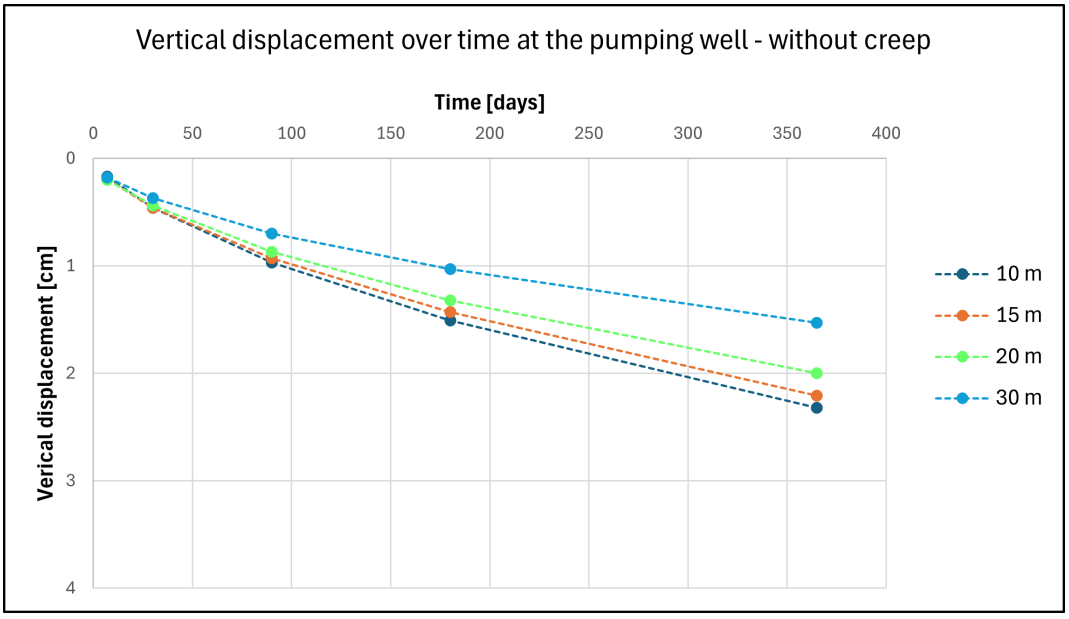

Figure 4.10: Vertical displacement of the clay, excluding creep, at the pumping well. Plotted over time for clay thicknesses 10, 15, 20 and 30 meters.

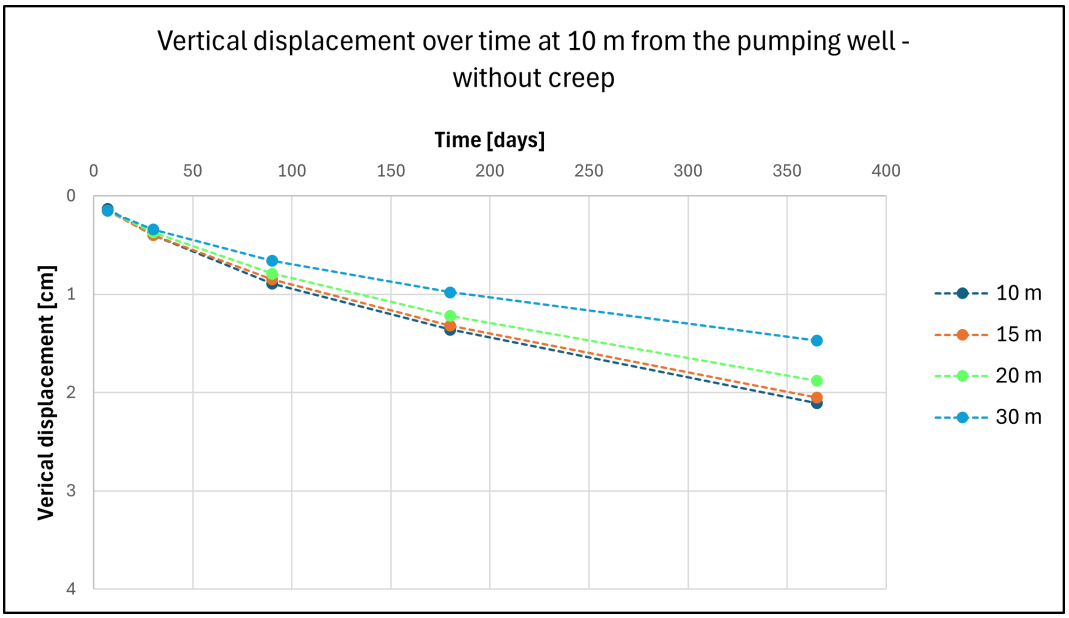

Figure 4.11: Vertical displacement of the clay, excluding creep, at the distance of 10 meters from the pumping well. Plotted over time for clay thicknesses 10, 15, 20 and 30 meters.

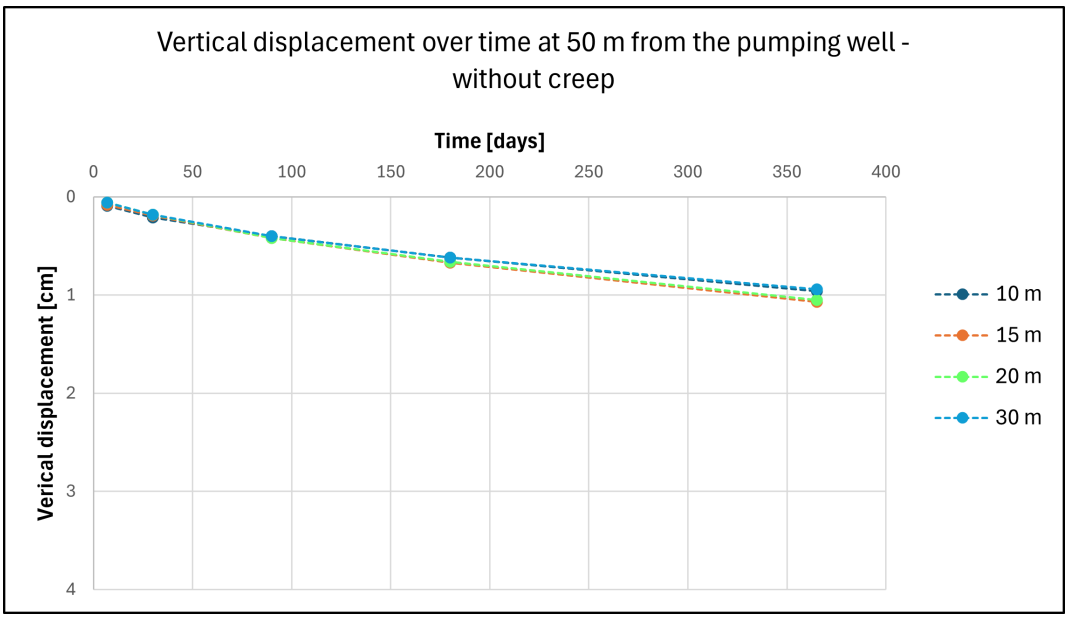

Figure 4.12: Vertical displacement of the clay, excluding creep, at the distance of 50 meters from the pumping well. Plotted over time for clay thicknesses 10, 15, 20 and 30 meters.

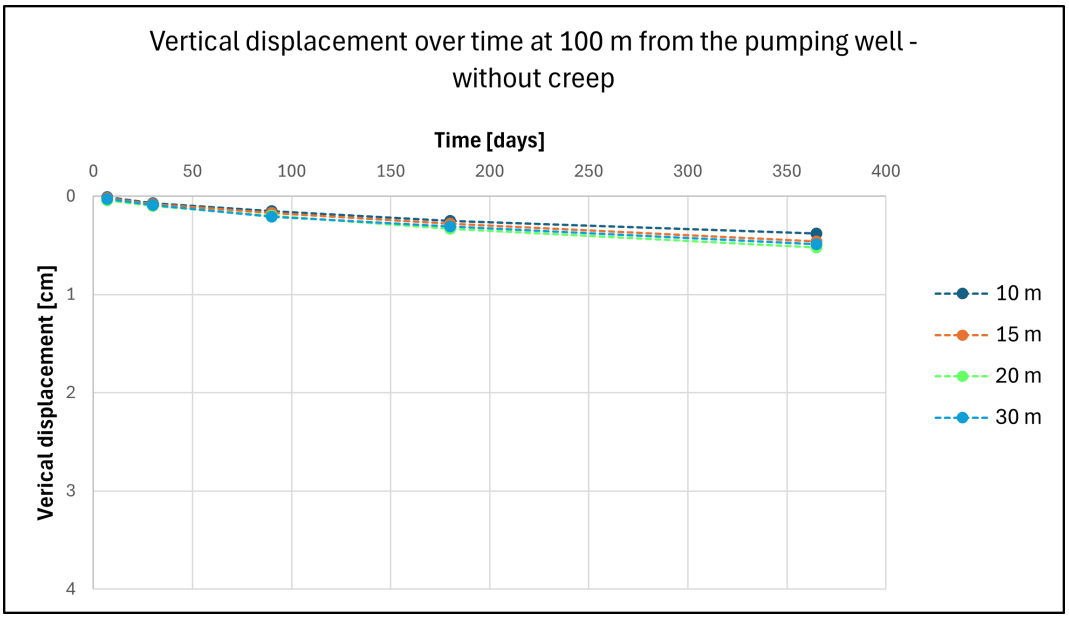

Figure 4.13: Vertical displacement of the clay, excluding creep, at the distance of 100 meters from the pumping well. Plotted over time for clay thicknesses 10, 15, 20 and 30 meters.

The amount of affected clay for various clay thicknesses and distances from the pumping well plotted over time are presented in Figures 4.14 - 4.17. The affected clay is considered to be the extent, seen from the bottom of the clay, to which the reduction in pore pressure is substantial compared to the initial pore pressure distribution. In this master thesis, a substantial reduction in pore pressure is considered to be greater than 1 kPa. When the values for the affected clay were derived, the pore pressure graphs for the different cases were examined, and these can be found in Appendix D. The pore pressure graphs in question had to be corrected for an unexpected numerical error in Plaxis. This error caused a pore pressure increase in the clay during the background creep phases. This error then in turn affected the pumping phases as the creep was included in these simulations as well. To correct for this, the value of how much the pore pressure exceeded the initial phase value in the creep phases was subtracted from the pore pressures when groundwater pumping was simulated.

In Figure D.17 in Appendix D an example of this is presented. The figure illustrates the distribution of the pore pressure during the initial phase, the isolated creep phase, and the uncorrected and corrected pore pressures after one year of pumping. This example demonstrates a 20-meter thick clay layer located 10 meters from the extraction well. The same methodology was applied to all other clay thicknesses and distances from the well.

The results show that the affected clay increases with increasing clay thickness. After 1 year of pumping, the amount of affected clay ranges between 6-10 meters at the well and between 4.5-5.5 meters at a distance of 100 meters from the well. This shows that the dispersion of affected clay, between different clay thicknesses, reduces

with distance from the well, but this is also valid for all investigated time steps. The results also show that the dispersion increases over time at all distances from the well.

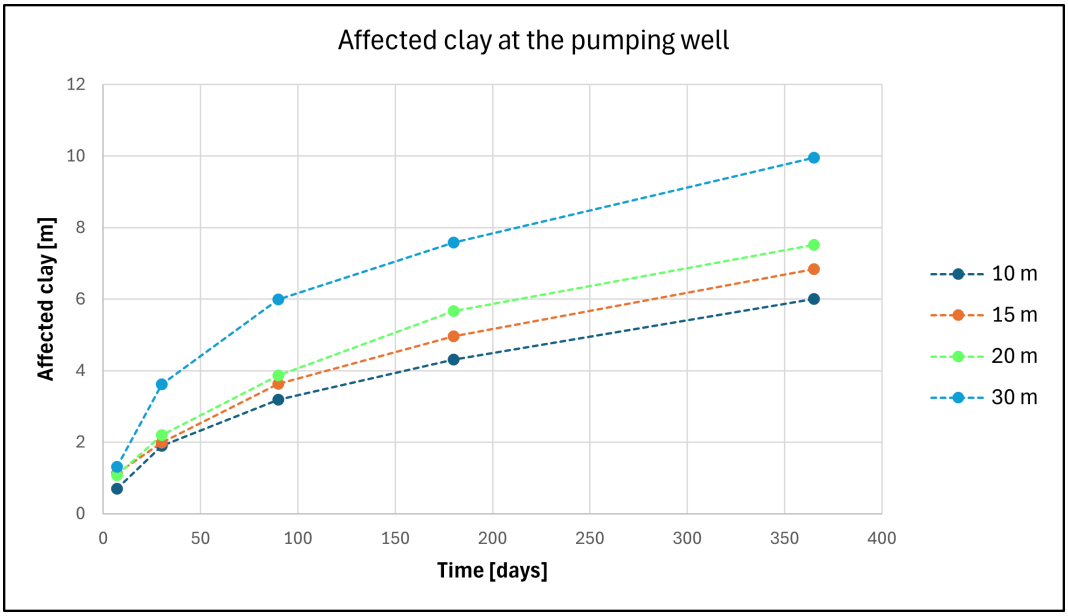

Figure 4.14: The affected clay at the pumping well. Plotted over time for clay thicknesses 10, 15, 20 and 30 meters.

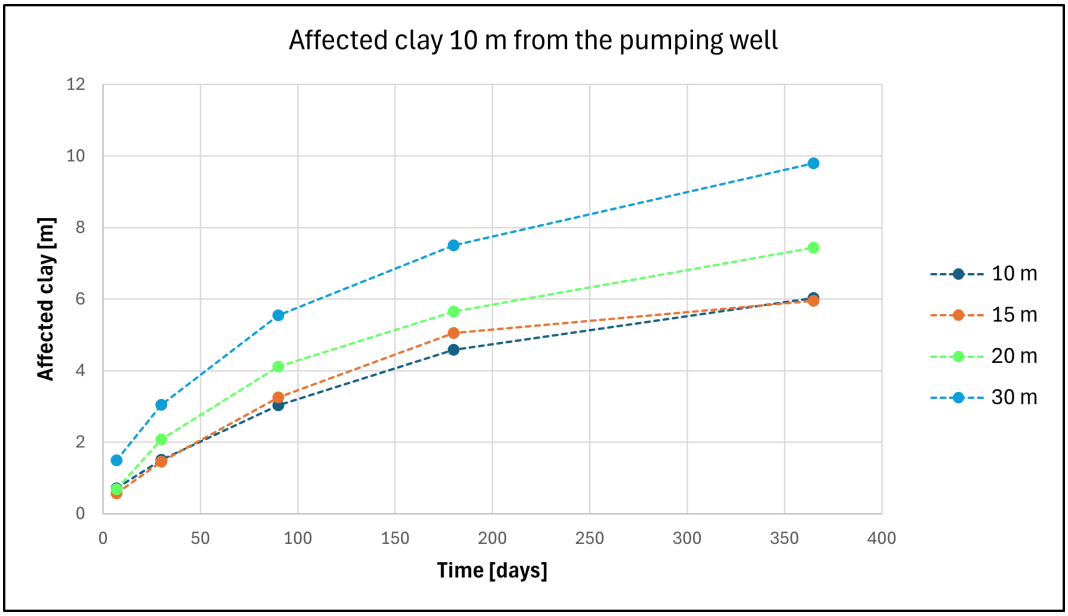

Figure 4.15: The affected clay 10 meters from the pumping well. Plotted over time for clay thicknesses 10, 15, 20 and 30 meters.

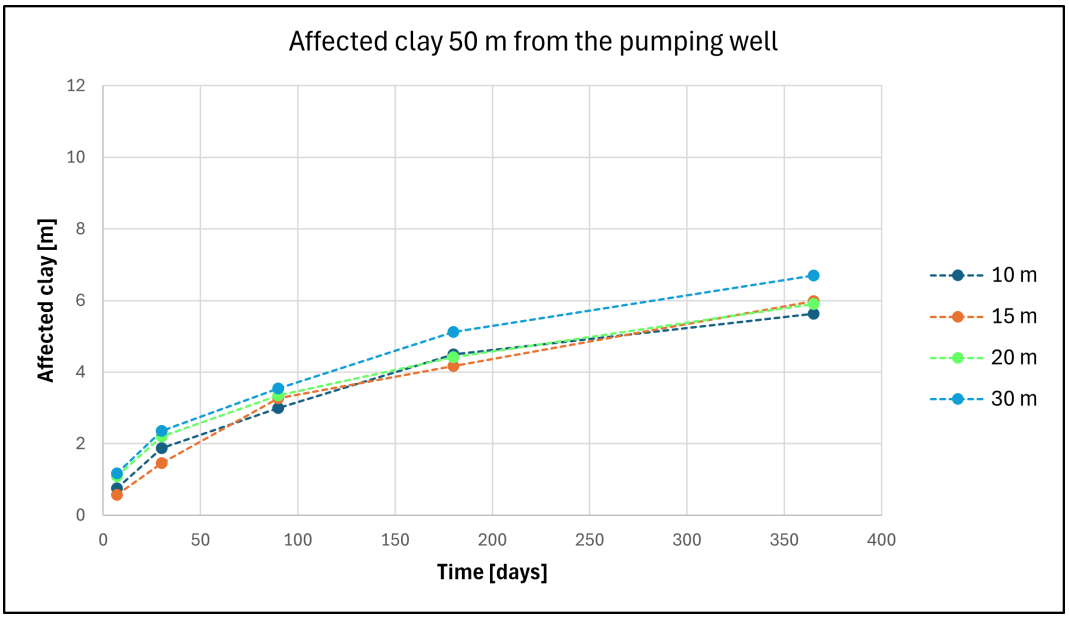

Figure 4.16: The affected clay 50 meters from the pumping well. Plotted over time for clay thicknesses 10, 15, 20 and 30 meters.

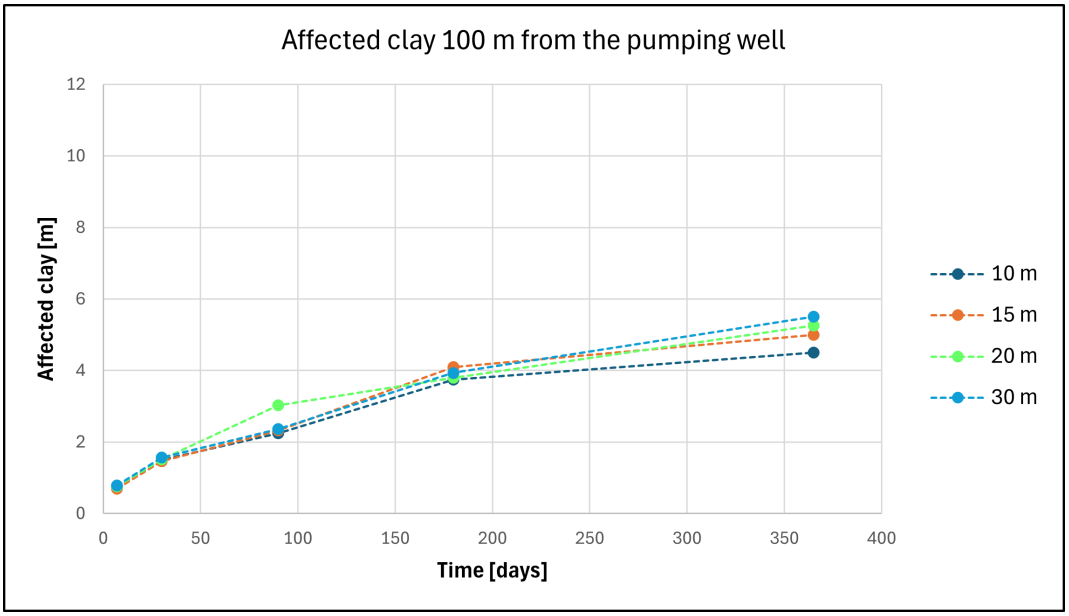

Figure 4.17: The affected clay 100 meters from the pumping well. Plotted over time for clay thicknesses 10, 15, 20 and 30 meters.

In Figure 4.18, the vertical displacements caused by the background creep are presented. These are plotted over time and includes the clay thicknesses 10, 15, 20 and 30 meters. The results show that a clay layer with a thickness of 10 meters will undergo vertical displacements due to background creep of approximately 0.07 centimeters after a year. Meanwhile, a clay layer with a thickness of 30 meters will undergo vertical displacements of around 0.92 centimeters after a year.

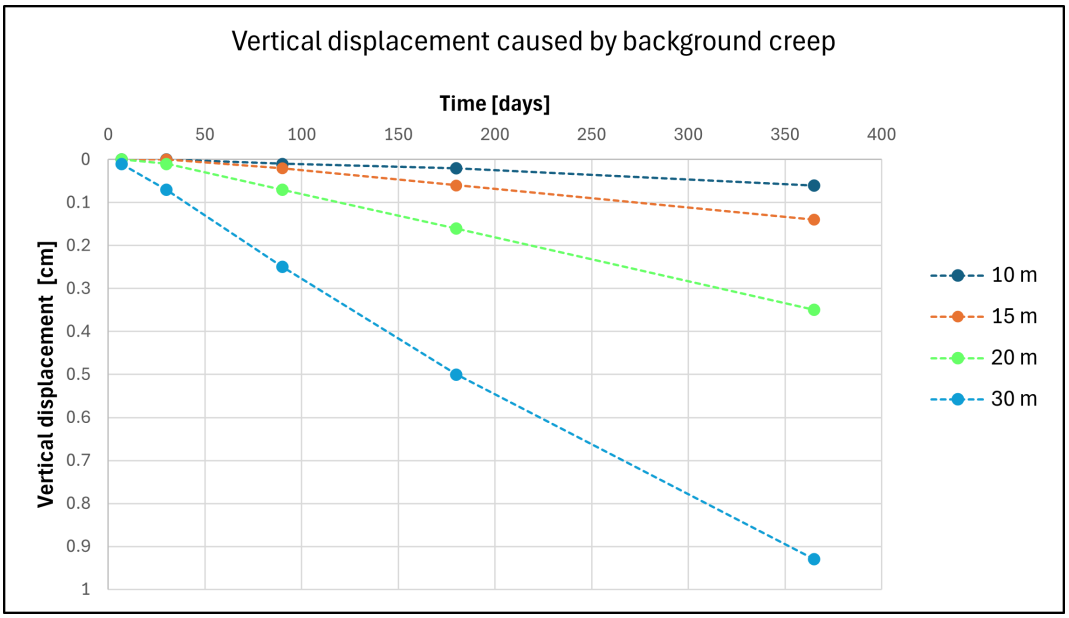

Figure 4.18: Vertical displacement of the clay caused by background creep for different clay thicknesses over time.

In Figure 4.19, the groundwater drawdown in the aquifer is presented, plotted against the distance from the pumping well. This drawdown is independent of the thickness of the clay. The results show that the largest drawdown occurs at the pumping well, which is about 2.8 meters. The magnitude of the drawdown decreases progressively with increasing distance from the pumping well, reaching approximately 0.7 meters at a distance of 100 meters from the well.

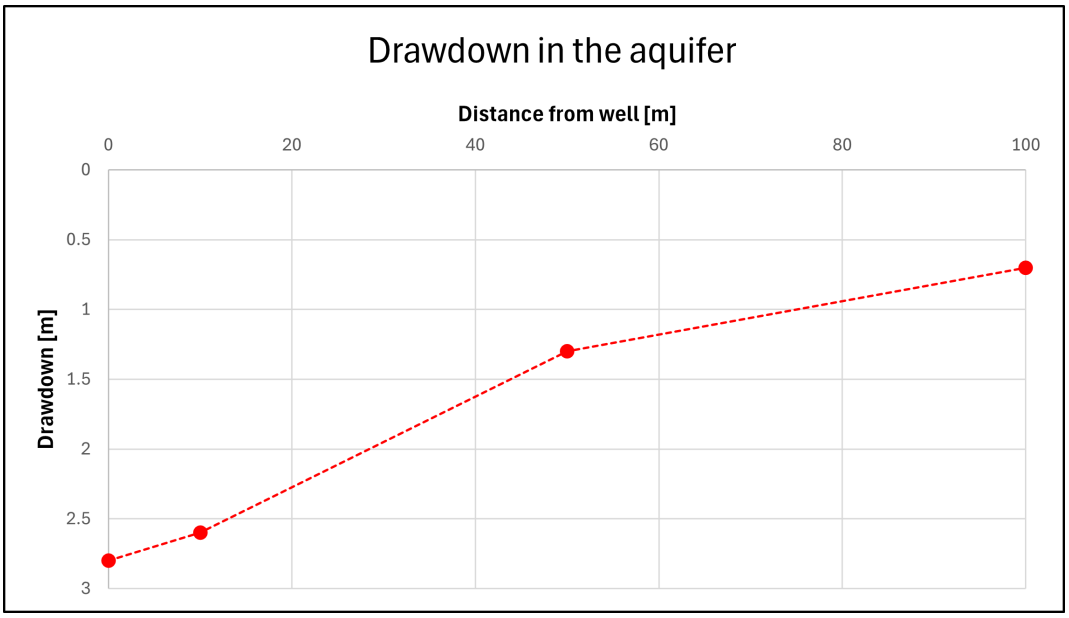

Figure 4.19: Aquifer drawdown due to pumping with a flow of 190 m^3/day, plotted over distance from the pumping well.

4.4 Results of the Hamnbanan pump test model

The modeling results of the pump test conducted within the Hamnbanan project are presented in this section. The results are shown after 1 month of pumping for the drawdown in the aquifer for the three different lengths of the model, the vertical displacement in the studied cross section, and also the predicted pore pressures of the model compared to the measured data.

The predicted drawdown throughout the cross section is shown in Figure 4.20 for both the groundwater extraction sources well and drain, for the three different model lengths of 230, 500, and 1000 meters. The modeling results are compared with the real-life measured drawdown. The results show that when modeling these kinds of complex problem in a two-dimensional model, both the way the extraction is modeled and the length of the model affect the results to a great extent. In this case, 500-meter models with the well and drain as the extraction source show the most similarity to the measured drawdown.

Furthermore, in Figures 4.21 and 4.22 the predicted pore pressure distribution at the beginning and at the end of the pump test for both 500-meter-long models are compared with the real-life measurements in boreholes VD4786 and VD4788 are presented. The results show that the different modeling techniques give approximately similar pore pressure distribution curves. However, when comparing the results to the measured data, there are rather large differences.

In Figure 4.23 the total vertical displacements for the 500 meter long well model in Plaxis are presented. The results show a vertical displacement of approximately 1-2 centimeters on the surface throughout the model, with the exception of the region located between 70 and 110 meters from the pumping well. In this region, the total vertical displacements exhibit a significant increase, up to 10 centimeters at certain locations.

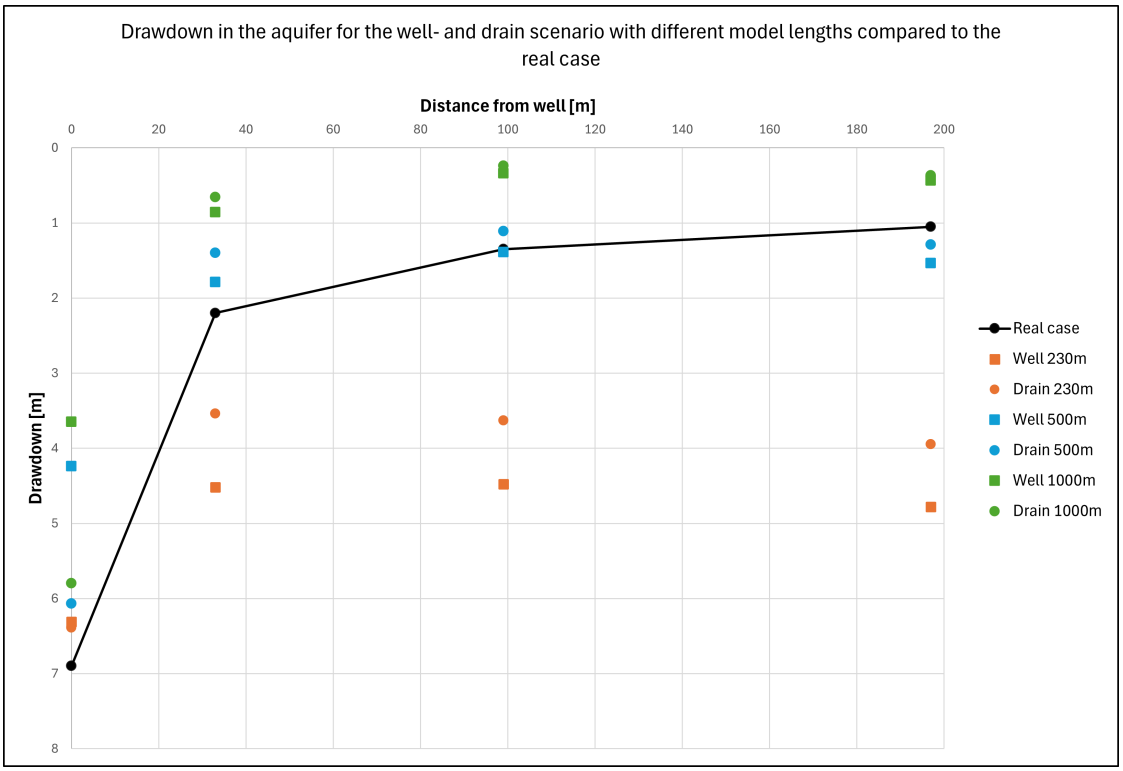

Figure 4.20: Drawdown in the aquifer for the well- and drain scenario for the model lengths 230, 500 and 1000 meters, compared to the real-life measured drawdown. Plotted against length from the extraction source.

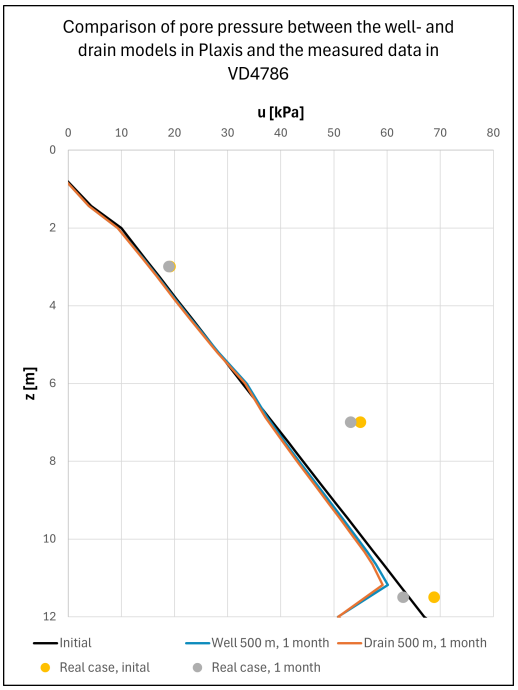

Figure 4.21: Measured pore pressures in VD4786 compared to the predicted pore pressures between the 500 meter well- and drain model in Plaxis.

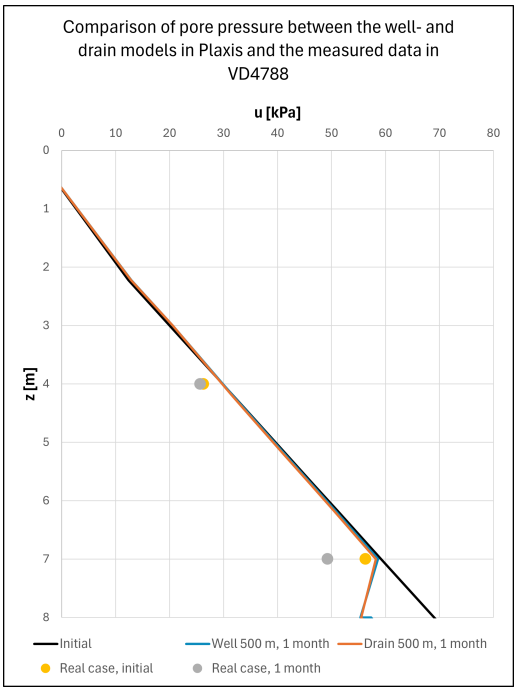

Figure 4.22: Measured pore pressures in VD4788 compared to the predicted pore pressures between the 500 meter well- and drain model in Plaxis.

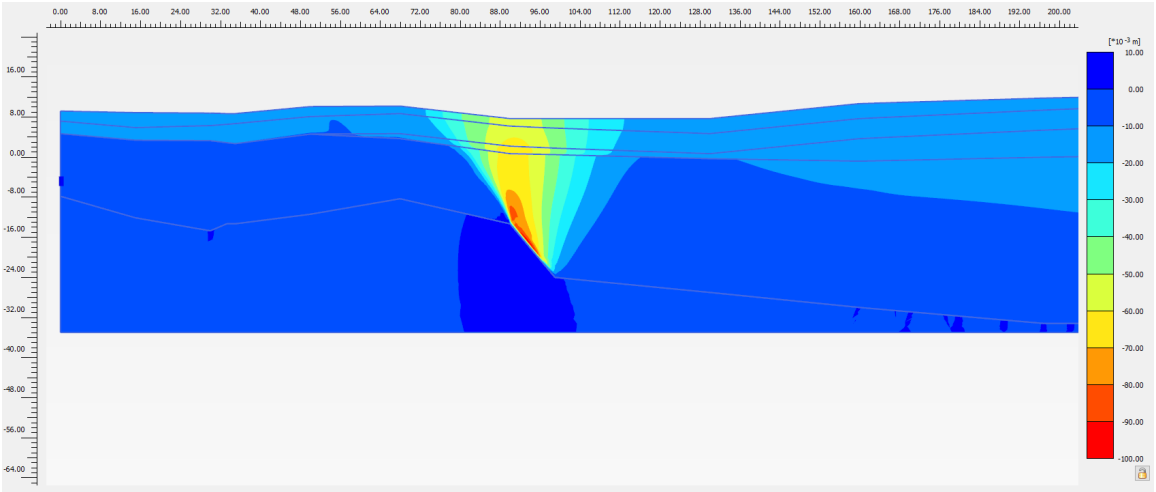

Figure 4.23: Predicted vertical displacements over the cross section in the 500 meter long well model.

5
Discussion

In this chapter, the modeling results and limitations for the 1D consolidation analyses and the 2D consolidation analyses are discussed.

5.1 1D consolidation analyses

The results of the 1D consolidation analysis for the analytical solution and the Plaxis model presented in Section 4.1 show similarities in terms of the dissipation of the pore pressures and the vertical displacements. The maximum difference observed in the predicted distributions of pore pressures was approximately 1 kPa, strongly suggesting that the two methodologies applied are comparable. As mentioned in the results, the Plaxis model predicts that the pore pressure increases slightly at the top of the clay layer. This phenomenon may be attributed to the modeling of groundwater level as static at the specified model coordinates, situated between the dry crust and the clay stratum. Consequently, upon the application of drawdown and the ensuing vertical displacements, the separation from the groundwater table is magnified, thus inducing a marginal elevation in pore pressure. However, this aspect has not been subjected to further examination.

The different models also show similarities in terms of the consolidation time. With the loading type, maximum excess pore pressure set as 1 kPa, the Plaxis model reaches the 'end of consolidation' after 5 years. At the same time step, the analytical solution predicts a very similar distribution of pore pressures, further underlining the similarities of the models.

The results also show similarities in the predicted vertical displacements for the clay, where the maximum difference is approximately 0.15 cm after 1 year of pumping. This also confirms the similarities of the model approaches. Given that the analytical model does not encompass the vertical displacements of the frictional soil, the comprehensive settlements observed in Plaxis have been incorporated into the analysis. This inclusion reveals that the vertical displacement of the frictional soil is approximately 1 cm. For practical applications, those displacements could be of importance.

5.2 Validation of the 1D analytical solution

When comparing the distribution of the pore pressures of the 1D analytical solution with the measured field data, several observations can be made. Initially, it can be seen that the initial pore pressure distribution of the analytical solution differs from the measured data. This is because the analytical solution is restricted to a linear distribution of initial pore pressures. This limitation is especially prominent in pore pressure profiles that have a clear drawdown at the bottom edge of the soil profile, as seen for VD4786 in Figure 4.4. However, when examining the pore pressure reduction for a certain drawdown in the underlying aquifer, the 1D analytical solution seems to be in line with the measured data. From a practical point of view, that is what matters in terms of stress increase and subsequent vertical displacements. However, while the analytical solution looks promising, further studies are needed to validate the method. Especially with respect to the effect of the initial pore pressure distribution on the drawdown. Furthermore, there are uncertainties related to the measured data. For example, the natural variation of the groundwater table due to precipitation, temperature, and human error could affect the measured data. The variation of data is evident in the figures presented in Appendix C, further underlining the importance of more studies being conducted to validate the model.

Other limitations of the analytical solution, apart from the restriction of the initial distribution of pore pressures, are that it is not optimized for different layers of clay or clays where the properties change with depth. It is most probable possible to incorporate this into the solution, but due to time restrictions, this has not been explored within the scope of this thesis.

5.3 Theoretical groundwater extraction model

The results of the theoretical local groundwater extraction model will be discussed in terms of how the thickness of the clay, the distance from the pumping well, and the duration of pumping affect the vertical displacements and the amount of affected clay. Furthermore, the effects of background creep on both the magnitude and the dispersion of vertical displacements will also be discussed. This discussion will be based on the results presented in Section 4.3.

When studying the results with respect to vertical displacements, an interesting observation regarding the magnitude of displacements can be made for different clay thicknesses. The results suggest that the largest vertical displacements, only due to groundwater extraction, occur in the thinnest clay layers. Meanwhile, when the creep effects are included, the largest displacements occur in the thickest clay layers. This indicates that consolidation proceeds more quickly in thinner clay layers. However, the creep will always be more prominent in the thickest clay layers, which is highlighted in Figure 4.18. This explains why vertical displacements are more significant in the thicker clay layers when creep is considered, despite the slower con-

solidation process. Nevertheless, in practical applications, the process that causes vertical displacements is not the primary concern, but is of great significance to understand and mitigate the problem.

The results of the vertical displacements show the expected trends with respect to time and distance from the pumping well. For all cases, the vertical displacements increase with time and reduce with distance. This is expected since the essence of time is in the very nature of the consolidation process and that the effect of the pumping decays with distance, which is highlighted in Figure 4.19.

Furthermore, the results show that the dispersion of vertical displacements between different clay thicknesses notably varies over time, with distance from the well and with inclusion or not of creep. With respect to time, the results indicate that the dispersion of vertical displacements will always increase with time. However, when examining short pumping durations up to approximately 1 month, the dispersion between different clay thicknesses is negligible.

In addition, in the case studied, the clay thickness does not affect the magnitude of vertical displacements close to the well when creep is included. However, this might just be the case for this specific clay. A parametric study of the clay properties would be necessary to evaluate the credibility of this conclusion. Especially since when the creep is excluded, the dispersion of vertical displacements near the well is prominent.

The results also indicate that vertical displacements at further distances from the well are highly dependent on the thickness of the clay when including creep. This is because the influence of the pumping reduces with distance, while the background creep remains constant, resulting in the dependence on the clay thickness, illustrated in Figures 4.9 and 4.13.

The findings related to the affected clay suggest that the influence of pumping is more significant near the pumping well and that there is more affected clay in the thicker layers across all distances from the well. The affected clay is, to a large extent, an indicator of how large vertical displacements can be expected. However, when comparing the vertical displacements without creep with the affected clay graphs, it is evident that the results do not align, at least not for 1 year of pumping. This, since vertical displacements increase with decreasing thickness, but for the affected clay, the relationship is the opposite. This is in line with the findings of Wikby et al. (2023), where the authors suggested that the most drawdown-induced deformations would occur, in the short term, in the thinnest clay layers. This could be explained by the drainage path being longer in the thicker clay layers and therefore resulting in a longer consolidation time, which could extend up to 30 years (Broms et al., 1976). However, over a longer period of time, vertical displacements are expected to be the largest in the thickest clay layers, due to the greater amount of affected clay.

Furthermore, in the affected clay graphs, there exist certain anomalous values between the amount of affected clay and the thickness of the clay. This is attributable

to the limitations in mesh refinement in Plaxis, as the mesh could not be refined as much as desired due to long simulation times. Due to the automated methodology used to extract the amount of affected clay, some outliers were included. This, since the methodology defined the amount of affected clay as the distance from the first mesh node that fell below the 1 kPa threshold to the bottom of the clay.

5.4 Hamnbanan pump test model

The results of the Hamnbanan pump test model show that with the modeling technique used, the results are highly dependent on the length of the model. This indicates that this modeling technique is not a viable method to use to predict aquifer drawdown and subsequent land subsidence due to groundwater extraction. However, there is the possibility that this modeling technique could be used to predict land subsidence if the drawdown of the model is validated with real-life data.
The findings indicate that the similarity of the models, with the groundwater extraction types well and drain, increases as the length of the model increases, exhibiting almost identical values when the model length is 1000 meters. This is illustrated in Figure 4.20.

However, it is evident from the results that the extent of the model has a great impact on the drawdown. This is mainly due to the fact that the closure of the x_{max} boundary and that no surface infiltration is considered fixates the volumetric capacity of the aquifer and prevents any potential for recharge. Hence, shorter models with a smaller volumetric capacity will experience a more pronounced drawdown, and the contrary for larger models. The closure of the x_{max} boundary was necessary due to substantial flow errors in the computational phases of the flow calculation within Plaxis when this boundary remained open. This resulted in the model becoming inoperable and unable to yield any results.

Furthermore, the fixed volumetric capacity of the aquifer will restrict the operational duration of the model. Having an extended pumping duration will, therefore, result in the depletion of water in the aquifer and a subsequent computational flow error in Plaxis. This highlights the need to obtain actual measured drawdowns to be able to validate the prediction accuracy of the model. Otherwise, the recharge capacity of the aquifer would need to be investigated further.

A comparison of pore pressure distributions was made between the 500-meter models, which resembled reality the most, and the real-life measured data in two boreholes. The results showed that the well and drain groundwater extraction methods exhibit a high degree of similarity but deviate from the measured data. Compared to the measurements in VD4786, see Figure 4.4, the models predict a reduction in the pore pressure similar to that of the measured data, but the initial distribution of the pore pressures differs significantly. The initial pore pressure distribution within the clay is linearly interpolated on the basis of the evaluated groundwater table and the pressure head of the aquifer across the cross section. This approach results in that the variation of pore pressures across the cross section resembles reality but is

necessarily not an exact match at a specific point. This is apparent for VD4786, where the measured initial distribution of the pore pressures is non-linear. The Plaxis models predicts rather similar pore pressures at the top and bottom of the clay but deviates clearly in between those.

For VD4788, the model predicts much less pore pressure reduction in the bottom part of the clay than the measured data suggest. This, despite the initial pore pressure distributions being rather similar. This is likely related to the fact that groundwater flow is a 3D problem, which has been compiled into a 2D model, using an axisymmetric model to resemble 3D conditions. The axisymmetric conditions assume that the soil geometry is the same in all directions from the rotation point x_{min}. As mentioned in the case study (Section 3.1), this is not the case at the site, further highlighting the limitations of this modeling technique. In addition to this, there are uncertainties related to the measured data, which is discussed previously in Section 5.2.

When examining the vertical displacements for the 500 meter long Hamnbanan pump test model presented in Figure 4.23, it can be seen that the vertical displacements at the ground surface are generally 1-2 cm. However, at a distance of approximately 70-110 meters from the extraction well, there are substantially larger vertical displacements. This behavior is seen in all models, but to various degrees. This is because of a slip surface created by the pronounced downward slope of the bedrock. The soil tries to settle due to groundwater extraction, but because of the high stiffness of the bedrock, the soil will slip along the bedrock interface. This is further emphasized by Figure E.1 in Appendix E, where the incremental shear strain developed at this interface is highlighted that will cause this local slip surface. This also highlights the risk associated with the development of deep failures due to the extraction of groundwater, which should also be taken into account when studying this type of problem.

A limitation of the entire Hamnbanan pump test model is that the spatial variation of the clay properties has not been taken into account. The soil profile within the area has been evaluated as two layers of clay over depth, with varying thickness. Furthermore, the soil data obtained from the soil tests show a rather large spread of the clay parameters within the area. However, the variations appear local and no pattern has been observed. Such variations could be of importance when modeling a groundwater extraction with this technique, since they could result in a large variation of the land subsidence and should be further investigated.

5.5 Plaxis limitations

In addition to the Plaxis limitations discussed in the previous chapter, there were other limitations that had to be considered when modeling the two-dimensional models, both the Hamnbanan pump test model and the theoretical model. One of these limitations was the placement of the well. In an axisymmetrical model, the x_{min} boundary must be closed. Should the well be placed on this boundary, this

x_{min} closed command overrides the pumping of the well, making the well inoperable. To solve this problem, the well was relocated inward by 0.2 meters within the model. The length of which the well was moved within the model was highly sensitive. Should the well be positioned closer than 0.2 meters to the boundary, there would be substantial flow errors, resulting in the model being unable to calculate any results. However, the drain in the Hamnbanan pump test model could be placed at the x_{min} boundary. The constraint associated with simulating an extraction in this way lies in the requirement for a drawdown input, rather than a flow rate, as in models that incorporate a well. This is attributed to the fact that prior to the actual extraction of water, the intended pumping rate of the well is typically predetermined, whereas the resulting drawdown induced by the pumping process can only be determined after the extraction.

Another limitation is related to the SSC constitutive model, where the creep causes the pore pressures to rise unexpectedly above the initial levels. This was deemed a numerical error in Plaxis since there is no evident reason for this behavior, and the phenomenon also occurs during the isolated creep phases. This behavior caused a heave in some parts of the soil profile but also had an impact on the amount of affected clay. These problems were corrected, but they need to be considered when modeling groundwater extraction problems with SSC.

6

Conclusions and suggestions for future studies

The following chapter presents the conclusions derived in this thesis as well as suggestions for future studies.

6.1 Conclusions

This thesis examines modeling approaches for land subsidence problems due to groundwater extraction in 1D and 2D, as well as identifying trends for how clay thickness affects the pore pressure reduction in a clay profile.

The 1D consolidation of a soil column subject to a uniform drawdown was compared for two different methods, an analytical solution and a finite element model in Plaxis. The results strongly suggest that the two different methods are comparable, as both showed similar results in terms of the distribution of pore pressures, consolidation time, and vertical displacements over time.

The 1D analytical solution was validated by comparing the predicted pore pressure reduction in 2 boreholes. The analytical solution predicted similar pore pressure reduction even though the magnitude of the pore pressures differed because of the restricted possibility of modeling nonlinear initial pore pressures.

A theoretical groundwater extraction model was created to investigate how clay thickness, distance from the pumping well, pumping time, and the effect of creep influence both vertical displacements and the amount of affected clay. The results showed that the vertical displacements, only due to groundwater extraction, increase with reduced clay thickness, but when the effects of creep are taken into account, the displacements increase with increased clay thickness. Furthermore, vertical displacements were found to increase with time and reduce with distance from the pumping well. The results also indicated that the clay thickness does not affect the vertical displacements for pumping durations up to 1 month. In addition, the results suggest that when creep is included, the magnitude of vertical displacements close to the pumping well is governed by the aquifer drawdown, while at a further distance, the clay thickness is the governing factor. In addition, the findings related to the affected clay indicate that the influence of pumping is most prominent near the well and that the affected clay increases with increasing clay thickness.

The pump test conducted within the Hamnbanan project was modeled in a 2D axisymmetric model to investigate how a land subsidence problem due to groundwater extraction could be modeled. The findings indicated that with the modeling technique used, the results are strongly dependent on the length of the model. This was because the x_{max} boundary in the axisymmetric model had to be closed, which led to that the volumetric capacity of the aquifer was governed by the model length. The fixed volumetric capacity was also found to affect the operational duration of the model, and therefore limiting the possibilities of modeling longer durations of pumping. For the case studied, by comparison to real-life measured data, it was found that a model with a length of 500 meters resembled reality the best and that the well and drain groundwater extraction method yielded comparable results. The models predicted distribution of the pore pressures in the clay after 1 month of pumping was compared with the measured data in two boreholes. It was found that the models predicted a similar reduction in pore pressures in one borehole, but underestimated the reduction in the bottom part of the clay in the other.

6.2 Suggestions for future studies

The findings of this study provide a foundational understanding of the relationship between groundwater extraction and land subsidence in the context of Gothenburg, Sweden. However, as with any complex geotechnical and hydrogeological phenomena, there remain several avenues for further exploration to improve the accuracy, applicability, and comprehensiveness of the results. This section outlines potential areas for future research, highlighting the need for extended studies, model enhancements, and practical applications that can build on the insights gained from this thesis.

For instance, the 1D analytical solution could be improved by incorporating a stepwise linear initial distribution of pore pressures and further validated for different clay properties. The findings of the theoretical groundwater extraction model could be supported by investigating the effects of different extraction rates and soil profiles. For application in Gothenburg, a more characteristic soft and loose "Gothenburg clay" could be investigated. Further improvements could also be made to the modeling technique used when examining groundwater extraction induced land subsidence. Modeling in 3D would address the issue of simplifying a 3D problem into a 2D model. There is also great potential in exploring alternative boundary conditions and model lengths in axisymmetric models to better replicate field conditions and to reduce the dependency of results on model dimensions.

Bibliography

Berntson, J. A. (1983). *Portrycksvariationer i leror i göteborgsregionen* (SGI Report, ISSN 0348-0755 ; 20). Swedish Geotechnical Institute. https://swedgeo.diva-portal.org/smash/record.jsf?pid=diva2%3A1299926&dswid=-3837

Blomén, H. (2017). *Pore pressure response in the uppermost part of a clay soil slope* [Licentiate dissertation, Chalmers University of Technology]. Chalmers Research. https://publications.lib.chalmers.se/records/fulltext/250093/250093.pdf

Broms, B. B., Fredriksson, A., & Carlsson, L. (1976). Land subsidence in Sweden due to water-leakage into deep-lying tunnels and its effects on pile supported structures. *International Association of Hydrological Sciences Proceedings of the Anaheim Symposium*, *121*, 375–388. https://www.landsubsidence-unesco.org/wp-content/uploads/2019/03/Proceedings_Anaheim.pdf

Cigna, F., & Tapete, D. (2021). Present-day land subsidence rates, surface faulting hazard and risk in Mexico City with 2014–2020 Sentinel-1 IW InSAR. *Remote Sensing of Environment*, *253*, 112–161. https://doi.org/10.1016/j.rse.2020.112161

Esteban, E., Dinar, A., Calvo, E., Albiac, J., Calatrava, J., Herrera, G., Teatini, P., Tomás, R., Ezquerro, P., & Li, Y. (2024). Modeling the optimal management of land subsidence due to aquifers overexploitation. *Journal of Environmental Management*, *349*, 119–333. https://doi.org/10.1016/j.jenvman.2023.119333

Galloway, D. L., & Burbey, T. J. (2011). Review: Regional land subsidence accompanying groundwater extraction. *Hydrogeology Journal*, *19*, 1459–1486. https://doi.org/10.1007/s10040-011-0775-5

Galloway, D. L., Jones, D., & Ingebritsen, S. (1999). *Land Subsidence in the United States* (USGS Circular 1182). U.S. Geological Survey. https://doi.org/10.3133/cir1182

Gambolati, G., Teatini, P., & Ferronato, M. (2006). Anthropogenic land subsidence. In *Encyclopedia of hydrological sciences* (pp. 2444–2459). John Wiley Sons, Ltd. https://doi.org/10.1002/0470848944.hsa164b

He, G., Yan, X., Zhang, Y., Yang, T., Wu, J., Bai, Y., & Gu, D. (2020). Experimental study on the vertical deformation of soils due to groundwater withdrawal. *International Journal of Geomechanics*, *20*(7), 04020076-1 - 04020076–12. https://doi.org/10.1061/(ASCE)GM.1943-5622.0001709

Jaky, J. (1944). A nyugalmi nyomas tenyezoje (The coefficient of earth pressure at rest). *Magyar Mernok es Epitesz-Egylet Kozlonye (Journal for Society of Hungarian Architects and Engineers)*, *78*(22), 355–358.

Karstunen, M., & Amavasai, A. (2017). *Best soil: Soft soil modelling and parameter determination* (Trafikverkets forskningsportföljer TRV 2015/2591). Chalmers. https://trafikverket.diva-portal.org/smash/record.jsf?pid=diva2%3A1746992&dswid=-2938

Lång, L.-O. (2009). *Grundvattenförekomster i Göteborgs kommun* (K 109). Geological Survey of Sweden, SGU. https://resource.sgu.se/dokument/publikation/k/k109beskrivning/k109-beskrivning.pdf

Larsson, R. (2008). *Jords egenskaper* (SGI Information 5). Swedish Geotechnical Institute. https://www.sgi.se/globalassets/publikationer/info/pdf/sgi-i1.pdf

Larsson, R., Bengtsson, P.-E., & Eriksson, L. (1997). *Prediction of settlements of embankments on soft, fine-grained soils. Calculation of settlements and their course with time* (SGI Information 13E). Swedish Geotechnical Institute. https://www.sgi.se/globalassets/publikationer/info/pdf/sgi-i13e.pdf

Larsson, R., Sällfors, G., Bengtsson, P.-E., Alén, C., Bergdahl, U., & Eriksson, L. (2007). *Skjuvhållfasthet - utvärdering i kohesionsjord* (SGI Information 3). Swedish Geotechnical Institute. https://www.sgi.se/globalassets/publikationer/info/pdf/sgi-i3.pdf

Lindskoug, N.-E., & Nilsson, L.-Y. (1974). *Grundvatten och byggande [Elektronisk resurs] STEGAS arbete 1966-73*. Stockholm: Svensk Byggtjänst.

Ma, J., Berggren, B., Bengtsson, P., Stille, H., & Hintze, S. (2006). Back analysis on a deep excavation in Stockholm with finite element method. *Numerical Methods in Geotechnical Engineering*, 423–429. https://www.researchgate.net/publication/290038608_Back_analysis_on_a_deep_excavation_in_Stockholm_with_finite_element_method

Merisalu, J., Sundell, J., & Rosén, L. (2023). Probabilistic cost-benefit analysis for mitigating hydrogeological risks in underground construction. *Tunnelling and Underground Space Technology*, *131*, 104815. https://doi.org/10.1016/j.tust.2022.104815

Olsson, M. (2010). *Calculating long-term settlement in soft clays* [Licentiate dissertation, Chalmers University of Technology]. Chalmers Research. https://www.sgi.se/globalassets/publikationer/rapporter/pdf/sgi-r74.pdf

Pratt, W. E., & Johnson, D. W. (1926). Local subsidence of the goose creek oil field. *The Journal of Geology*, *34*(7), 577–590. http://www.jstor.org/stable/30056838

Shen, S.-L., Zhu, H., & Zhang, X.-L. (2004). Land subsidence due to groundwater drawdown in Shanghai. *Geotechnique*, *54*(2), 143–147. https://doi.org/10.1680/geot.54.2.143.36332

Sun, H., Grandstaff, D., & Shagam, R. (1999). Land subsidence due to groundwater withdrawal: Potential damage of subsidence and sea level rise in southern New Jersey, USA. *Environmental Geology*, *37*, 290–296. https://doi.org/10.1007/s002540050386

Swedish Transport Administration. (2011). *TK Geo 11* (Trafikverkets publikationer 2011:047). https://trafikverket.diva-portal.org/smash/record.jsf?pid=diva2%3A1542349&dswid=-4196

Swedish Transport Administration. (2015a). Markteknisk undersökningsrapport (MUR), Hydrogeologi. (108793-18-081-001). https://bransch.trafikverket.se/contentassets/

704ec2d97a0344b1ad5ab7ee2020035a/0210_markteknsik-undersokningsrapport-hydregeologi-542-mb.pdf.pdf

Swedish Transport Administration. (2015b). Projekterings PM - Hydrogeologi. (108793-18-080-001). https://tinyurl.com/mw7ds4jc

Swedish Transport Administration. (2015c). Projekterings-PM, Geoteknik. (108793-08-080-001). https://tinyurl.com/25wm9y4e

Swedish Transport Administration. (2015d). Teknisk handling Geoteknik. (108793-15-010-001). https://tinyurl.com/2dtf4zsk

Swedish Transport Administration. (2018a). Hamnbanan Göteborg, dubbelspår Eriksberg – Pölsebo, Vattenverksamhet, PM Sättningsrisker på grund av grundvattensänkning. (108793-04-025-204). https://bransch.trafikverket.se/contentassets/704ec2d97a0344b1ad5ab7ee2020035a/0215_sattningsrisker-8.97mb.pdf.pdf

Swedish Transport Administration. (2018b). Markteknisk undersökningsrapport (MUR), Hydrogeologi.

Swedish Transport Administration. (2022). Hamnbanan Göteborg. https://www.trafikverket.se/vara-projekt/projekt-i-vastra-gotalands-lan/hamnbanan-goteborg/

Swedish Transport Administration. (2023). *Geokonstruktion, dimensionering och utformning* (TRVINFRA-00230). https://puben.trafikverket.se/dpub/visa-dokument/3e52866e-9e63-494f-ba77-7d6de6d91bd4

Tahershamsi, H., & Dijkstra, J. (2021). Towards rigorous boundary value level sensitivity analyses using fem. *IOP Conference Series: Earth and Environmental Science*, *710*(1), 012072. https://doi.org/10.1088/1755-1315/710/1/012072

Tahershamsi, H., & Dijkstra, J. (2022). Using experimental design to assess rate-dependent numerical models. *Soils and Foundations*, *62*(6), 101244. https://doi.org//10.1016/j.sandf.2022.101244

Wikby, P., Abed, A., Karlsson, M., Sundell, J., & Karstunen, M. (2023). The influence of parameter variability on subsidence. *10th European Conference on Numerical Methods in Geotechnical Engineering*. https://doi.org/10.53243/NUMGE2023-325

Xie, K.-H., Tao, L.-W., Wang, Y.-l., & Li, C.-X. (2012). One-dimensional consolidation solution and analysis for aquitard in leakage system. *Journal of Shenyang University of Technology*, *34*(5), 582–585.

A

Soil parameters

Test data and evaluated profiles for the water content W_N and the liquid limit W_L are presented in Figures A.1 and A.2.

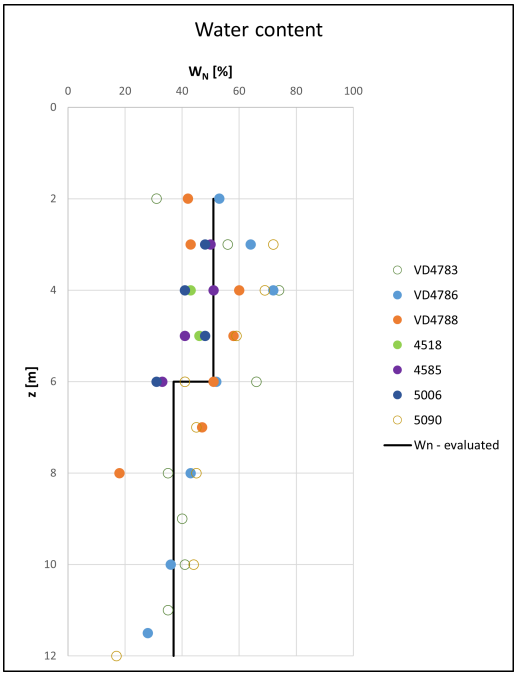

Figure A.1: Test data and evaluated profile for the water content W_N.

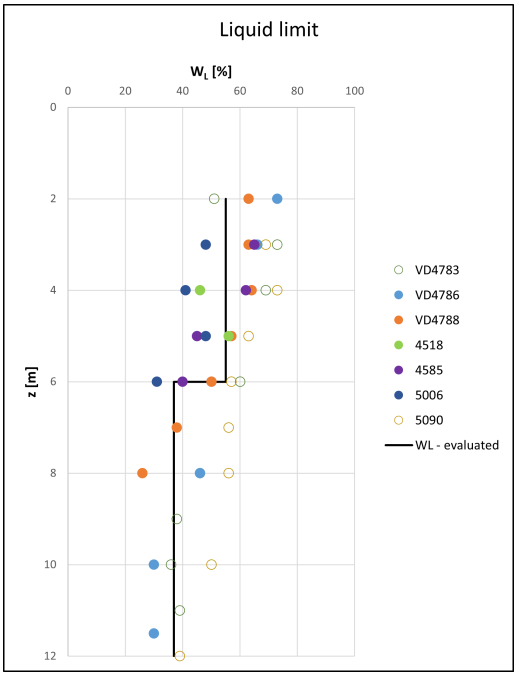

Figure A.2: Test data and evaluated profile for the liquid limit W_L.

B

Matlab code for the 1D analytical solution

```
%% 1D Consolidation analytical solution
% AUTHORS: MAANS PAULSSON AND MARCUS TRAPP
% BASED ON THE WORK OF Xie et. al. (2012). "One-
   dimensional consolidation solution and analysis for
   aquitard in leakage system". Published in the Journal
   of Shenyang University of Technology
clc
clear all
close all

% Input data for analytical solution
yw = 10;                                    % unit weight of
   water [kN/m^3]
dh = 2;                                     % groundwater
   drawdown in aquifer [m]
H = 9;                                      % thickness of
   aquitard [m]
z_values_analytical = 0:0.1:H;              % range of depths
    of investigated points for analytical solution [m]
h0 = 0;                                     % distance from
   top of aquitard to GWL [m]
ha = 12;                                    % pressure head
   of aquifer [m]
k_m_day= 8.64*10^(-5);                      % hydraulic
   conductivity, aquitard [m/day], recalculate into m/s.
k = k_m_day/86400;                          % hydraulic
   conductivity, aquitard [m/s]
E_oed = 4000;                               % oedometer
   modulus [kPa] be aware of precon

% Create values for Tv
t = [2, 7, 30, 90, 180, 365, 1825, 2500]          % number
    of days
```

```
Tv_values=(k * E_oed * t*86400)/(yw * (H)^2)

% Adjustment of u due to non hydrostatic conditions
u_bottom_aquitard_hydro = yw * (H+h0);
u_top_aquifer = yw * ha;
du_a= u_top_aquifer - u_bottom_aquitard_hydro;
u_extra = du_a / H * z_values_analytical;

%
   ----------------------------------------------------------------

% Colors for plotting
colors = lines(length(Tv_values));

% Initialize cell arrays to store values (Export to excel
   )
u_numeric_cells = cell(length(Tv_values), 1);
delta_u_numeric_cells = cell(length(Tv_values), 1);
%
   ----------------------------------------------------------------

 %% Delta u
 %Calculation of delta u, (deltasigma'v = -delta u)

% Initialize figure
figure;

% Loop through Tv values
for i = 1:length(Tv_values)
    Tv = Tv_values(i);

    syms m;

    % Series term
    series_term = (-1)^(m-1) * (1/m) * sin(m * pi *
       z_values_analytical / H) * exp(-m^2 * pi^2 * Tv);
    delta_u_series_sum = symsum(series_term, m, 1, 100);

    % Entire expression
    delta_u = -yw * dh * z_values_analytical / H + (2 *
       yw * dh / pi) * delta_u_series_sum;
    delta_u_numeric = vpa(delta_u); % Convert the series
       sum to a numeric value

    % Store in cell array
    delta_u_numeric_cells{i} = double(delta_u_numeric);
```

```
    % Plot analytical solution
    plot(delta_u_numeric, -z_values_analytical, '
       DisplayName', ['Analytical, t = ' num2str(t(i)), '
       d'], 'Color', colors(i, :));
    hold on;


end


% Add labels and legend
xlabel('\Deltau [kPa]');
ylabel('z [m]');
title('\Deltau');
legend('Location', 'Best');
grid on;

% Hold off to stop superimposing plots
hold off;

%
   ------------------------------------------------------------------

%% u
% Calculation of u

% Initialize figure
figure;

% Loop through Tv values
for i = 1:length(Tv_values)
    Tv = Tv_values(i);

    syms n;

    % Series term
    series_term2 = (2 * yw * dh / (n * pi)) * (-1)^(n-1)
       * sin(n * pi * z_values_analytical / H) * exp(-n^2
        * pi^2 * Tv);
    u_series_sum = symsum(series_term2, n, 1, 100);

    % Entire expression
    u = (yw * (h0 + z_values_analytical - dh *
       z_values_analytical / H) + u_series_sum) + u_extra
       ;
```

```
    u_numeric = vpa(u); % Convert the series sum to a
       numeric value

    % Store in cell array
    u_numeric_cells{i} = double(u_numeric);

    % Plot analytical solution
    plot(u_numeric, -z_values_analytical, 'DisplayName',
       ['Analytical, t = ' num2str(t(i)), 'd'], 'Color',
       colors(i, :));
    hold on;


end

    %Plot inital u
    u_initial= h0*yw + (ha-h0)*yw*z_values_analytical/H;
    plot(u_initial,-z_values_analytical, 'DisplayName', '
       Inital','Color','black');

% Add labels and legend
xlabel('u [kPa]');
ylabel('z [m]');
title('u');
legend('Location', 'Best');
grid on;

%
   ----------------------------------------------------------------

% Hold off to stop superimposing plots
hold off;

% For export to excel
delta_u_numeric_matrix = vertcat(delta_u_numeric_cells
   {:});
u_numeric_matrix = vertcat(u_numeric_cells{:});

%
   ----------------------------------------------------------------


%% Vertical displacement
figure;

% Loop through Tv values
```

```
for i = 1:length(Tv_values)
    Tv = Tv_values(i);

    syms b;

    % Series term
    series_term3 = symsum(2 * exp(-4 * (pi*(b-1/2))^2 *
       Tv) / ((pi* (b - 1/2))^2), b, 1, 100);

    % Entire expression
    S = (yw * dh * H) / (2 * E_oed) *(1 - series_term3);
    S_numeric(i) = vpa(S); % Convert the series sum to a
       numeric value

    % Store in cell array
    settlement_numeric_cells{i} = double(S_numeric);
    hold on;
end
% Plot analytical solution
    semilogx(t, -S_numeric,'o-')
    hold on

% Add labels and legend
xlabel('time [days]');
ylabel('Vertical displacement [m]');
title('Vertical displacement');
grid on;

%
   ----------------------------------------------------------------------
```

C

Pore pressure measurements

The measured pore pressure data over time in the boreholes VD4783, VD4786, VD4788 and 5090 are presented in Figures C.1-C.4. In addition, the measurements in VD4786 and VD4788 during the course of the pump test are highlighted in Figures C.5 and 4.5.

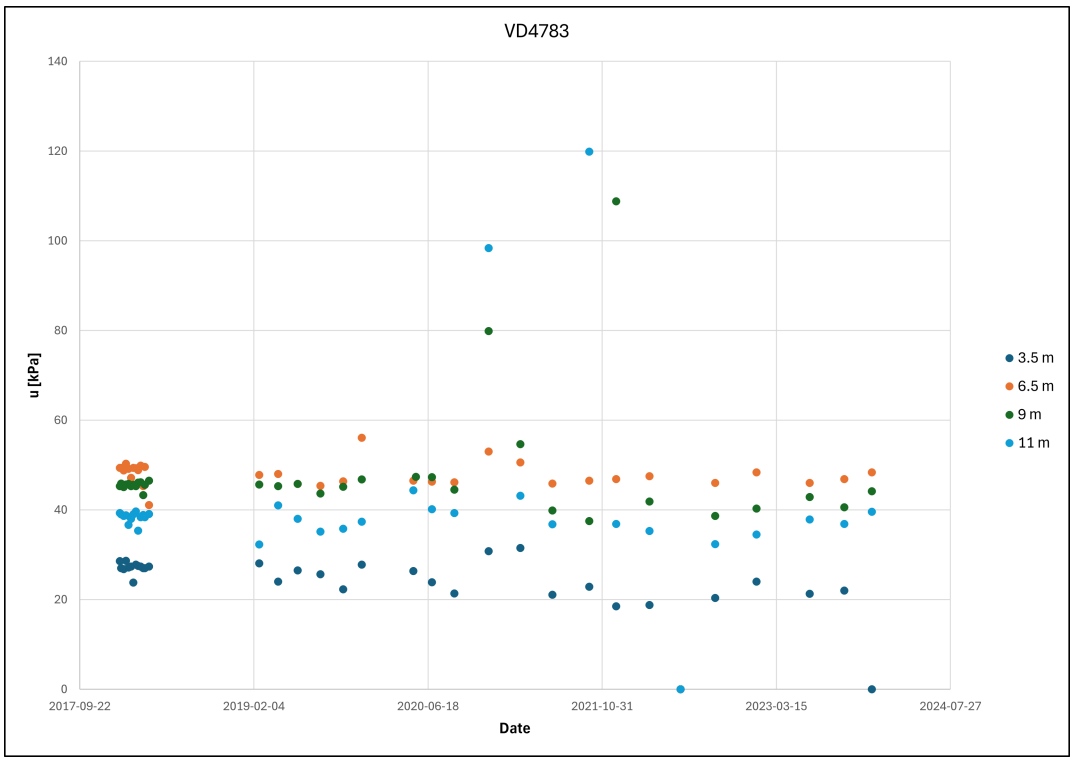

Figure C.1: Pore pressure measurements for borehole VD4783.

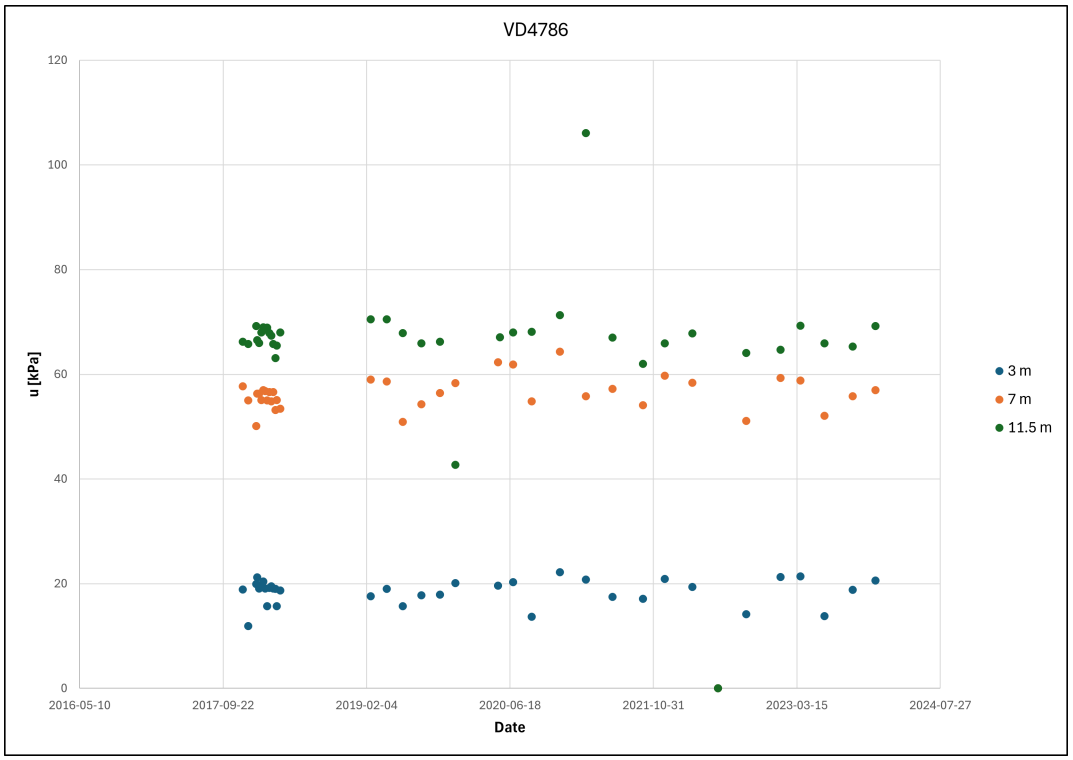

Figure C.2: Pore pressure measurements for borehole VD4786.

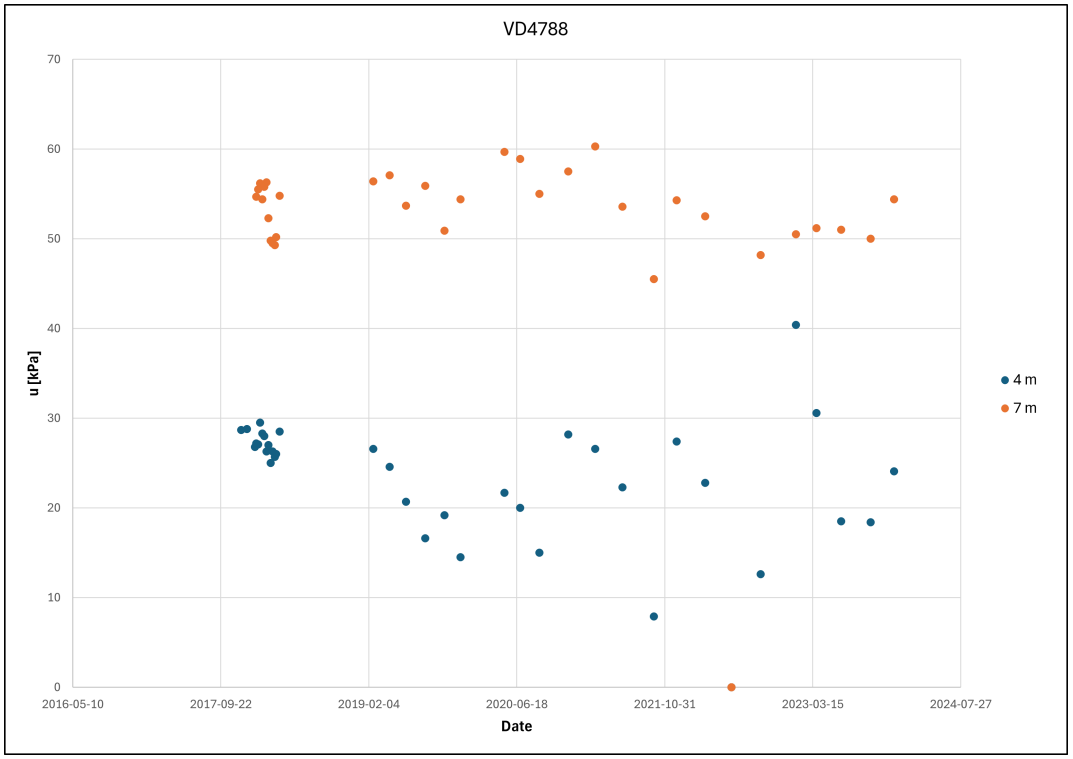

Figure C.3: Pore pressure measurements for borehole VD4788.

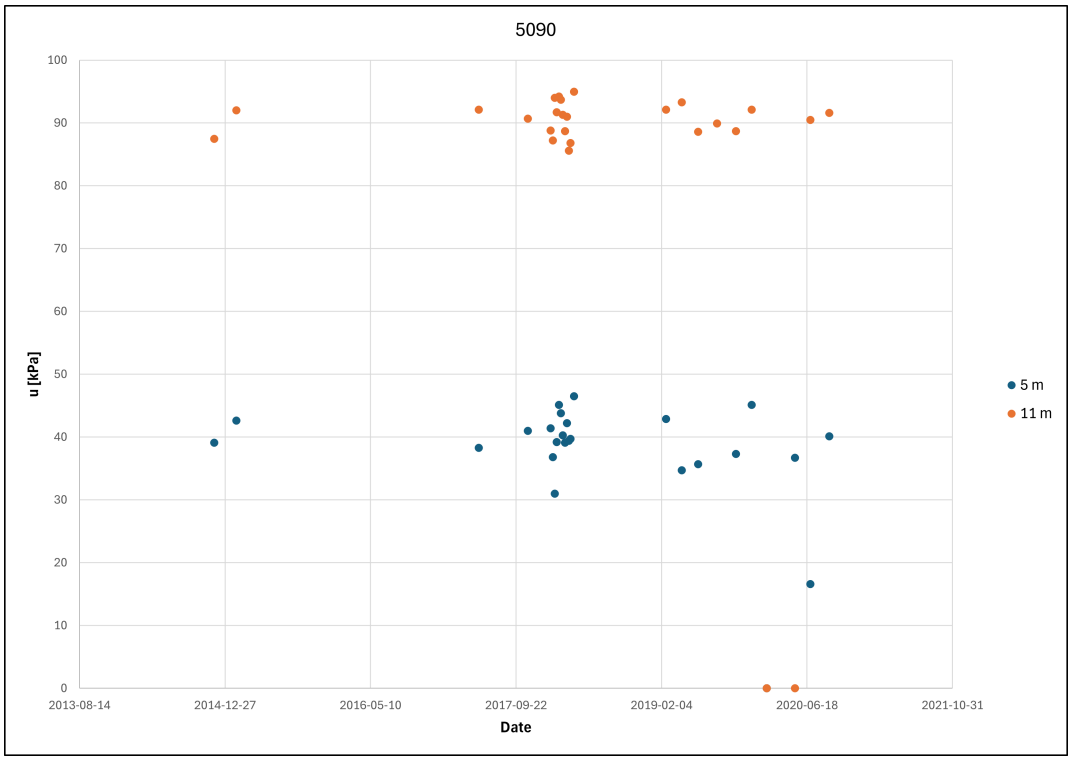

Figure C.4: Pore pressure measurements for borehole 5090.

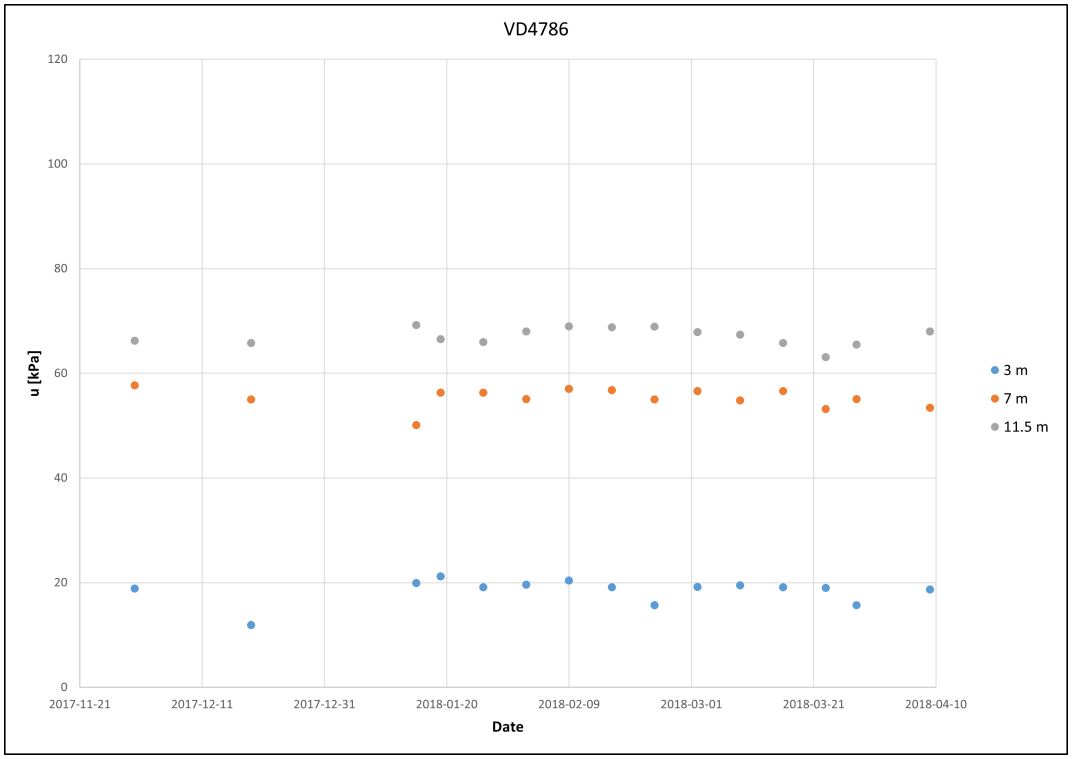

Figure C.5: Pore pressure measurements for borehole VD4786 during the pump test.

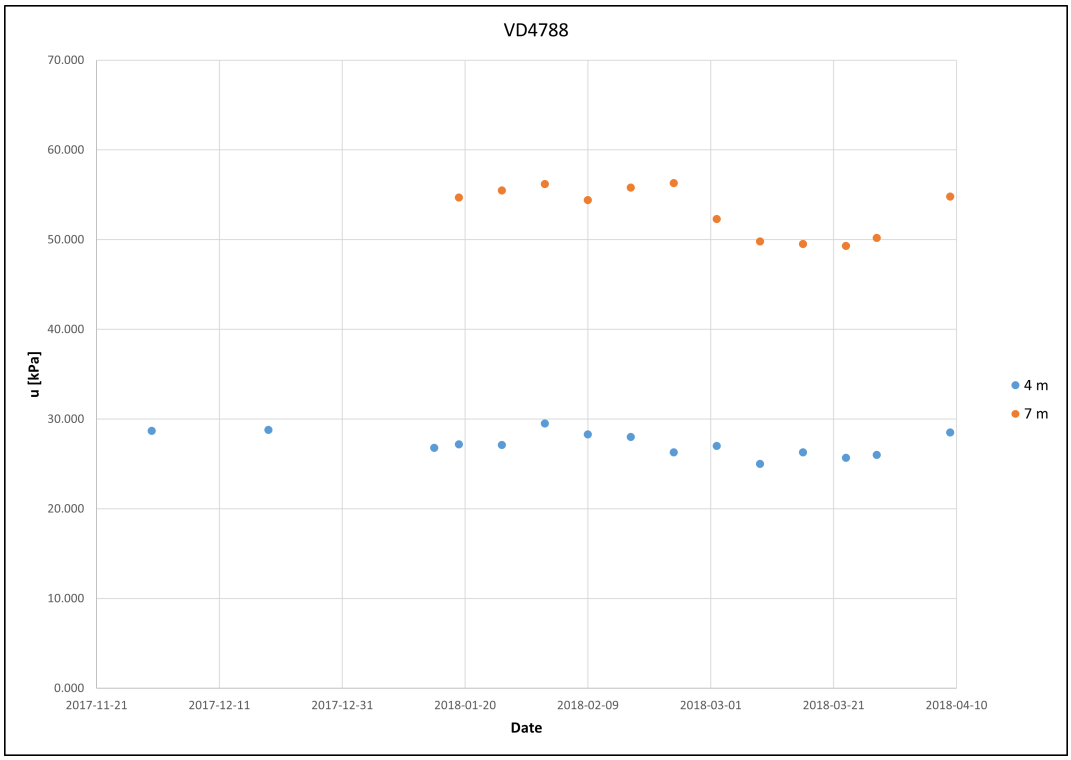

Figure C.6: Pore pressure measurements for borehole VD4788 during the pump test.

D

Distribution of pore pressures in the theoretical local groundwater extraction model

The distribution of pore pressures for different pumping durations at the distances 0, 10, 50 and 100 meters from the pumping well and the clay thicknesses 10, 15, 20 and 30 meters are shown in Figures D.1 - D.16. The pore pressures in the theoretical local groundwater extraction model were corrected due to the increase in pore pressures due to background creep. An example of the corrected and uncorrected pore pressures in relation to the pore pressures during the background creep phase is shown in Figure D.17.

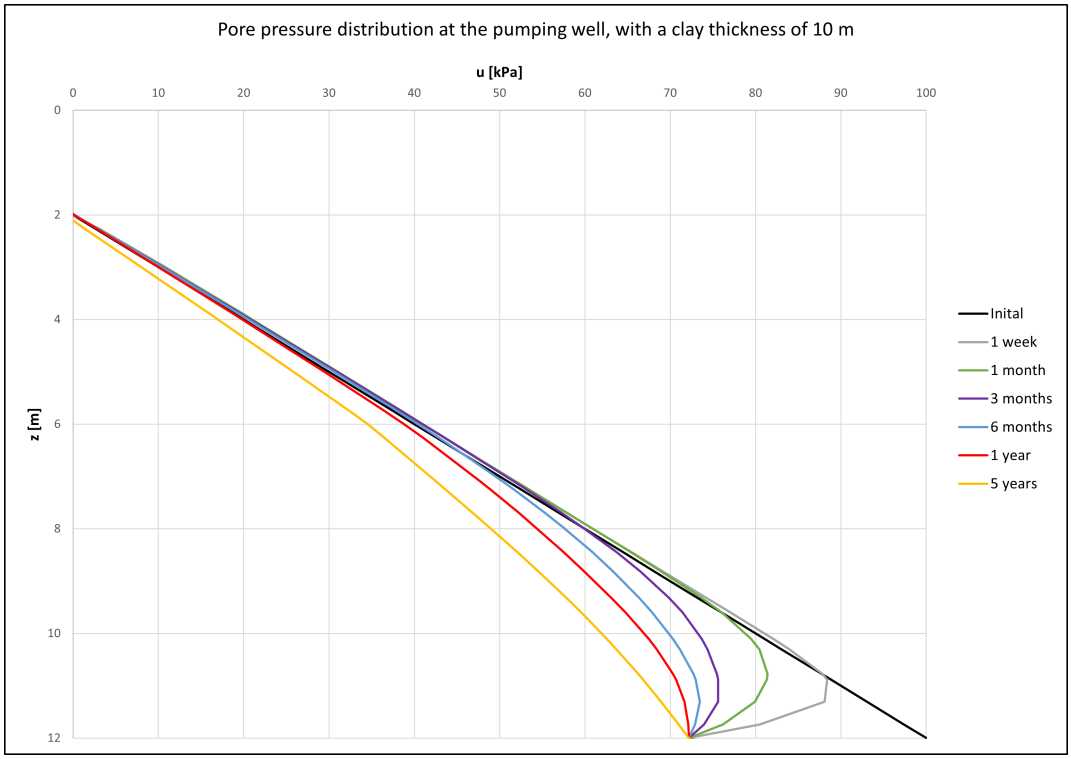

Figure D.1: The pore pressure distribution at the pumping well, with a clay thickness of 10 meters. Plotted over depth for different pumping durations.

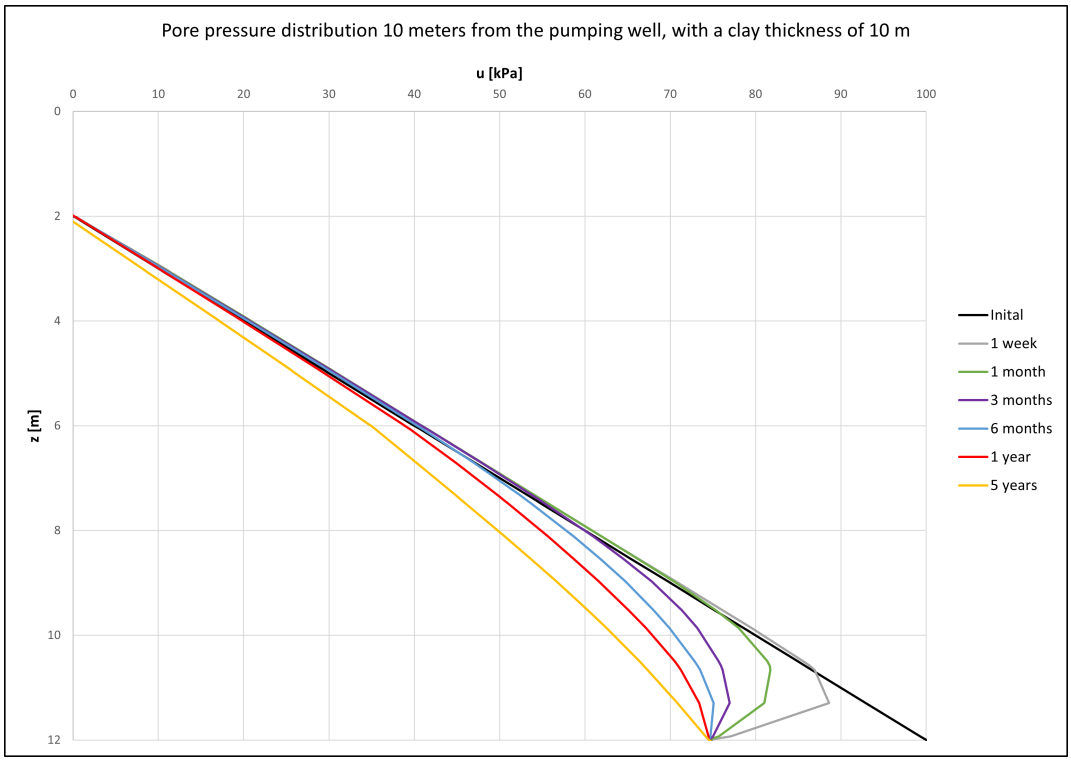

Figure D.2: The pore pressure distribution 10 meters from the pumping well, with a clay thickness of 10 meters. Plotted over depth for different pumping durations.

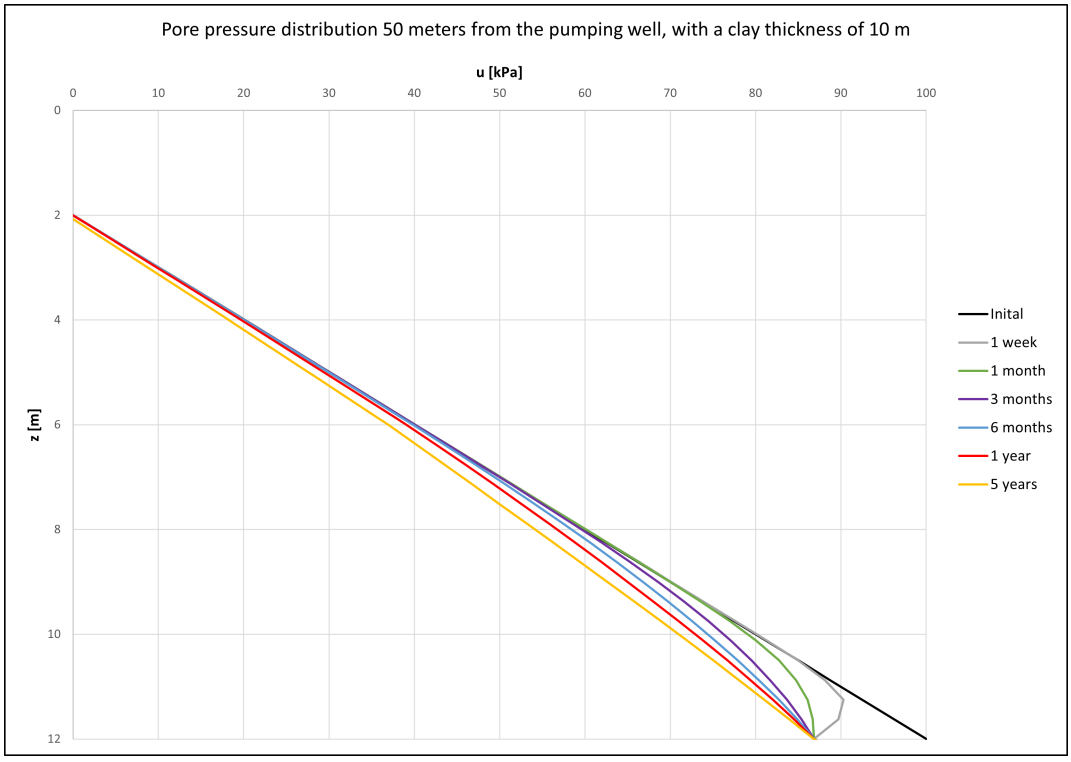

Figure D.3: The pore pressure distribution 50 meters from the pumping well, with a clay thickness of 10 meters. Plotted over depth for different pumping durations.

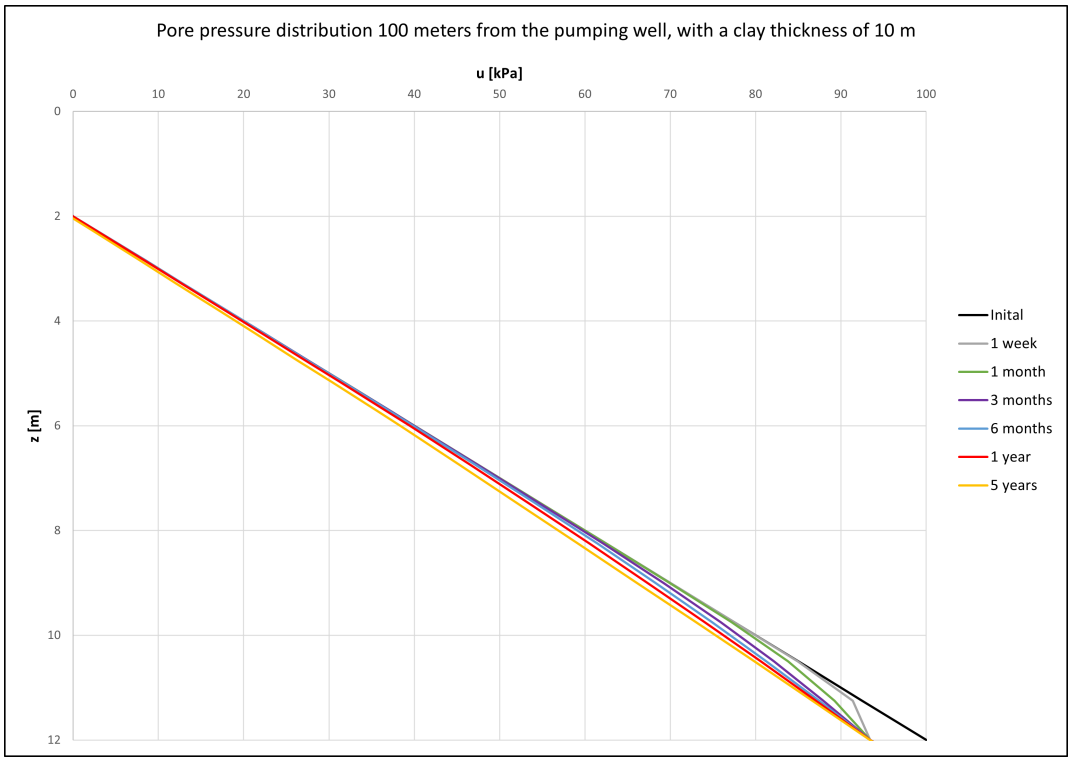

Figure D.4: The pore pressure distribution 100 meters from the pumping well, with a clay thickness of 10 meters. Plotted over depth for different pumping durations.

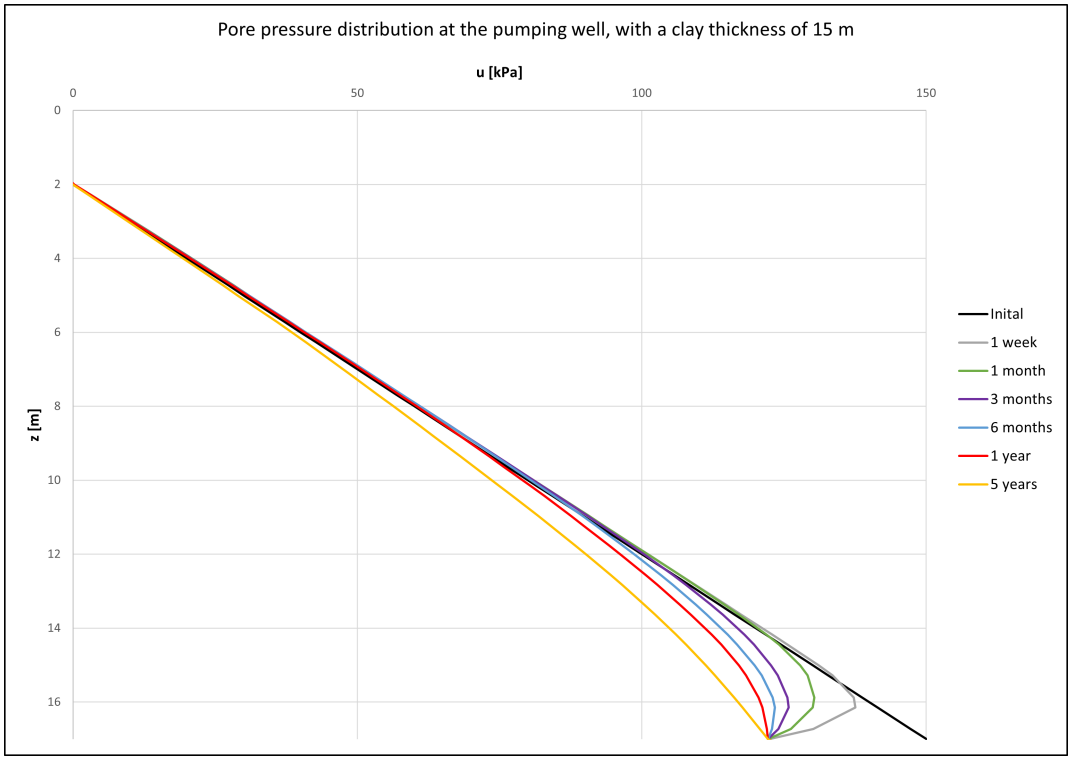

Figure D.5: The pore pressure distribution at the pumping well, with a clay thickness of 15 meters. Plotted over depth for different pumping durations.

Figure D.6: The pore pressure distribution 10 meters from the pumping well, with a clay thickness of 15 meters. Plotted over depth for different pumping durations.

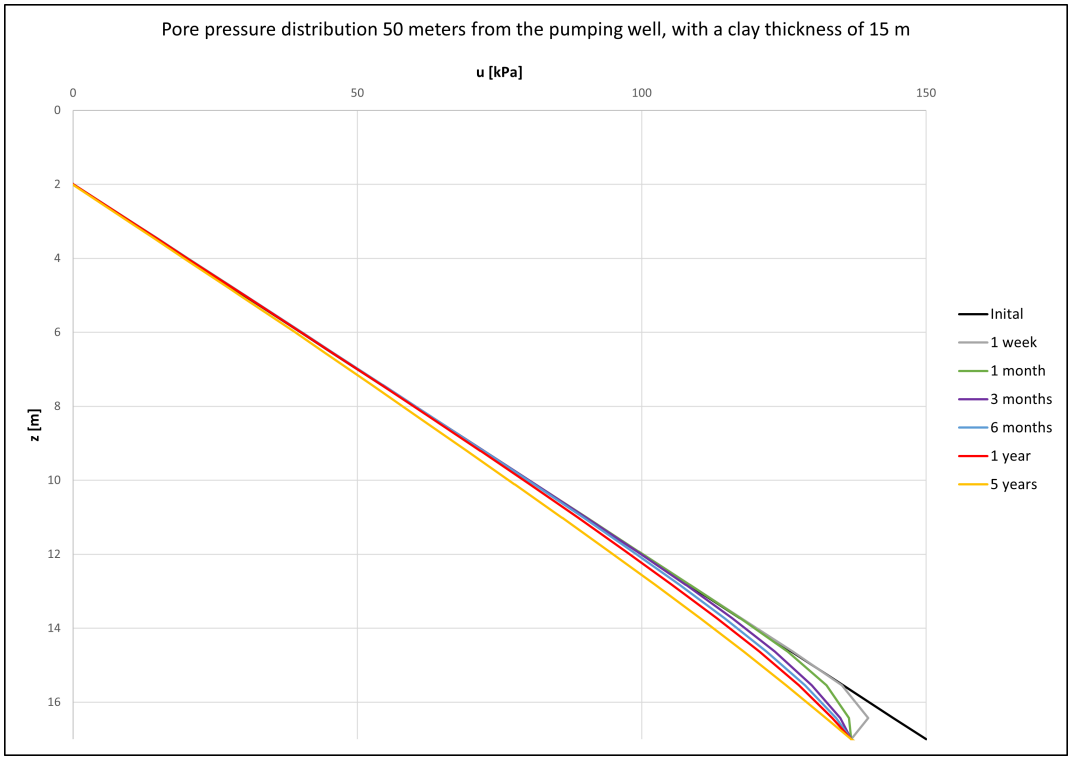

Figure D.7: The pore pressure distribution 50 meters from the pumping well, with a clay thickness of 15 meters. Plotted over depth for different pumping durations.

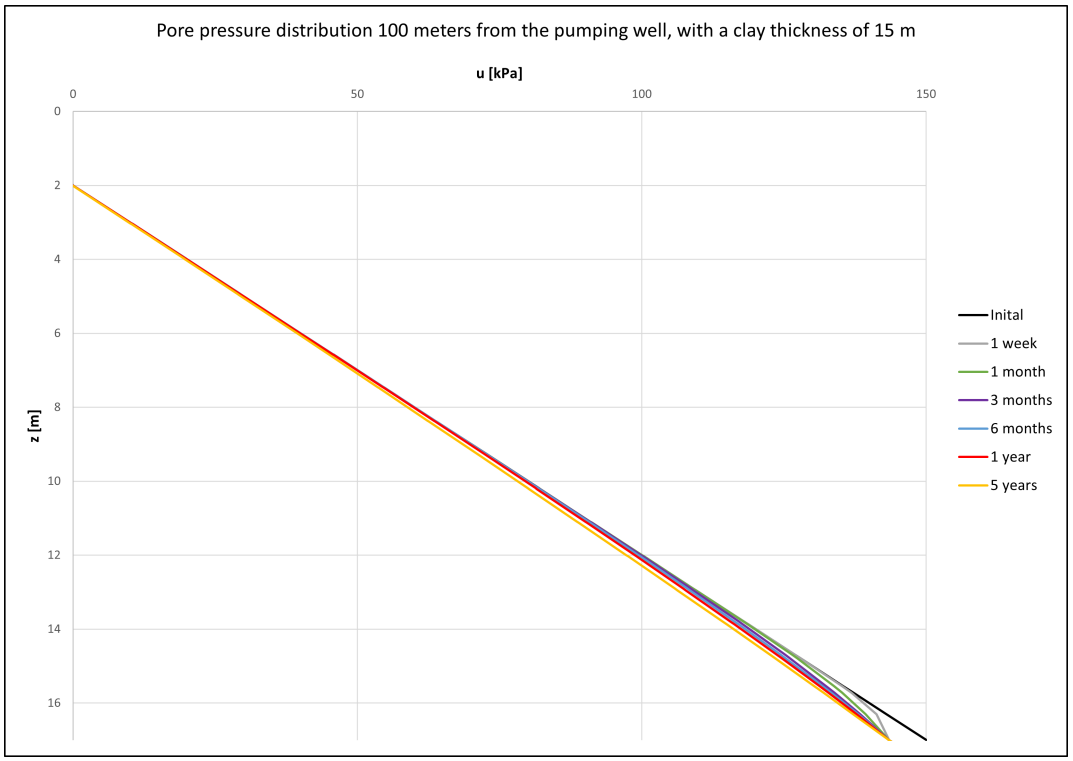

Figure D.8: The pore pressure distribution 100 meters from the pumping well, with a clay thickness of 15 meters. Plotted over depth for different pumping durations.

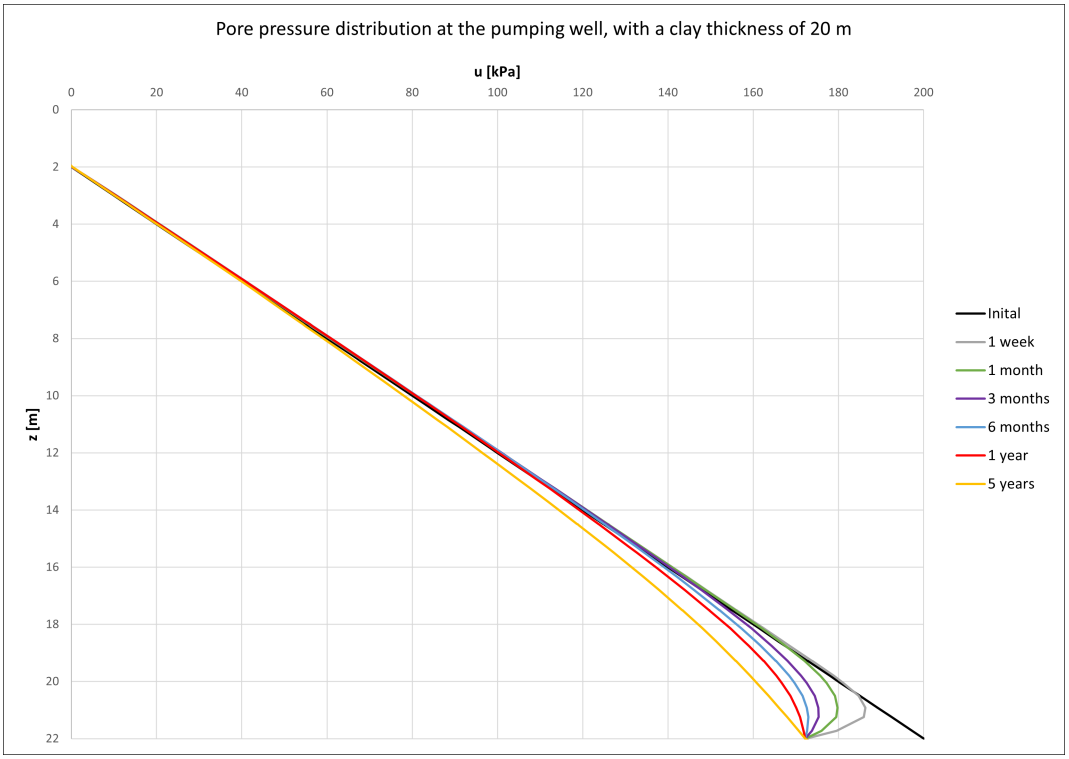

Figure D.9: The pore pressure distribution at the pumping well, with a clay thickness of 20 meters. Plotted over depth for different pumping durations.

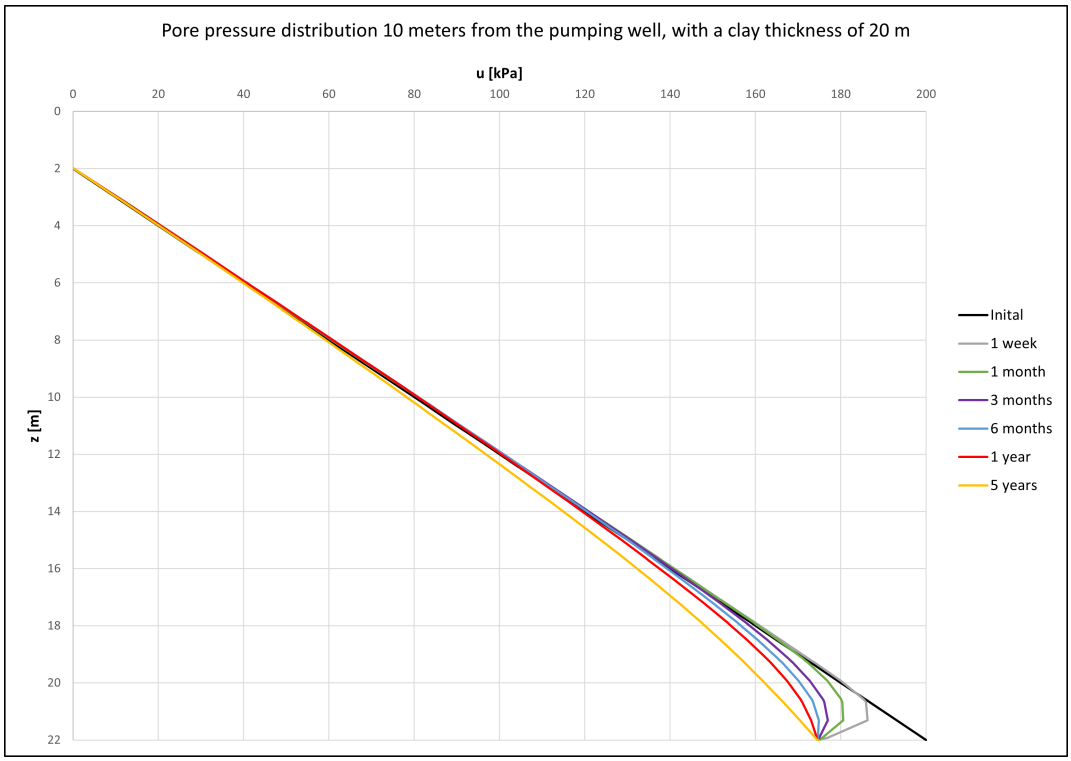

Figure D.10: The pore pressure distribution 10 meters from the pumping well, with a clay thickness of 20 meters. Plotted over depth for different pumping durations.

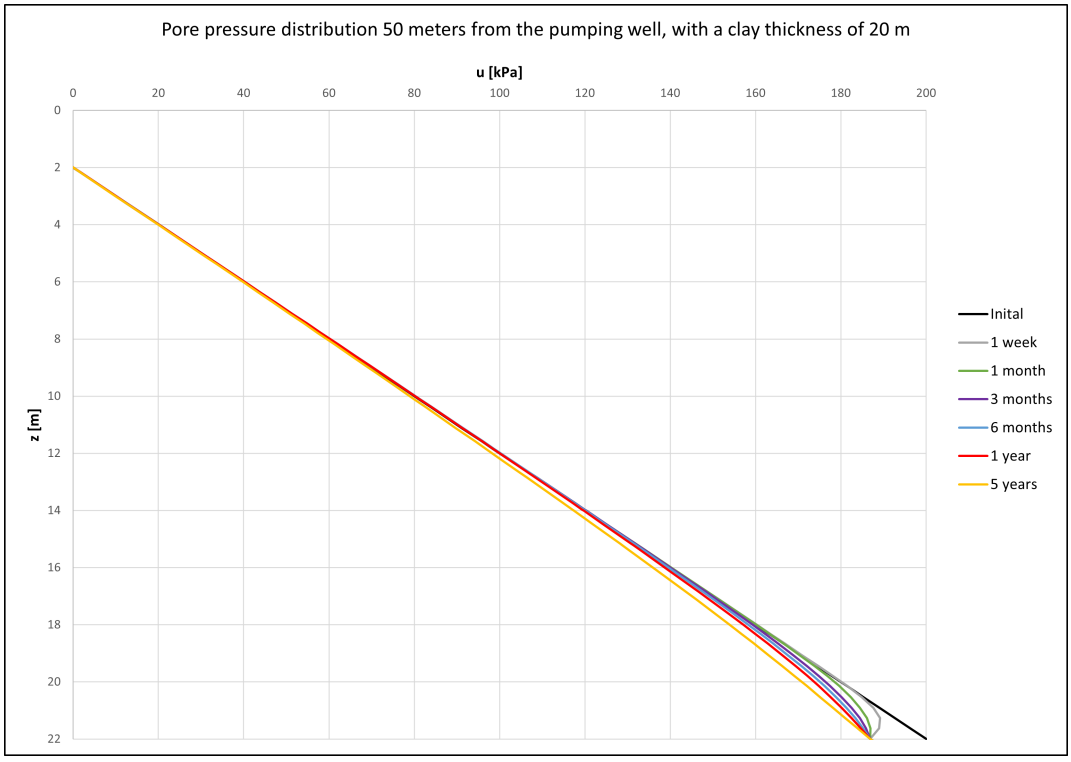

Figure D.11: The pore pressure distribution 50 meters from the pumping well, with a clay thickness of 20 meters. Plotted over depth for different pumping durations.

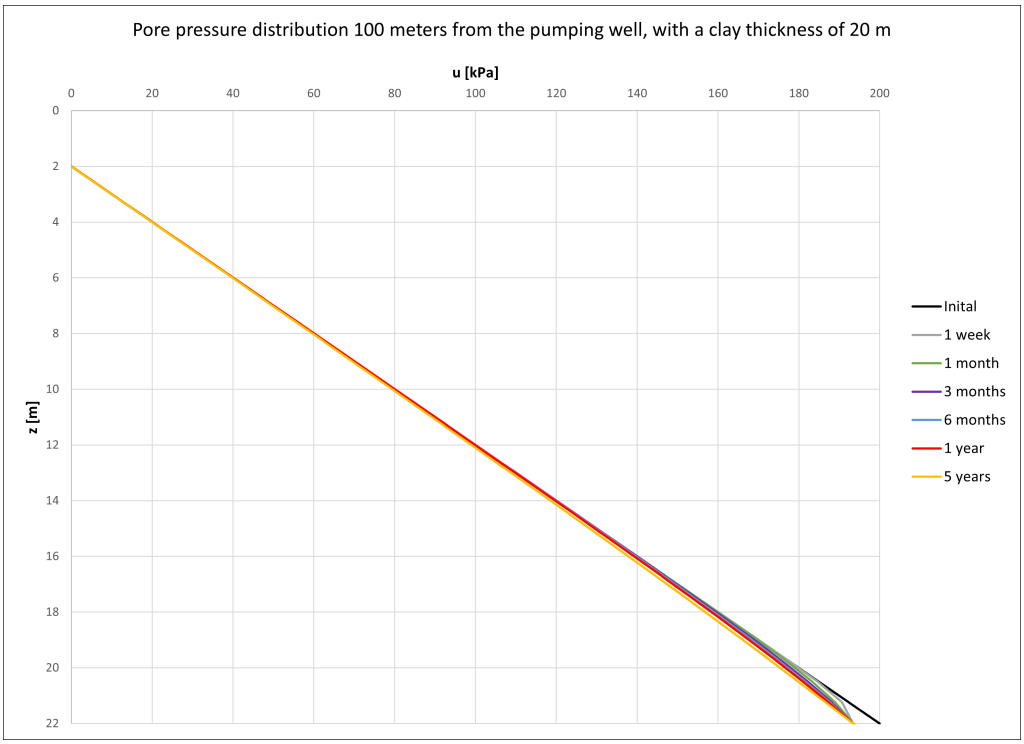

Figure D.12: The pore pressure distribution 100 meters from the pumping well, with a clay thickness of 20 meters. Plotted over depth for different pumping durations.

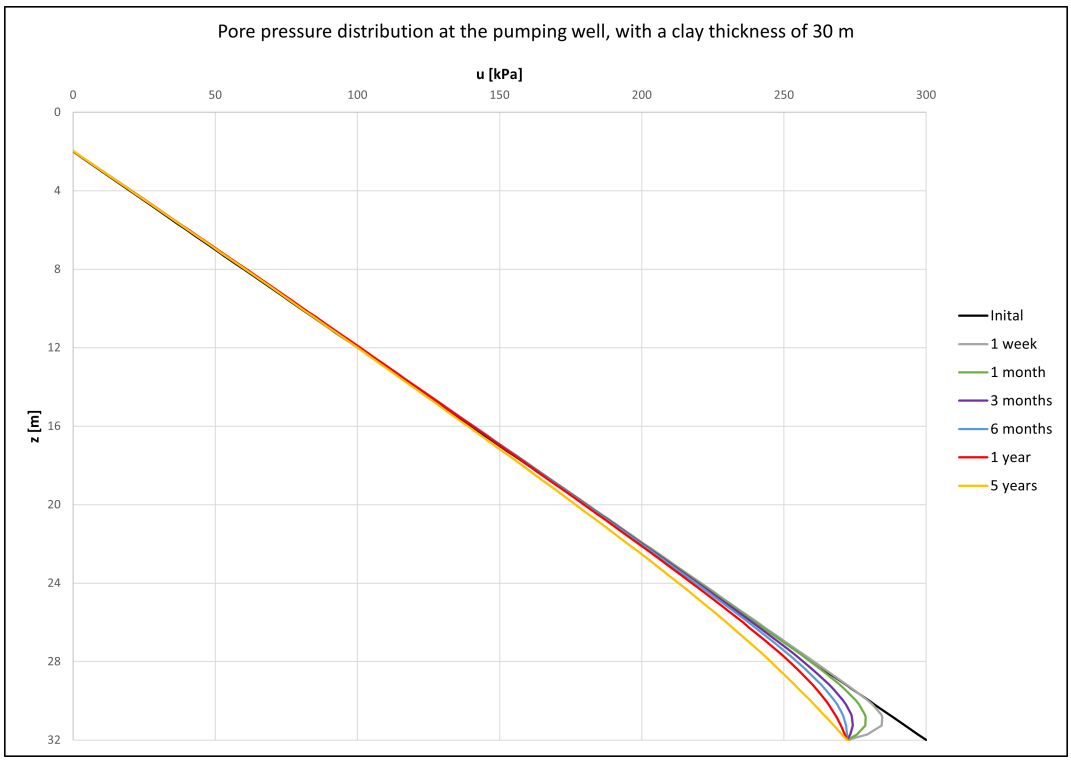

Figure D.13: The pore pressure distribution at the pumping well, with a clay thickness of 30 meters. Plotted over depth for different pumping durations.

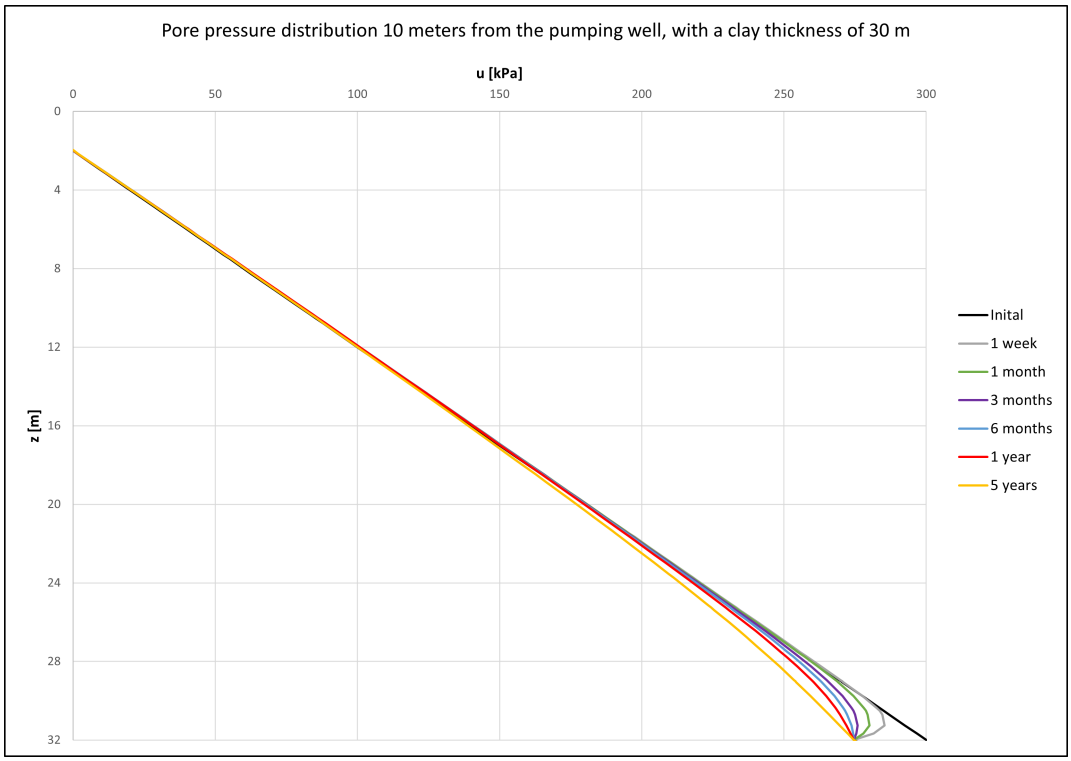

Figure D.14: The pore pressure distribution 10 meters from the pumping well, with a clay thickness of 30 meters. Plotted over depth for different pumping durations.

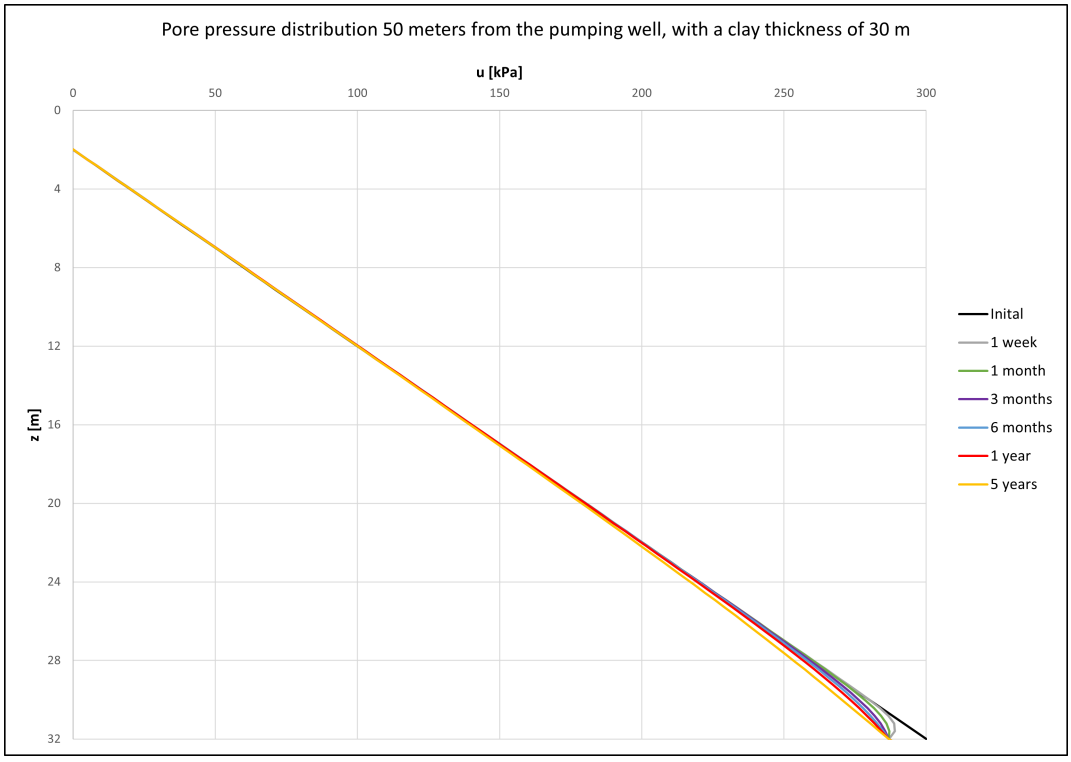

Figure D.15: The pore pressure distribution 50 meters from the pumping well, with a clay thickness of 30 meters. Plotted over depth for different pumping durations.

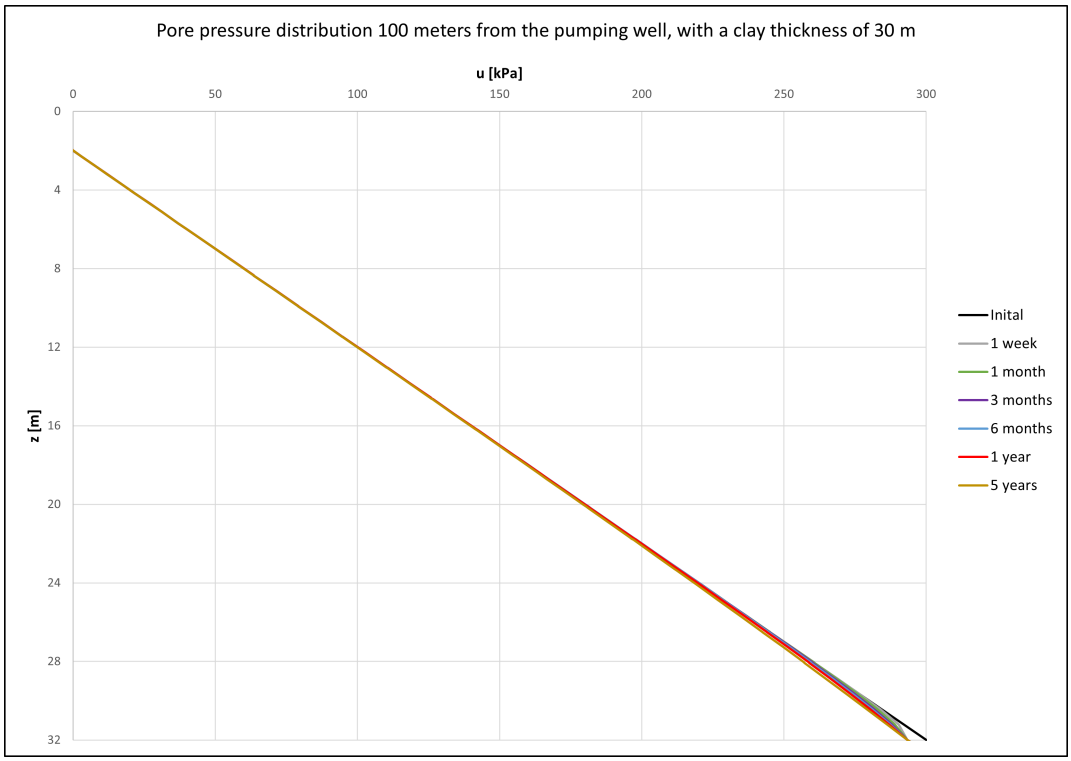

Figure D.16: The pore pressure distribution 100 meters from the pumping well, with a clay thickness of 30 meters. Plotted over depth for different pumping durations.

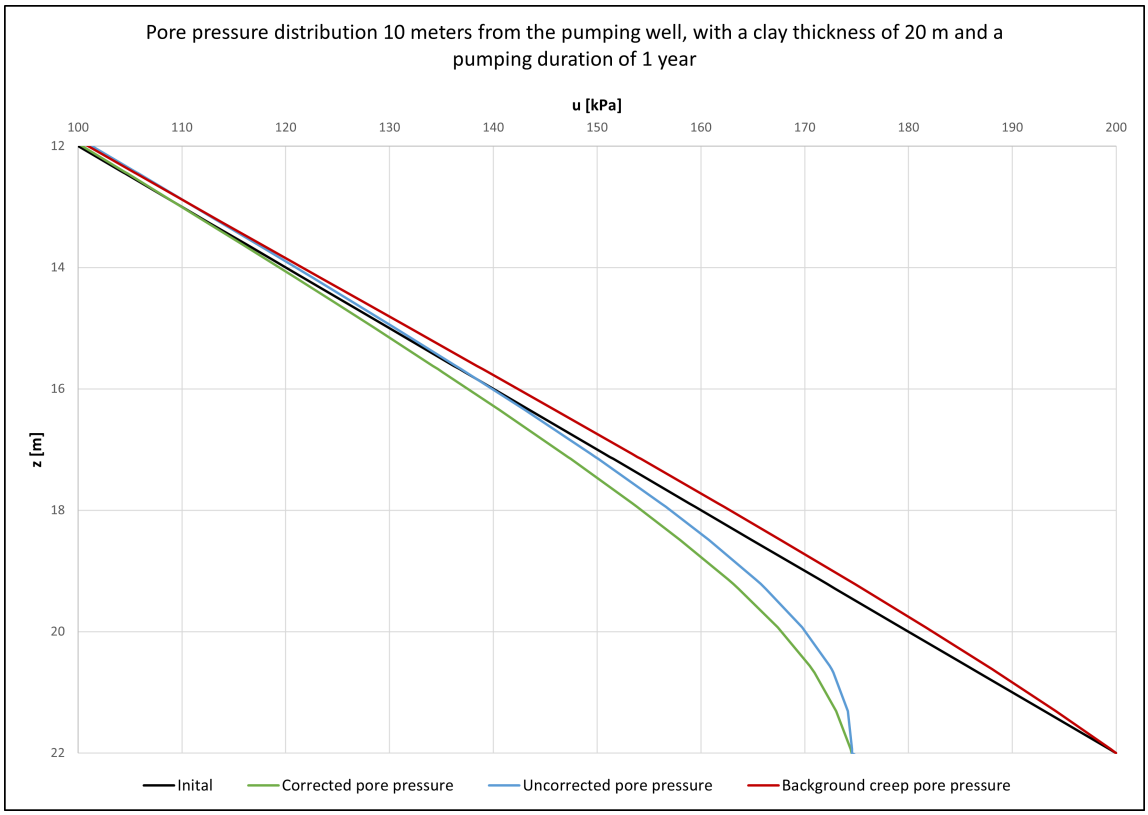

Figure D.17: The pore pressure distribution during the initial phase, the background creep phase, and the uncorrected as well as corrected pore pressures after one year of pumping.

E

Complimentary Plaxis output

In Figure E.1 below, the incremental shear strain developed at the interface between the bedrock and the frictional material is shown. The model shown in the figure is the 500-meter long Hamnbanan pump test model, modeled with a well as the extraction source.

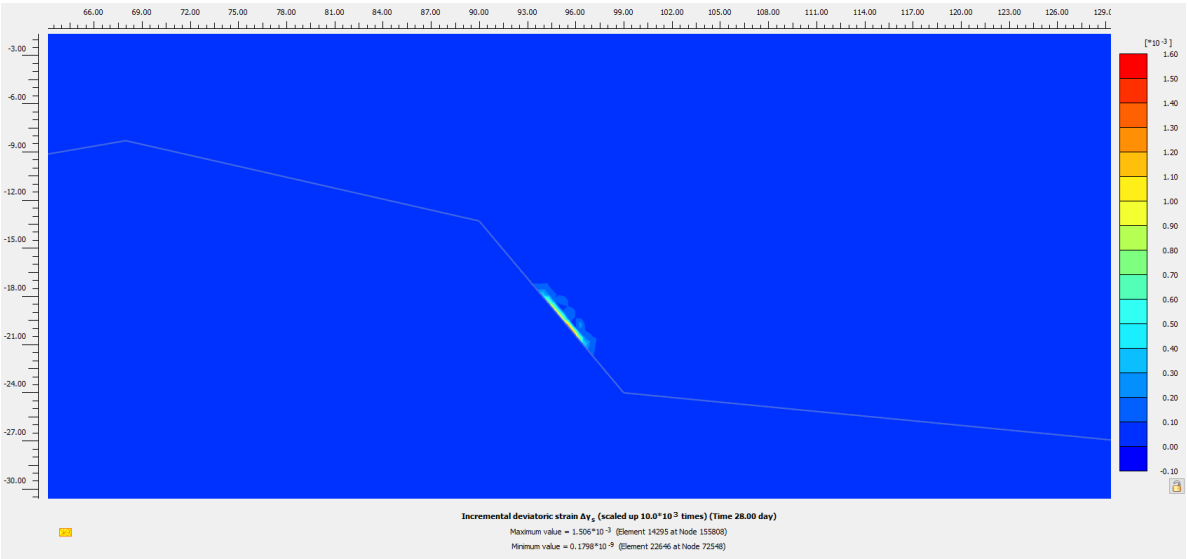

Figure E.1: The incremental shear strains in the interface between the bedrock and the frictional material.

DEPARTMENT OF Architecture and Civil Engineering
CHALMERS UNIVERSITY OF TECHNOLOGY
Gothenburg, Sweden
www.chalmers.se

CHALMERS
UNIVERSITY OF TECHNOLOGY